THE UNIVERSITY OF CALGARY

Interfacial Crack Problems in Layered Materials

by

Mingzheng Li

A DISSERTATION

SUBMITTED TO THE FACULTY OF GRADUATE STUDIES

IN PARTIAL FULFILLMENT OF THE REQUIREMENTS FOR THE DEGREE

OF DOCTOR OF PHILOSOPHY

DEPARTMENT OF MECHANICAL ENGINEERING

CALGARY, ALBERTA

OCTOBER, 1998

Abstract

Interfacial cracking and toughening in metal/ceramic layered materials are investigated in this dissertation. This work stems from the fact that mechanical properties of metal/ceramic layered materials are, to a large extent, determined by the deformation and failure mechanisms at the interface. With the wide use of metal/ceramic layered materials in electronic packaging, ceramic actuators, coatings of fine length scale, the characterization of the basic properties of the layered materials can be quite different from that of the corresponding bulk materials, and provides challenges for both theoretical modelling and experimental measurements. Two fundamental issues are analyzed in detail in present work with considering the fine length scale (from micrometer to nanometer): ductile versus brittle behaviour of metal/ceramic layered materials, and interfacial toughening in metal/ceramic layered materials under mixed mode load condition.

The ductile versus brittle behaviour of the metal/ceramic layered materials is examined by considering the energy conditions for dislocation initiation (layered materials behaviour is denoted as ductile) and interface debonding (layered materials behaviour is denoted as brittle). It is demonstrated that dislocation emission is obvious when the metal layer thickness is above several micrometer; on the other hand, the metal/ceramic layered material is brittle when the metal layer thickness is in the order of nanometer. The mode mixity effect on this ductile versus brittle behaviour is also investigated in terms of loading phase angle.

The interfacial toughening in metal/ceramic layered materials is analyzed by considering the dislocation behaviour in the metal layer. Superdislocation approach is employed to analyze the effects of blunting and shielding on the interfacial crack. A model of periodically enabling dislocation emission and interface debonding is established to simulate the interfacial crack initiation and propagation process. The interface fracture toughness is investigated and steady-state interfacial crack propagation is achieved such that provides some basic parameters, such as length scale and mode mixity, for the safe design of metal/ceramic layered materials.

Acknowledgements

I would like to express my deep gratitude to my advisor Professor X. Mao for his guidance, advice, and encouragement throughout this research work.

I am very grateful to Dr. J. S. Wang at Harvard University, Dr. H. J. Gao at Stanford University for their invaluable discussions and suggestions on this work.

I would like to thank Dr. L. J. Qiao, Mr. X. J. Li, Dr. X. P. Li, and the rest of my colleagues for their assistance and cooperation. Also, I wish to acknowledge the staff of the Department of Mechanical Engineering at the University of Calgary for the support of my study and research, and the staff of the Computing Center of University of Calgary for the help with my finite element calculation.

This dissertation is dedicated to my wife, Changyu Wang, for her patience, understanding, and encouragement during the preparation of this work. It is also dedicated to my little daughter, Linna (Wen Jia), for the forgiving cheer throughout the writing of this dissertation.

Table of Contents

List of Tables

List of Figures

Nomenclature

$b, \bar{b}$	Burgers vector
E, E_j	Young's modulus
E_*	effective Young's modulus
$f, \bar{f}, f_{crack}, f_{interface}, f_K$	force on dislocation
f_{glide}	dislocation gliding force
G	energy release rate
G_c	critical strain energy release rate
G_{disl}	energy release rate for dislocation emission
G_{cleav}	energy release rate for cleavage
h	layer thickness
h_i	location for i'th dislocation
$K, K^{tip'}$	complex interface stress intensity factor
K_c	critical stress intensity factor, fracture toughness
K^{∞}	far field stress intensity factor
K_I, K_{II}, K_1, K_2	stress intensity factor of mode I, II, respectively
k^D	stress intensity factor due to dislocation
$\bar{n}$	unit vector
n	dislocation emission number

n'	critical dislocation emission number
r_c	dislocation core size
R_o	plastic zone length scale
U_{act}	activation energy
W_{ad}	adhesion energy
W_o, W_d', W_d	dislocation self-energy
W_k', W_k	interaction energy between dislocation and crack
W_L', W_L	ledge energy
α	Dundurs parameter
β	Dundurs parameter
γ	surface energy
ε	singularity index
μ, μ_j	shear modulus
ν, ν_j	Poisson's ratio
σ_b	interfacial tensile strength
σ_Y	yield stress
σ_m	mean stress
$\tilde{\sigma}$	stress tensor
$\sigma_{11}, \sigma_{22}, \sigma_{33}$	tensile stress component
σ_{xx}, σ_{yy}	tensile stress component

$\sigma_{rr}, \sigma_{\theta\theta}$	tensile stress component in polar coordinate system
σ^{max}	maximum tensile stress
σ^{tip}	crack tip tensile stress
$\sigma_{xy}, \sigma_{12}, \sigma_{r\theta}$	shear stress component
τ_b	interfacial shear strength
τ, τ_{xy}	shear stress
τ^{max}	maximum shear stress
τ^{tip}	shear stress at crack tip
φ	slip plane inclination angle
Γ	fracture toughness
Γ_i	fracture toughness for crack initiation
Γ_R	fracture resistance, fracture toughness
Γ_{ss}	steady-state fracture toughness
$\Sigma^{I}_{mn}, \Sigma^{II}_{mn}, \Sigma^{III}_{mn}$	Angular distribution function
$\Psi, \Psi^{\infty}, \Psi^{tip}, \Psi^{tip'}, \Psi'$	phase angle
$\Omega, \Omega_x, \Omega_y$	Airy stress function
χ	Airy stress function

Chapter 1

Introduction

1.1 Prologue

Layered materials made from constituents with different physical properties have been widely used to achieve functional requirements, such as the attainment of damage tolerance while maintaining high strength. Some of the important application areas of layered materials include: electronic packaging (Evans and Hutchinson, 1995), ceramic actuators (Furuta and Uchino, 1993; Aburatani et al., 1994; Uchino, 1995; Gong and Suo, 1996), and coatings used for either thermal protection (Kokini and Takenchi, 1995) or for abrasion, oxidation and corrosion resistance. These layered materials usually combine a hard brittle material with a softer ductile material in order to achieve optimal combination of damage tolerance, stiffness, and strength. Generally, they have involved combinations of a ceramic with a polymer or metal and an intermetallic with a metal. Some example brittle materials of interest include silicon, and various oxides and nitrides. The typical ductile materials include aluminum, copper, nickel, and gold.

The dissimilar nature of the constituents challenges the thermomechanical integrity and reliability of the layered material (Evans and Hutchinson, 1995). One of the dominant factors affecting reliability is the deformation and failure mechanisms at the interfaces which are both numerous and susceptible to decohesion and sliding. There are two basically different interface responses: "strong" and "weak" (Evans and Dalgleish, 1992). If one of the constituent materials fails prior to interface rupture, the interface is

designated "strong". Conversely, if failure occurs by interface separation, the interface is considered "weak".

The "weak" interface is the focus of recent research because defects such as voids, gas pores and cracks, are generated easily in the process of layered materials thus make interfaces susceptible to failure. As mentioned by Evans and Hutchinson (1995), there are several basic mechanisms of interfacial failure in metal/ceramic layered materials as shown in Figure 1-1.

Emphasis of this dissertation will be put on the mechanism of brittle debonding with no reaction products or interphase on the interface in metal/ceramic layered materials. For this mechanism, the fracture behavior of the interfacial crack will be investigated by considering both the microstructure and macro performance of the layered materials.

1.2 Objectives

Recently, a lot of work (Leung, He and Evans 1995; Leung et al., 1995; Turner and Evans, 1996; Embury et al., 1996; Mao and Evans, 1997) has been done on metal/ceramic layered materials with micrometer to nanometer length scale. In these thin layered materials, the characterization of basic properties, which can be quite different from that in corresponding bulk materials, provides challenges for both theoretical modelling and experimental measurement. For example, because of the issue of length scale, the characterizations of interface toughness and elastic-plastic transition mechanism are needed.

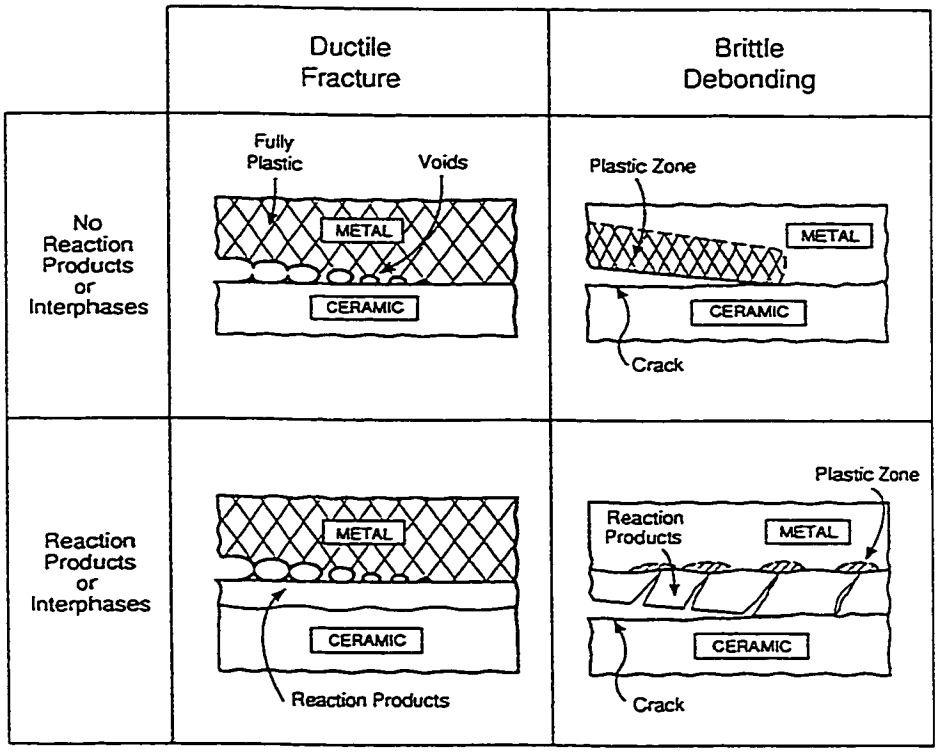

Figure 1-1 Different mechanisms of interface failure in metal/ceramic materials.

This dissertation is aimed to examine two fundamental issues in such thin metal/ceramic layered materials: ductile versus brittle behavior and interfacial toughening. These two fundamental issues become more complicated because of two major factors: the interfacial crack and the fine length scale in the material. Due to the existing of the interfacial crack, interfacial fracture mechanics approaches should be used. For example, the effect of mode mixity, which is the measure of the relative amount of mode II interface stress intensity factor to mode I interface stress intensity factor at the interfacial crack tip, on the performance of the material should be investigated.

To look at the effect of length scale, consider, for example, a layered material consisting of alternating ductile and brittle layers with a pre-existing crack at the interface (Figure 1-2).

Upon loading, the ductile phase flows and blunts the crack tip. If the ductile layer thickness h is sufficiently large, the flow and blunting events at the crack tip will proceed until a limiting event intervenes. Depending on the material system, the limiting event can be cleavage at the blunted crack tip, or void growth and its linkage with the blunted crack tip (see Figure 1-1). It is assumed here that the limiting event does not occur such that only the plastic flow itself is presented (Hsia et al., 1994).

For the example layered materials presented above, Tvergaard and Hutchinson (1994) proposed a material-based length quality, R_o, to estimate the plastic zone size (show as dark area in Figure 1-2) around the crack tip.

$$R_o = \frac{1}{3\pi}\left(\frac{K_c}{\sigma_Y}\right)^2 \tag{1.1}$$

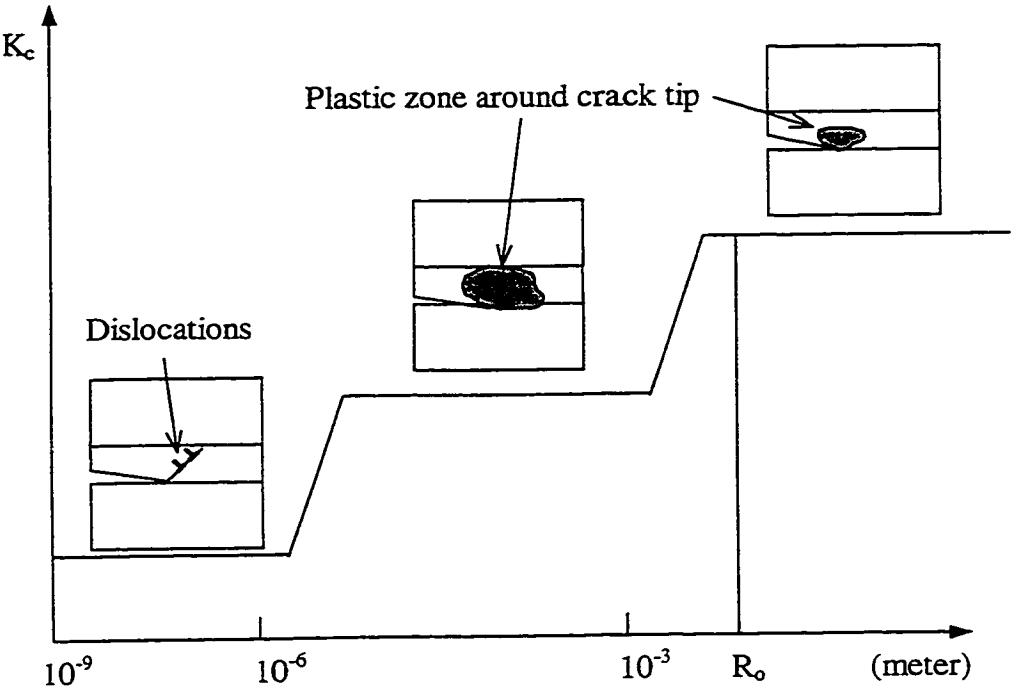

Figure 1-2 Plasticity for different length scale in layered materials.

where K_c is the fracture toughness (material resistance for crack propagation) of the ductile material and σ_Y is the yield strength. For a typical ductile material such as steel, the crack tip plastic zone size is of the order of millimeters to centimeters. If the ductile layer thickness is larger than a few centimeters (e.g. $h/R_o = 6$), no confinement exists and the measured fracture toughness is independent of the layer thickness.

However, the plastic flow becomes confined when $h \sim R_o$ (e.g. $h/R_o = 1.5$), resulting in a lower fracture toughness. This is in agreement with experimental results (Evans and Dalgleish, 1992) which indicate that as the ductile layer thickness decreases, the material appears increasingly more brittle, absorbing smaller amounts of energy at fracture, even though the volume fraction of the ductile is substantial in these layered materials.

When h approaches the micron level, the plasticity within the thin ductile layer can no longer be treated with continuum theory. The interaction between individual dislocation and the crack tip will be considered. This is the regime to be studied in the present dissertation. The ductile layer is assumed as metal in this dissertation. The confining metal layer thickness considered in this study is about a few microns, thus the metal is treated as crystal and the effects of the dislocations within the crystal will be analyzed.

1.3 Original contributions

Some work on the two fundamental issues mentioned previously is listed in Table 1-1 and Table 1-2. Considering what were done, the original contributions of this dissertation are:

Table 1-1 Outline of work on ductile versus brittle behavior of materials

Material	Contributors
Homogeneous, Isotropic	Kelly et al. (1967); Rice and Thomson (1974); Manson (1979)
Bimaterial	Rice et al. (1990); Wang and Anderson (1991); Beltz and Wang (1992); Beltz and Rice (1992)
Layered materials	Will be investigated in this dissertation

Table 1-2 Outline of work on toughening in layered materials

Crack Morphology and Load Condition	Contributors and Comments
Crack within metal layer, Mode I load	Hsia et al. (1994) Using dislocation model and fracture mechanics in homogeneous material. Only crack initiation was analyzed
Interfacial crack, Mixed mode (mode I + mode II) load	Tvergaard and Hutchinson (1994) Addressed interfacial crack propagation. A stress-displacement relationship was assumed at the crack tip. Finite element method was used.
Interfacial crack, Mode I load	Mao and Evans (1997) Using fracture mechanics approaches in homogeneous material. Metal was treated as crystal and dislocation model was used. Analyzed the interfacial crack propagation.
Interfacial crack, Mixed mode (mode I + mode II) load	Will be investigated in this dissertation Using interfacial fracture mechanics approaches. Addressing interfacial crack initiation and propagation. Employing dislocation model.

1. Investigating the condition for the ductile versus brittle behavior of metal/ceramic layered material.
2. Examing the effects of length scale and mode mixity on the ductile behavior of the metal/ceramic layered material.
3. Analyzing the interfacial toughening in metal/ceramic layered material under mixed mode load condition with interfacial crack fracture mechanics approaches.
4. Establishing a model to simulate the interfacial crack propagation process by considering the crystal structure of the metal layer.
5. Investigating the effects of length scale and mode mixity on the interfacial crack fracture toughness in metal/ceramic layered material.

1.4 Organization of text

After a review on the work about interfacial crack and dislocation in layered materials in Chapter 2, the fundamentals about interfacial crack fracture mechanics and edge dislocation theory are introduced in Chapter 3 and Chapter 4, respectively. Considering the two fundamental issues mentioned previously, the ductile versus brittle behavior of metal/ceramic layered materials is examined in Chapter 5 in terms of the competition between atomic decohesion (cleavage) and dislocation nucleation at the interface crack tip. In Chapter 6, the interfacial crack toughening mechanism is investigated by addressing interfacial crack initiation and propagation process. Based on the equilibrium dislocation emission concept and superdislocation approach, the dislocation behavior and its effect on

interfacial toughening are examined. The conclusions and recommendations are summarized in Chapter 7.

Chapter 2

Literature Review

In this chapter, the literature is reviewed on layered materials from both a macro continuum fracture mechanics viewpoint and a micro standpoint in terms of dislocation theory and application. Even though research on layered materials stems from the study of composites, it is remarked here that the recent research interest of layered materials originally stems from testing the fracture toughness of bimaterial system (see the review by Hutchinson and Suo, 1992), only some recent work sheds directly light on layered materials modeling (Hsia et al., 1994; Tvergaard and Hutchinson, 1994, 1996; Wei and Hutchinson, 1996; Mao and Evans, 1997).

2.1 Macro continuum fracture mechanics in layered materials

The original interest in layered materials stems from their applications in composites decades ago. Conventional plate or shell theories were used to analyze the stress and strain field by considering the boundary conditions across layers. But, research on layered materials in the presence of defects has only been done recently. The main reason for this trend is due to the fine length scale in these layered materials. Therefore, even some initially small defects will significantly change the performance of the system. The defects include voids, inclusions, gas pores and cracks etc.

Because of the high stress singularity at crack tip, the fracture behavior of layered materials has been the focus of recent research. Erdogan and Gupta (1971) employed

integral equation to provide the theoretical tools for studying the fracture of layered composites with flaws. Some basic methodologies and results based on fracture mechanics concepts were presented in a recent review by Hutchinson and Suo (1992).

Even though layered materials may consist of many layers with different material for each layer, most widely used layered materials are composed of alternating two different materials, wherein, one constituent has high strength and another constituent has excellent toughness. The typical application areas of such layered materials include micro-electronic packaging (Hutchinson and Evans, 1995), ceramic multilayer actuators (Furuta and Uchino, 1993; Aburatani et al., 1994; Yang and Suo, 1994; Uchino, 1995; Rogers, 1995; Gong and Suo, 1996), and coatings (Kokini and Takenchi, 1995).

For modelling, three layers are usually used to investigate the performance of the layered materials system, as illustrated in Figure 2-1. The middle layer is denoted as material 1, and two outer layers are assumed identical and denoted as material 2.

Generally, material 2 is brittle such as ceramic and glass, and material 1 is either brittle, such as epoxy, or ductile, such as metal. If material 1 is brittle, or the plastic behavior of material 1 can be ignored, such layered material is denoted as elastic/elastic/elastic type material; when the plastic behavior of material 1 should be considered, the layered material is denoted as elastic/elastic-plastic/elastic type material. It is noted here that the ductile or brittle behavior of materials will change under some circumstance. For example, the brittle material at room temperature may be ductile at high temperature and a ductile bulk material may be brittle when the dimension of the material

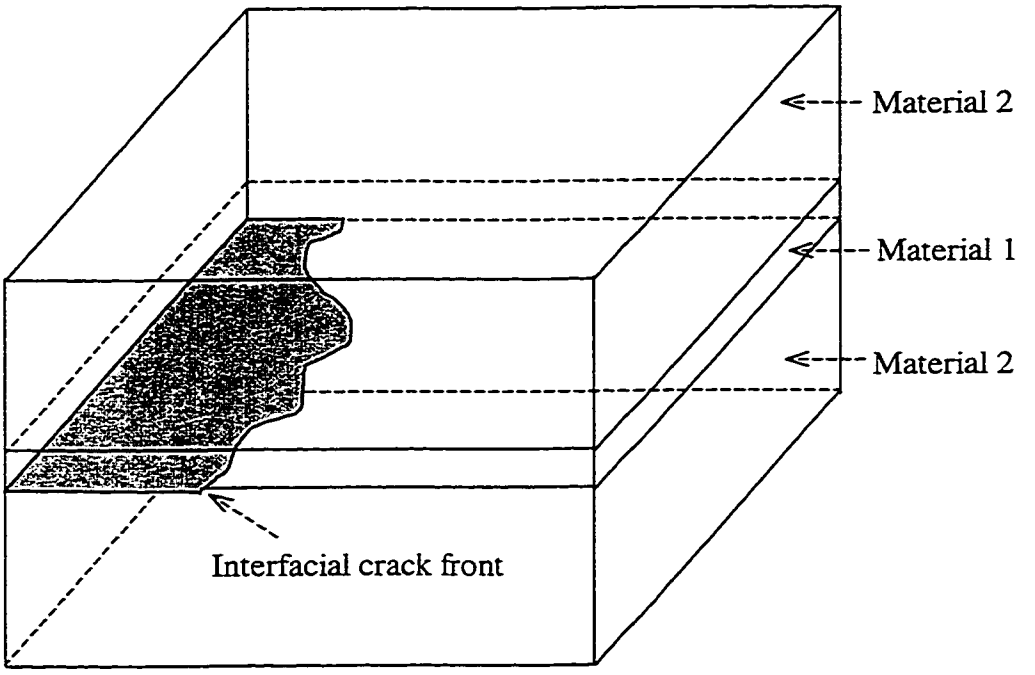

Figure 2-1 Layered materials model with three layers.

sample becomes very small. The definitions of brittle and ductile used in this dissertation are from the conventional standpoint, such as bulk homogeneous media.

2.1.1 Elastic/elastic/elastic layered materials

Comprehensive work has been done about elastic/elastic/elastic type layered materials because the middle layer is susceptible to induce crack, and plasticity in such system is ignored, which makes analysis simpler. The original purpose of using such system is to measure interface fracture toughness of a bimaterial system (Suo and Hutchinson, 1989). Suo (1990) analyzed the parallel debonding, which was observed in an Al_2O_3-SiC-Al_2O_3 laminate. Various modes of cracking in a thin brittle adhesive layer joining two identical bulk solids were reviewed by Hutchinson and Suo (1992). The objectives of these work can be concluded as two groups: (1) the cracking morphology investigation, including straight crack within layer, interfacial crack, alternating crack between two interface and wavy crack within adhesive layer; (2) interface fracture toughness analysis and testing for various cracking morphologies.

Two main factors to affect the system performance, namely, residual stress in the adhesive layer and loading phase angle which measures the ratio of shear load to tensile load, were investigated in detail in recent work (Hutchinson and Suo, 1992).

It was widely reported that the different levels of elastic mismatch and residual stress induce different crack morphology (Fleck et al., 1991; Hutchinson and Suo, 1992). Therefore, different interface fracture toughness is predicted.

Recent experiments have been accomplished to examine the strong dependence of interface toughness on mode mixity in terms of loading phase angle. Cao and Evans (1989) and Liechti and Chai (1992) have studied an epoxy/glass system. Wang and Suo (1990) examined an epoxy on metal and Plexiglass substrates. All these systems exhibit rapidly increasing interfacial fracture toughness at large phase angles. Various aspects of methods for measuring interface fracture toughness can be found in articles by Suo and Hutchinson (1989), Charalabgides et al. (1989), Evans et al. (1990), Rice et al. (1990), Hutchinson and Suo (1992) and Shih (1991), and in a volume edited by Ruhle et al. (1990).

2.1.2 Elastic/elastic-plastic/elastic layered materials

Comparing to elastic/elastic/elastic system, elastic/elastic-plastic/elastic type layered materials are more complicated to analyze because of the involvement of plasticity. Although defects are easily generated within middle layer in elastic/elastic/elastic system, cracks are usually found at the interfaces in elastic/elastic-plastic/elastic systems because of the weakness of interface. Two main mechanisms contribute such creation of interfacial cracks. Firstly, in the process of layered materials, the middle layer is deposited on the substrate and some defects will be generated on the interface. These defects will nucleate the interfacial crack. Secondly, the adjacent brittle layers are cracking susceptible. Once the crack is generated in the brittle layer, it is likely to propagate to the interface and cause the interface cracking (Shaw et al., 1996).

Because of the stress concentration near the interfacial crack tip, plasticity can be easily generated in the middle layer. Therefore, to investigate the properties of elastic/elastic-plastic/elastic system, it must consider the role of plasticity.

Some basic phenomena that control crack propagation at metal/oxide interfaces have been reported (Reimanis et al., 1991; Evans and Dalgleish, 1992; Leung et al., 1995; Shen and Suresh, 1995a and 1995b; Turner and Evans, 1996; Finot and Suresh, 1996). Previous studies on comparable interfaces have indicated strong effects on the fracture toughness, Γ, of plasticity, of reaction products and of the atmosphere, coupled through the interface fracture mechanism. Crack extension along interfaces without reaction products may occur either by ductile void growth (ductile mode), by brittle debonding (brittle mode) or by coupled with plasticity. Interfacial cracking involving plasticity often occurs by a failure mechanism operating at interfacial defects ahead of the interfacial crack front, whereas brittle debonding occurs by direct bond rupture at the crack front itself. The dominant mechanism (among these possibilities) is governed by such parameters as yield strength, work of adhesion, metal thickness and interface defect population.

Some criteria were suggested to distinguish brittle mode and ductile mode. As mentioned by Turner and Evans (1996), ductile mode occurs when the bonding at the interface is capable of sustaining stresses in the range, $\sigma_m / \sigma_Y \approx 5$, where σ_m is the mean stress $[\frac{1}{3}(\sigma_{11} + \sigma_{22} + \sigma_{33})]$ and σ_Y is the uniaxial yield strength of the metal. When this stress is reached, defects in the metal near the interface are unstable against plastic hole growth and ductile rupture is inevitable. When the interface bonding is less strong, fracture

can occur by debonding along the interface with essentially no metal attached to the oxide and vice versa.

Recently, many experiments (Leung et al., 1995; Turner and Evans, 1996) and theories (Hsia et al., 1994; Evans and Hutchinson, 1995; Mao and Evans, 1997) have been proposed to investigate the properties of such system, especially metal/oxide combination. A fundamental understanding now exists for the ductile fracture mechanism. However, basic issues remain to be understood when fracture occurs by brittle bond rupture, particularly with regard to the role of the work of adhesion, W_{ad}. Recent work focusing on brittle mode analysis indicated that even when interface fracture involves bond rupture, there can be a substantial influence of plastic dissipation Γ_p on the fracture toughness Γ. Moreover, Γ_p is affected by the mode mixity at the crack tip and the metal layer thickness.

Reimanis et al. (1992) investigated the effects of plasticity on the crack propagation resistance of a metal/ceramic interface by conducting experiments on a gold/sapphire interface. The interface was found to fail by interface separation in a nominally "brittle" manner with a critical strain energy release rate, $G_c = 50\ Jm^{-2}$, substantially larger than the work of adhesion, $W_{ad} = 0.5\ Jm^{-2}$. Evidence of plastic deformation on the gold fracture surface, such blunting steps and slip steps, suggested that plastic dissipation is the primary contribution to the measured G_c. Their calculations indicated that the majority effect occurs in the plastic zone through the crack wake. The interface was also found to be susceptible to slow crack growth.

The effects of interface structure and microstructure on the fracture toughness, Γ, of metal-ceramic interfaces were reviewed by Evans and Dalgleish (1992). Some systems exhibited a ductile fracture mechanism and others failed by brittle mechanism. In the absence of either interphase or reaction products, Γ is dominated by plastic dissipation (for both fracture mechanisms). Additionally, Γ, is larger when fracture occurs by ductile void growth (for the same layer thickness, h, and yield stress σ_Y). Interpahses and reaction products have been shown to have an important effect on Γ. A general trend found by experiment is that Γ scales with the fracture toughness of the interphase itself. The important effects of the residual stresses in the interface (which influence the fracture mechanism) and the layer thickness were examined as well.

De Graef et al. (1992) studied the structure, bonding and fracture resistance of interfaces between alumina and platinum. O'Dowd et al. (1992) addressed the fracture toughness of alumina-niobium interfaces. A model system was developed to measure the interfacial strength and fracture toughness. Interface fracture toughness experiments were carried out for phase angle between 0 and 45 degree. For positive phase angles less than 45, fracture along the interface was observed in most cases. The measured interfacial fracture toughness shows a strong dependence on phase angle. They suggested that interface toughening with increased mode mixity in the alumina/niobium system is due to two phenomena. Firstly, because the fracture toughness of the niobium is much greater than that of the interface, the crack is constrained to grow on the interface. Crack growth along the interface requires a sufficiently high interfacial hoop stress. Mixed mode loading redistributes the stresses which results in lower hoop stresses across the interface at a

fixed magnitude of stress intensity factor, K. Therefore the magnitude of K must be increased in order to produce the hoop-stress levels similar to those for small mode mixity. Secondly, plastic flow in the niobium results in stress relaxation. Under conditions of high mode mixity, stress relaxation becomes particularly important, further elevating by a significant amount of remote loads that are necessary to raise the near-tip stresses to the levels required to fracture interface.

To facilitate comparison with theory, plastic dissipation effects for confined metal layers subject to mode I (tensile) loading was explored experimentally by Turner and Evans (1996). The mechanism of mode I crack propagation along gold/sapphire interfaces in both humid and dry environments have been investigated. It was reported that interface failure occurs by bond separation at the interfaces accompanied by substantial deformation of the gold along intersecting slip planes. In a dry environment, crack extension occurs by interfacial decohesion at multiple sites ahead of the main crack front. The associated fracture toughness is of order $\Gamma = 50\ \mathrm{Jm}^{-2}$. The debonding initiates from interfacial defects. The main crack experiences extensive plastic blunting; whereas debonds ahead of the crack have diminished blunting and propagate, subject to rising resistance curve. Because of the small blunting displacements, the stresses ahead of the debonds are sufficient to cause rupture of the interface bonds. In a humid environment, the crack propagation mechanism changes. In this case, the crack front itself extends, when $\Gamma = 10\ \mathrm{Jm}^{-2}$, subject to small blunting displacements.

Some theoretical models have been provided recently to address the interfacial crack problems in layered materials. Tvagaard and Hutchinson (1994, 1996) proposed a model

to consider the plasticity role by establishing a stress-displacement relationship at the interfacial crack tip and FEM (Finite Element Method) simulations were implemented to investigate the model. The steady-state is attained and the strong dependency of interface toughness on mode mixity is analyzed. Wei and Hutchinson (1996) used the FEM model to analyze the joints and strain plasticity theory was suggested to modify the model.

2.2 Micro viewpoint of plasticity – application of dislocation theory

Since the edge dislocation was proposed by Orowan (1934), Polanyi (1934), and Taylor (1934) to explain the discrepancy between theoretical strength and experimental result in crystal, dislocation theory has been widely used to investigate the property of materials. Some basic concepts and results of dislocation theory will be presented in Chapter 4. The emphasis here is on the applications of dislocation theory in bimaterial system and layered materials for non-cracked media and cracked media, respectively.

2.2.1 Dislocation in non-cracked media

For bimaterial system, Head (1953) analyzed the stress of the edge dislocation with different interface boundary condition. Dundurs (1969) reviewed some basic approaches and results for both edge dislocation and screw dislocation.

Using the complex potential and conformal mapping techniques, Chu (1982) analyzed the stress field of a straight screw dislocation lying parallel to the surface of a two-phase isotropic thin film of equal thickness in each phase with a welded interface.

Due to the misfit dislocations introduced at the interface, Freund (1987) investigated the stability of dislocation threading a strained layer on a substrate in terms of critical layer thickness at which interface dislocation can form "spontaneously". Beltz and Freund (1994) redressed this critical layer thickness issue using a Peierls-Nabarro model for the dislocation.

For bimaterial interfaces with arbitrary stiffness, Shilkrot and Srolovitz (1998) examined the interaction between an array of dislocations and the interface with general bond condition.

For the dislocation in layered materials, Chou (1966) used the method of images to determine the stress field of a screw dislocation in and near a lamellar inclusion. Kamat et al. (1987) extended Chou's approach to get the image force on screw dislocations in n-multilayer structures. Embury and Hirth (1994) analyzed the dislocation storage and the mechanical response of fine scale microstructures using the edge dislocation array model. Considering dipole screw dislocations embedded within a multilayer which was modeled as alternating layers of material 1 and material 2, Anderson and Li (1995) predicated the Hall-Petch relations for multilayered materials in terms of critical local resolved shear stress on a slip plane to produce slip transmission across an interface.

2.2.2 Dislocation in cracked media

Considering the dislocation in bicrystal system, Beltz and Wang (1990) predicated the brittle or ductile behavior of an interfacial crack (with regard to particular slip systems). To avoid the assumption of the effective core size of the emitted dislocation in the

approach proposed by Beltz and Wang (1990), Beltz and Rice (1992) solved the elasticity problem of a traction-free crack with a Peierls-type stress versus displacement relationship being satisfied as a boundary condition along a slip plane ahead of the crack tip.

Suo (1989) analyzed the dislocation interaction with interfacial crack in terms of the interface stress intensity factor due to the dislocation.

Crack tip dislocation emission and arrangements were investigated experimentally for bimaterial system (Lii et al., 1990; Zielinski et al., 1992; Huang and Gerberich, 1992; Marsh et al., 1992). In the work, a superdislocation model, in which the image force is already included, was developed to determine the shielding effect of assays of dislocation on interfacial crack.

So far, the work on dislocation in cracked layered materials is not advanced. Anderson and Li (1993) employed screw dislocation model to investigate the ductile-to-brittle transitions in multilayered materials under mode III (anti-shear) condition.

The effects of dislocation confinement on fracture behavior in laminates consisting of alternating submicron ductile and brittle layers were studied by Hsia et al (1994). The crack is within the ductile layer. Employing superdislocation model, the crack tip field was analyzed. It was indicated that cleavage can even occur in ductile metals such as copper and aluminum if the constraining layer is sufficiently thin.

Considering an interfacial crack within the metal/ceramic layered materials, Mao and Evans (1997) analyzed the blunting effects on interfacial crack initiation and propagation in metal/ceramic layered materials under mode I loading. Because the metal layer thickness

is in the order of micrometer, the metal was treated as crystal and superdislocation approach was used to analyze the blunting effect.

Chapter 3

Fundamentals of Interfacial Crack Fracture Mechanics

After an introduction about some concepts in linear fracture mechanic, some fundamentals of interfacial crack fracture mechanics are reviewed in this chapter. The elastic fields are analyzed for bimaterial system, and the fracture mechanics result for layered material with an interfacial crack is presented. The fundamentals herein and those in the next chapter are the grounds for Chapter 5 and Chapter 6 to address the interfacial crack problems in metal/ceramic layered materials.

3.1 Fundamental definitions and basic formulations in linear fracture mechanics

3.1.1 Modes of crack propagation

Three loading situations are summarized in fracture mechanics to analyze different types of stresses. Figure 3-1 shows the three modes and directions of crack propagation.

These modes are generally identified by subscripts I, II and III. Mode I, which is also called the opening or tensile mode, refers to cases in which the crack surfaces move directly apart and the traction on xz plane ahead of the crack tip is pure tensile. Mode II, usually called the sliding mode or in-plane shear mode, refers to cases in which the crack surfaces slide over one another in a direction perpendicular to the leading edge of the crack and the traction on xz plane ahead of the crack tip is pure in-plane shear. Mode III, also referred to as the tearing or antiplane shear mode, is those cases in which the crack surfaces move relative to one another and parallel to the leading edge of the crack and the

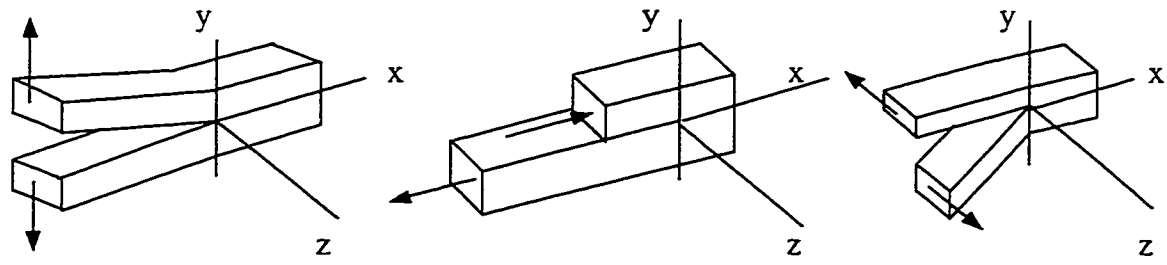

Mode I Mode II Mode III

Figure 3-1 Basic modes of loads and cracking propagation.

traction on xz plane ahead of the crack tip is pure anti-plane shear.

These three modes essentially describe three independent movements of the upper and lower crack surfaces with respect to each other and are sufficient to describe all possible modes of crack propagation in an elastic material. If subject to more than one mode, the material is referred to as under mixed mode condition.

3.1.2 Stress distribution in vicinity of crack tip

The plane problem of elasto-statics in the absence of body force for the homogeneous isotropic solid, either in plane strain or idealized plane stress, reduces to the solution of a biharmonic function

$$\nabla^2\nabla^2\chi(r,\theta)=0. \tag{3.1}$$

Here, χ is Airy stress function, ∇^2 is Laplacian operator in polar coordinates and $\nabla^2=\frac{\partial^2}{\partial r^2}+\frac{1}{r}\frac{\partial}{\partial r}+\frac{1}{r^2}\frac{\partial^2}{\partial\theta^2}$. r and θ are shown in Figure 3-2 and measured from the crack tip. The stress components can be determined according to the relations

$$\begin{aligned}\sigma_{rr}&=\frac{1}{r}\frac{\partial\chi}{\partial r}+\frac{1}{r^2}\frac{\partial^2\chi}{\partial\theta^2},\\ \sigma_{\theta\theta}&=\frac{\partial^2\chi}{\partial r^2},\\ \sigma_{r\theta}&=\frac{1}{r^2}\frac{\partial\chi}{\partial\theta}-\frac{1}{r}\frac{\partial^2\chi}{\partial r\partial\theta}.\end{aligned} \tag{3.2}$$

Williams (1957) solved the above plane problem by using the eigenfunction expansion method. The stresses and displacements in the vicinity of the crack tip can be expressed in the polar coordinate system as

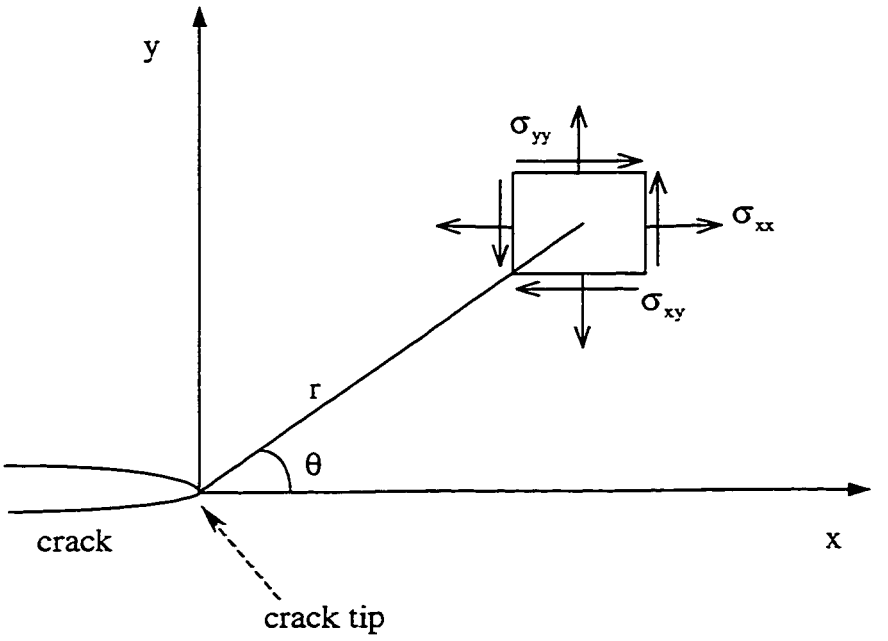

Figure 3-2 Stress distribution in the vicinity of crack tip.

$$\sigma_{rr} = \frac{K_I}{\sqrt{2\pi r}}\cos\frac{\theta}{2}(1+\sin^2\frac{\theta}{2}) + \frac{K_{II}}{\sqrt{2\pi r}}\sin\frac{\theta}{2}(1-3\sin^2\frac{\theta}{2}),$$

$$\sigma_{r\theta} = \frac{K_I}{\sqrt{2\pi r}}\cos^3\frac{\theta}{2} - \frac{K_{II}}{\sqrt{2\pi r}}(3\sin\frac{\theta}{2}\cos^2\frac{\theta}{2}),$$

$$\sigma_{r\theta} = \frac{K_I}{\sqrt{2\pi r}}\sin\frac{\theta}{2}\cos^2\frac{\theta}{2} + \frac{K_{II}}{\sqrt{2\pi r}}\cos\frac{\theta}{2}[1-3\sin^2\frac{\theta}{2}],$$

$$\begin{aligned} u_r = {} & \frac{K_I}{2E}\sqrt{\frac{r}{2\pi}}(1+\nu)[(2\kappa-1)\cos\frac{\theta}{2} - \cos\frac{3\theta}{2}] \\ & + \frac{K_{II}}{2E}\sqrt{\frac{r}{2\pi}}(1+\nu)[-(2\kappa-1)\sin\frac{\theta}{2} + 3\sin\frac{3\theta}{2}], \end{aligned}$$

$$\begin{aligned} u_\theta = {} & \frac{K_I}{2E}\sqrt{\frac{r}{2\pi}}(1+\nu)[-(2\kappa+1)\sin\frac{\theta}{2} - \sin\frac{3\theta}{2}] \\ & + \frac{K_{II}}{2E}\sqrt{\frac{r}{2\pi}}(1+\nu)[-(2\kappa+1)\cos\frac{\theta}{2} + 3\cos\frac{3\theta}{2}]. \end{aligned} \qquad (3.3)$$

Here, u_r and u_θ are radial and tangential components of displacement field. E is Young's modulus and ν is Poisson's ratio.

In the Cartesian coordinate system the above expressions can be written as

$$\sigma_{xx} = \frac{K_I}{\sqrt{2\pi r}}\cos\frac{\theta}{2}[1-\sin\frac{\theta}{2}\sin\frac{3\theta}{2}] - \frac{K_{II}}{\sqrt{2\pi r}}\sin\frac{\theta}{2}[2+\cos\frac{\theta}{2}+\cos\frac{3\theta}{2}],$$

$$\sigma_{yy} = \frac{K_I}{\sqrt{2\pi r}}\cos\frac{\theta}{2}[1+\sin\frac{\theta}{2}\sin\frac{3\theta}{2}] + \frac{K_{II}}{\sqrt{2\pi r}}\sin\frac{\theta}{2}\cos\frac{\theta}{2}\cos\frac{3\theta}{2},$$

$$\sigma_{xy} = \frac{K_I}{\sqrt{2\pi r}}\sin\frac{\theta}{2}\cos\frac{\theta}{2}\cos\frac{3\theta}{2} + \frac{K_{II}}{\sqrt{2\pi r}}\cos\frac{\theta}{2}[1-\sin\frac{\theta}{2}\sin\frac{3\theta}{2}],$$

$$\begin{aligned} u = {} & \frac{K_I}{2E}\sqrt{\frac{r}{2\pi}}(1+\nu)[(2\kappa-1)\cos\frac{\theta}{2} - \cos\frac{3\theta}{2}] \\ & + \frac{K_{II}}{2E}\sqrt{\frac{r}{2\pi}}(1+\nu)[(2\kappa+3)\sin\frac{\theta}{2} + \sin\frac{3\theta}{2}], \end{aligned}$$

$$v = \frac{K_I}{2E}\sqrt{\frac{r}{2\pi}}(1+\nu)[(2\kappa+1)\sin\frac{\theta}{2} - \sin\frac{3\theta}{2}] + \frac{K_{II}}{2E}\sqrt{\frac{r}{2\pi}}(1+\nu)[-(2\kappa-3)\cos\frac{\theta}{2} + \cos\frac{3\theta}{2}]. \tag{3.4}$$

Here, u and v are displacement components in Cartesian coordinate system. In Equations (3.3) and (3.4), σ_{xx}, σ_{yy}, σ_{rr} and $\sigma_{\theta\theta}$ are normal components of the stress tensor, σ_{xy} and $\sigma_{r\theta}$ are shear components of the stress tensor, and

$$\kappa = \begin{cases} \dfrac{3-\nu}{1+\nu} & \text{if plane stress,} \\ 3-4\nu & \text{if plane strain.} \end{cases} \tag{3.5}$$

The asymptotic singular field around the crack tip for anti-plane deformation of the medium can be expressed as

$$\tau_{xz} = -\frac{K_{III}}{\sqrt{2\pi r}}\sin\frac{\theta}{2},$$

$$\tau_{yz} = -\frac{K_{III}}{\sqrt{2\pi r}}\cos\frac{\theta}{2},$$

$$w = -\frac{K_{III}}{\mu}\sqrt{\frac{r}{2\pi}}\sin\frac{\theta}{2}. \tag{3.6}$$

Here, w is anti-plane displacement. τ_{xz} and τ_{yz} are anti-plane shear stresses and μ is the shear modulus. In anti-plane deformation, expressions in polar coordinate system are the same as expressions in Cartesian coordinate system.

K_I, K_{II}, and K_{III} in the foregoing expressions, are defined as the stress intensity factors for the three respective modes. The stress intensity factor depends on the geometry of the body and the loading configuration.

3.1.2 Stress intensity factor

From Equation (3.4), the stress field near a crack tip for Mode I can be written as

$$\sigma_{xx} = \frac{K_I}{\sqrt{2\pi r}}\cos\frac{\theta}{2}\left[1-\sin\frac{\theta}{2}\sin\frac{3\theta}{2}\right],$$

$$\sigma_{yy} = \frac{K_I}{\sqrt{2\pi r}}\cos\frac{\theta}{2}\left[1+\sin\frac{\theta}{2}\sin\frac{3\theta}{2}\right],$$

$$\sigma_{xy} = \frac{K_I}{\sqrt{2\pi r}}\sin\frac{\theta}{2}\cos\frac{\theta}{2}\cos\frac{3\theta}{2}. \qquad (3.7)$$

An important feature of the above expression is the fact that the stress distribution around any crack in a structure is similar and depends only on the parameters r and θ. The difference between one cracked component and another lies in the magnitude of the stress intensity factor K_I. In essence, K_I serves as a scale factor to define the magnitude of the crack-tip stress field. K_I depends on the loading configuration and the geometry of the system. In general, the stress intensity factor can be expressed as

$$K_I = f(\sigma, a) \qquad (3.8)$$

where the functionality depends on the configuration of the cracked component and the manner in which the loading is applied. Many functions have been determined for various specimen configurations and are available from the fracture mechanics literature (e.g. Tada et al., 1985). For example, a central crack in an infinite body, subjected to a uniform stress, σ, the stress intensity factor is

$$K_I = \sigma\sqrt{\pi a} \qquad (3.9)$$

Once the stress intensity factor for a given test sample is known, it is then possible to determine the maximum stress intensity factor that would cause failure (crack

propagation). This critical value K_{IC} is described in the literature as the fracture toughness, Γ, of the material. The fracture toughness is one of the materials properties, and interacts with the design stress and crack size to control the conditions for fracture in a component. For the example of a central crack in an infinite body subjected to a uniform stress, the fracture toughness, Γ, is

$$\Gamma = K_{IC} = \sigma_f \sqrt{\pi a} \tag{3.10}$$

where σ_f is the fracture stress of the material.

3.1.3 Energy release rate

The strain energy stored per volume of material, U, for a general three-dimensional loading system can be expressed by the stress components as

$$U = \frac{1}{2E}[\sigma_x^2 + \sigma_y^2 + \sigma_z^2 - 2\nu(\sigma_x\sigma_y + \sigma_y\sigma_z + \sigma_z\sigma_x) + 2(1+\nu)(\tau_{xy}^2 + \tau_{yz}^2 + \tau_{zx}^2)]. \tag{3.11}$$

Crack instability is associated with the stationary value of the strain energy curve. Beyond this stationary value the energy release during an incremental crack extension exceeds the energy required to create new crack surfaces. The energy release rate, G, is defined by Irwins (1957) as

$$G = \frac{\partial U}{\partial a}. \tag{3.12}$$

G is also termed as the crack driving force. G can be interpreted as the energy required for crack extending one unit length, and includes all energy dissipation in the material such as crack surface energy and plastic work. If the fracture occurs via mode I, then G is expressed as G_I, and similarly G_{II} and G_{III} for the other modes.

It was demonstrated in fracture mechanics literature (e.g. Hutchinson and Suo, 1992) that the relationship between stress intensity factor and energy release rate can be generalized as

$$G = \begin{cases} \dfrac{K_I^2 + K_{II}^2}{E} & \text{if plane stress,} \\ \dfrac{K_I^2 + K_{II}^2}{E}(1-\nu^2) & \text{if plane strain.} \end{cases} \tag{3.13}$$

Similar to the critical stress intensity factor, the critical energy release rate, G_c, is described in literature as the fracture toughness of the material such as

$$\Gamma = G_c . \tag{3.14}$$

3.2 Interfacial crack in bimaterial system

Bimaterial system, which consists of two type of materials, are shown in Figure 3-3 with material 1 above the interface and material 2 below. Some results for anisotropic materials can be found in the review by Hutchinson and Suo (1992), this part will focus on plane problem for isotropic materials. Let μ_j, E_j and ν_j be the shear modulus, Young's modulus, Poisson's ratio of the respective materials.

3.2.1 Dundurs parameters

Dundurs (1969) has observed that a wide class of elastic plane problems for bimaterial depends on only two (rather than three) nondimensional combinations of the elastic moduli. With the convention set in Figure 3-2, the Dundurs' elastic mismatch parameters are

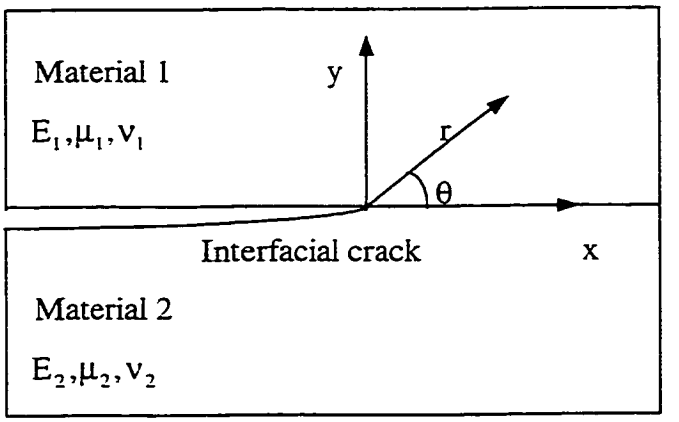

Figure 3-3 Interfacial crack illustration.

$$\alpha = \frac{\mu_1(\kappa_2+1)-\mu_2(\kappa_1+1)}{\mu_1(\kappa_2+1)+\mu_2(\kappa_1+1)} \text{ and } \beta = \frac{\mu_1(\kappa_2-1)-\mu_2(\kappa_1-1)}{\mu_1(\kappa_2+1)+\mu_2(\kappa_1+1)}. \tag{3.15}$$

Here,

$$\kappa_j = \begin{cases} \dfrac{3-\nu_j}{1+\nu_j} & \text{if plane stress,} \\ & \qquad (j=1,2) \\ 3-4\nu_j & \text{if plane strain.} \end{cases} \tag{3.16}$$

A more revealing expression for α is

$$\alpha = (\overline{E}_1 - \overline{E}_2)/(\overline{E}_1 + \overline{E}_2) \tag{3.17}$$

where $\overline{E}_j = E_j/(1-\nu_j^2)$ in plane strain and $\overline{E}_j = E_j$ in plane stress. Thus, α measures the mismatch in the plane tensile modulus across the interface. It approaches +1 when material 1 is extremely stiff compared to material 2, and approaches -1 when material 1 is extremely compliant. When $\nu_1 = \nu_2$, α is the same in plane strain and plane stress.

The parameter β is a measure of the mismatch in the in-plane bulk modulus. In plane strain,

$$\beta = \frac{1}{2}\frac{\mu_1(1-2\nu_2)-\mu_2(1-2\nu_1)}{\mu_1(1-\nu_2)+\mu_2(1-\nu_1)}. \tag{3.18}$$

Thus, in plane strain, β vanishes when both materials are incompressible ($\nu_1 = \nu_2 = 1/2$), and $\beta = \alpha/4$ when $\nu_1 = \nu_2 = 1/3$. In plane stress, $\beta = \alpha/3$ when $\nu_1 = \nu_2 = 1/3$.

Both α and β vanish when there is no mismatch, and both change signs when the materials are switched. To describe the singularity around crack tip (see section 3.1.2), another index ε is defined as

$$\varepsilon = \frac{1}{2\pi} \ln\left(\frac{1-\beta}{1+\beta}\right). \tag{3.19}$$

In plane strain, the physical admissible values of α and β are restricted to lie within a parallelogram enclosed by $\alpha = \pm 1$ and $\alpha - 4\beta = \pm 1$ in the (α, β) plane (see Figure 3-4), by requiring $0 < \nu < 1/2$ and $\mu > 0$. The range of α and β in plane stress in somewhat more restricted.

Table 3-1 Dundurs parameters and the oscillatory index

Bimaterial (material 1 / material 2)	α	β	ε
Al / Sapphire	-0.69	-0.143	0.046
Au / Sapphire	-0.62	-0.053	0.17
Cu / Sapphire	-0.47	-0.096	0.031
Nb / Sapphire	-0.55	-0.056	0.018
Ni / Sapphire	-0.26	-0.063	0.020
Fe / Sapphire	-0.30	-0.065	0.021
Au / MgO	-0.53	-0.062	0.020
Ni / MgO	-0.13	-0.079	0.025
Cu / Si	-0.04	0.038	-0.012

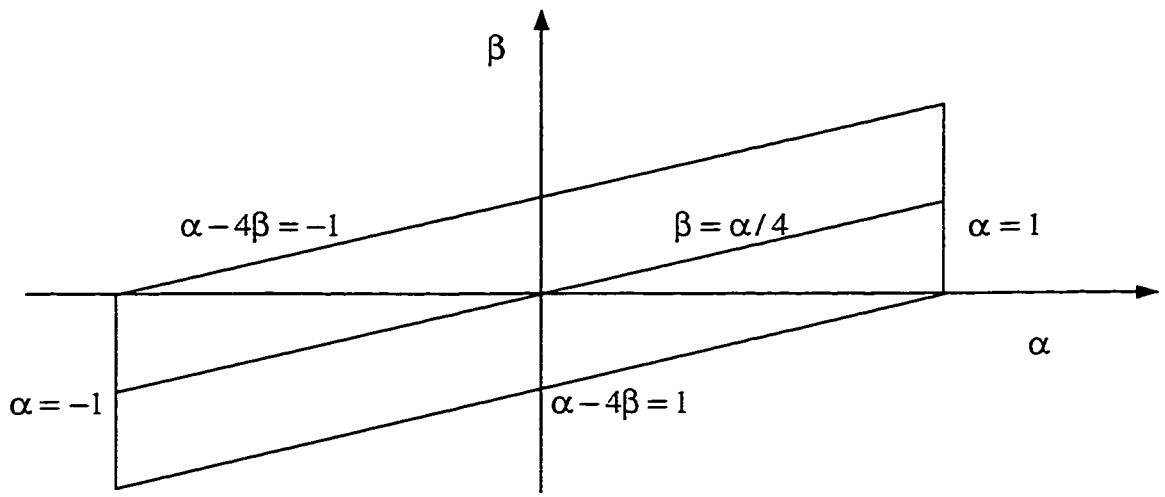

Figure 3-4 Dundurs parameters.

It is demonstrated (Hutchinson and Suo, 1992) that most of the (α, β) combinations fall between $\beta = 0$ and $\beta = \alpha/4$. Some example values are listed in Table 3-1. Note that α, β and ε reverse sign when material 1 and 2 are interchanged.

Combinations that satisfy $\beta = 0$ give rise to simpler crack tip fields than combinations with $\beta \neq 0$, and special attention will be paid to this restricted family of materials in Chapter 5 and Chapter 6.

3.2.2 Interfacial crack stress field

Solutions to bimaterial interfacial crack problems were presented in the earlier papers on the subject by Williams (1959), Cherepanov (1962), England (1965), Erdogan (1965), Rice and Sih (1965), and Willis (1971). Here, the notations and definitions of Rice (1988) for the crack tip fields will be adopted since these reduce to the conventional notation when the mismatch vanishes. Coordinate system is set to take the origin at the crack tip, as in Figure 3-5, with the crack flakes lying along the negative x-axis. The dominant stress singularity for any plane problem in which zero tractions are prescribed on the portion of the negative x-axis ending at the origin is of the form

$$\sigma_{mn} = \mathrm{Re}[Kr^{i\varepsilon}](2\pi r)^{-1/2}\Sigma^{I}_{mn}(\theta,\varepsilon) + \mathrm{Im}[Kr^{i\varepsilon}](2\pi r)^{-1/2}\Sigma^{II}_{mn}(\theta,\varepsilon) \quad (m, n = r, \theta) \quad (3.20)$$

where $i = \sqrt{-1}$, r and θ are defined in Figure 3-5, Re denotes real part of a complex and Im refers to the imaginary part of a complex, and ε is the index defined in Equation (3.19). The quantities Σ^{I}_{mn} and Σ^{II}_{mn} are given by Rice et al. (1990) as follows,

$$\Sigma^{I}_{rr} = -\frac{\sinh \varepsilon(\pi-\theta)}{\cosh \pi\varepsilon}\cos\frac{3\theta}{2} + \frac{e^{-\varepsilon(\pi-\theta)}}{\cosh \pi\varepsilon}\cos\frac{\theta}{2}\left(1+\sin^2\frac{\theta}{2}+\varepsilon\sin\theta\right),$$

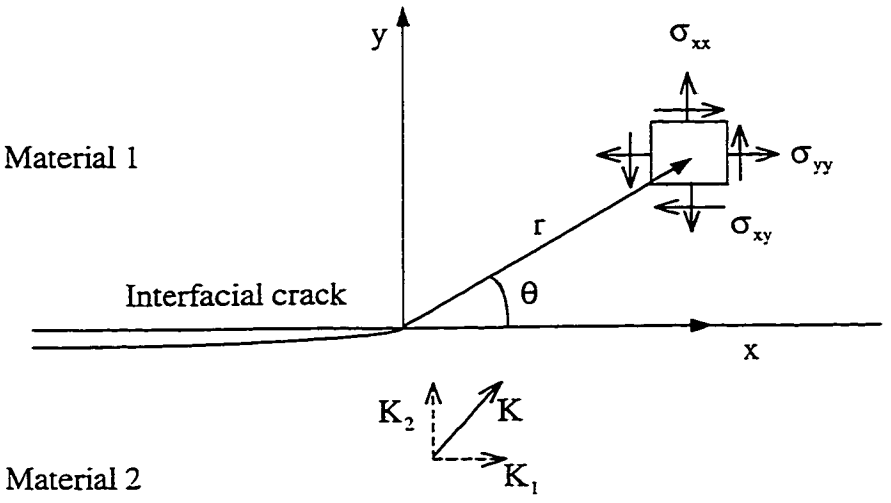

Figure 3-5 Stress distribution and interface stress intensity factor.

$$\Sigma^{I}_{\theta\theta} = \frac{\sinh\varepsilon(\pi-\theta)}{\cosh\pi\varepsilon}\cos\frac{3\theta}{2} + \frac{e^{-\varepsilon(\pi-\theta)}}{\cosh\pi\varepsilon}\cos\frac{\theta}{2}(\cos^2\frac{\theta}{2} - \varepsilon\sin\theta),$$

$$\Sigma^{I}_{r\theta} = \frac{\sinh\varepsilon(\pi-\theta)}{\cosh\pi\varepsilon}\sin\frac{3\theta}{2} + \frac{e^{-\varepsilon(\pi-\theta)}}{\cosh\pi\varepsilon}\sin\frac{\theta}{2}(\cos^2\frac{\theta}{2} - \varepsilon\sin\theta),$$

$$\Sigma^{II}_{rr} = \frac{\cosh\varepsilon(\pi-\theta)}{\cosh\pi\varepsilon}\sin\frac{3\theta}{2} - \frac{e^{-\varepsilon(\pi-\theta)}}{\cosh\pi\varepsilon}\sin\frac{\theta}{2}(1+\cos^2\frac{\theta}{2} - \varepsilon\sin\theta),$$

$$\Sigma^{II}_{r\theta} = -\frac{\cosh\varepsilon(\pi-\theta)}{\cosh\pi\varepsilon}\sin\frac{3\theta}{2} - \frac{e^{-\varepsilon(\pi-\theta)}}{\cosh\pi\varepsilon}\sin\frac{\theta}{2}(\sin^2\frac{\theta}{2} + \varepsilon\sin\theta),$$

$$\Sigma^{II}_{\theta\theta} = \frac{\cosh\varepsilon(\pi-\theta)}{\cosh\pi\varepsilon}\cos\frac{3\theta}{2} + \frac{e^{-\varepsilon(\pi-\theta)}}{\cosh\pi\varepsilon}\cos\frac{\theta}{2}(\sin^2\frac{\theta}{2} + \varepsilon\sin\theta), \qquad (3.21)$$

and $\Sigma_{zr} = \Sigma_{z\theta} = 0$, $\Sigma_{zz} = v(\Sigma_{rr} + \Sigma_{\theta\theta})$.

In Equation (3.20), $K = K_1 + iK_2$, the complex interface stress intensity factor, has real and imaginary parts K_1 and K_2, respectively, which play similar roles to the conventional mode I and mode II intensity factors in isotropic solids. It is noted here that throughout this dissertation, subscripts I and II to K indicate in homogeneous medium, and subscripts 1 and 2 to K refer to interfacial crack problem involving two types of material. Superscript ∞ to K refers to far field loading or boundary condition.

Generally, the singular fields are normalized so that the traction on the interface directly ahead of the tip are given by

$$\sigma_{yy} + i\sigma_{xy} = (K_1 + iK_2)(2\pi r)^{-1/2} r^{i\varepsilon} \qquad (3.22)$$

or

$$\sigma_{yy} = \mathrm{Re}[Kr^{i\varepsilon}](2\pi r)^{-1/2}, \quad \sigma_{xy} = \mathrm{Im}[Kr^{i\varepsilon}](2\pi r)^{-1/2} \qquad (3.23)$$

where $r^{i\varepsilon} = \cos(\varepsilon \ln r) + i\sin(\varepsilon \ln r)$. The associated crack flank displacements at distance

r behind the crack tip, $\delta_i = u_i(r,\theta=\pi) - u_i(r,\theta=-\pi)$, are given by

$$\delta_y + i\delta_x = \frac{8}{(1+2i\varepsilon)\cosh(\pi\varepsilon)} \frac{(K_1 + iK_2)}{E_*} \left(\frac{r}{2\pi}\right)^{1/2} r^{i\varepsilon} \tag{3.24}$$

where

$$\frac{1}{E_*} = \frac{1}{2}\left(\frac{1}{\bar{E}_1} + \frac{1}{\bar{E}_2}\right) \tag{3.25}$$

Compared to the $r^{-\frac{1}{2}}$ singularity of the stress field in homogeneous material (see Equation (3.7)), Equation (3.22) indicates that the stress filed for interfacial crack is $r^{-\frac{1}{2}+i\varepsilon}$ singularity. This is the so-called oscillatory singularity in interfacial crack fracture mechanics, which brings in some complications that are not present in elastic fracture mechanics of homogeneous solids. To solve this unrealistic phenomenon, contact zone model was proposed by assuming a contact zone on the interface behind the crack tip (Comninou, 1977a, 1977b and 19977c; Gautesen and Dundurs, 1987; Gautesen and Dundurs, 1988). Rice (1988) readdressed the interfacial crack problem, and indicated that the oscillatory singularity zone is so close the crack tip that the results based on Equation (3.20) are valid to investigate the fracture behavior of the bimaterial system. If $\varepsilon = 0$, which is a reasonable approximation for most materials (see Table 3-1), the singularity of the interfacial stress field is the same as that of the homogeneous material and the oscillatory behavior can be neglected.

3.2.3 Energy release rate

In plane problem, the energy release rate for crack advance on the interface is related

with the interface stress intensity factor as (Malyshev and Salganik, 1965)

$$G = \frac{(1-\beta^2)}{E_*}|K|^2 = \frac{(1-\beta^2)}{E_*}(K_1^2 + K_2^2) \tag{3.26}$$

where β is one of the Dundurs parameters defined in Equation (3.15). Consider the relationship between β and ε, $1-\beta^2 = 1/\cosh^2(\pi\varepsilon)$, G can be expressed by ε as

$$G = \frac{(K_1^2 + K_2^2)}{E_* \cosh^2(\pi\varepsilon)}. \tag{3.27}$$

3.2.4 Mode mixity and Interfacial crack toughness

In isotropic solids, pure loading mode results in pure stress distribution on the plane ahead crack tip. For example, a central crack with length of 2a in an infinite body subject to a uniform stress σ_{yy}^{∞}, stress intensity factors are

$$K_I = \sigma_{yy}^{\infty}\sqrt{\pi a} \quad \text{and} \quad K_{II} = 0. \tag{3.28}$$

The stress field ahead crack tip can be derived from Equation (3.7) by setting $\theta = 0$

$$\sigma_{yy} = \frac{K_I}{\sqrt{2\pi r}} = \sigma_{yy}^{\infty}\sqrt{\frac{a}{2r}}, \quad \sigma_{xy} = 0. \tag{3.29}$$

On the other hand, the interfacial crack is not free to evolve with pure mode stressing at its tip. If a central crack with length of 2a lying on the interface between two semi-infinity media under uniform stress σ_{yy}^{∞}, the interface stress intensity factor is

$$K = K_1 + iK_2 = \sigma_{yy}^{\infty}(1+2i\varepsilon)(\pi a)^{1/2}(2a)^{-i\varepsilon} \tag{3.30}$$

and the stress filed ahead the interfacial crack is expressed in Equation (3.22). It can be seen that shear stress σ_{xy} is involved into the bimaterial system and mode II stress

intensity factor is presented at the interfacial crack tip. In interfacial crack fracture mechanics, mode mixity is defined as the term to describe the relative amount of mode II to mode I at crack tip and measured by the phase angle Ψ,

$$\tan \Psi = \frac{K_2}{K_1}. \tag{3.31}$$

In this dissertation, Ψ^{∞} is used for far field load with $K^{\infty} = K_I^{\infty} + iK_{II}^{\infty}$,

$$\tan \psi^{\infty} = \frac{K_I^{\infty}}{K_{II}^{\infty}}, \tag{3.32}$$

and Ψ^{tip} for interface crack tip with $K = K_1 + iK_2$,

$$\tan \psi^{tip} = \frac{K_2}{K_1}. \tag{3.33}$$

Similarly to homogeneous material, both the crack interface stress intensity factor for interfacial crack propagation, K_C, and the critical energy release rate, G_C, are used to measure the fracture toughness for interfacial crack. But the interface fracture toughness is not a single material parameter (as it would be in homogeneous solid), rather it is a function of the mode mixity. The fracture toughness of the interface is generalized as

$$G_C = \Gamma(\Psi^{\infty}) = \Gamma(\Psi^{tip}), \tag{3.34}$$

and can be interpreted as an effective surface energy that depends on the mode of loading. The above relationship is also assumed to hold for quasi-static crack advance when crack growth resistance effects can be disregarded.

Although there are lots of methods to measure the fracture toughness in homogeneous material, the progress in interfacial crack is not advanced. Efforts to measure interfacial toughness under mixed mode conditions go back some years (e.g.

Trantian, 1972; Anderson et al., 1974), as reviewed by Liechti and Hanson (1988). Parallel efforts have also been underway to develop mixed mode fracture specimens designed to measure the delamination toughness associated with ply separation in polymermatrix composites (e.g. Kinloch, 1987). A series of recent experiments (Cao and Evans, 1989; Wang and Suo, 1990; Liechti and Chai, 1992) have focused on the interface between epoxy and glasses, metals and plastics. Thouless (1990) has carried out mixed mode toughness experiments for crack propagation in the interface between a brittle wax and glass.

An overview of various mechanisms responsible for the strong dependence of interfacial toughness on mode mixity was given by Evans et al. (1990). Two primary mechanisms are asperity contact and plasticity. Asperity on the fracture surfaces will tend to make contact for some distance behind the tip when mode II is presented along with mode I. A micromechanics model of shielding of the tip due to asperity interaction was presented by Evans and Hutchinson (1989), which led to a prediction of $\Gamma(\Psi^{\infty})$ in terms of a nondimensional measure of fracture surface roughness.

The role of plasticity on the interface fracture toughness has been widely investigated (Evans et al, 1990; Shih, 1991; Zywicz and Parks, 1992; Liang and Liechti, 1995). Shih and Asaro (1988) demonstrated that the nature of crack tip plasticity depending on Ψ^{∞}, by observing that the plastic zone in plane strain increases in size as $|\Psi^{\infty}|$ increase with G fixed. When an interface between a bimaterial system is actually a very thin layer of a third phase, the details of the cracking morphology in the thin interface layer can also play a role in determining the mixed mode toughness. Tvergaard and Hutchinson (1993, 1994 and

1996) used a stress-displacement relationship at the interfacial crack tip to investigate the effect of plasticity on the interfacial fracture toughness.

3.3 Result for layered materials with interfacial crack

Several elasticity solutions for mixed mode cracks in multilayers were obtained in recent years by analytical and numerical methods, and have been used to calibrate fracture specimens and assess technically representative structures (Hutchinson and Suo, 1992). One example, which is related to the topics that I will address in this dissertation, is cited here in details.

Suo and Hutchinson (1989) analyzed a sandwich sample as illustrated in Figure 3-6. The discussion was restricted to brittle systems for which any inelastic behavior occurs on a scale that is small compared with the layer thickness h. The layer thickness is assumed to be very small compared with the in-plane dimensions of the joint or of the sandwich specimen. At the macroscopic level, the tip of a crack along the joint or layer is characterized by macroscopic, or applied stress intensity factors K_I^∞ and K_{II}^∞ which are determined from a standard analysis that ignored the existence of the thin layer.

Employing energy conservation principle proposed by Rice (1968), the global energy release rate, G^∞, and local energy release rate at interface crack tip, G, are the same:

$$G = \frac{1}{\bar{E}_1}[(K_I^\infty)^2 + (K_{II}^\infty)^2] = \frac{1-\beta^2}{E_*}|K|^2 . \tag{3.35}$$

This relationship gives

$$K = h^{-i\varepsilon}\left(\frac{1-\alpha}{1-\beta^2}\right)^{1/2}(K_I^\infty + iK_{II}^\infty)e^{i\omega}, \tag{3.36}$$

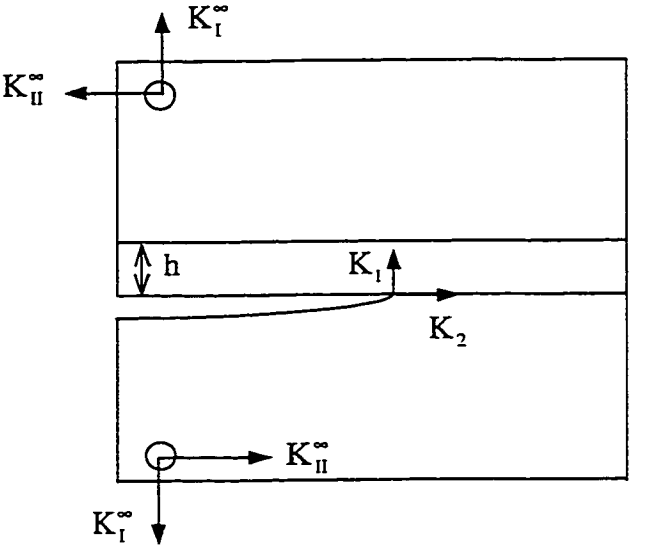

Figure 3-6 Layered material with interfacial crack.

where α and β are defined in Equation (3.15). From numerical calculations (Suo and Hutchinson, 1989), the angle shift ω, which is due exclusively to the moduli dissimilarity, ranges between $5°$ to $-15°$, depending on α and β.

The fracture toughness of the joint as determined in a test is identified with the critical value of the overall energy release rate at crack advance according to

$$\Gamma(\Psi^{\infty}) = G_c^{\infty} \tag{3.37}$$

where $\Psi^{\infty} = \tan^{-1}(K_{II}^{\infty} / K_I^{\infty})$.

Chapter 4

Fundamentals of Edge Dislocation Theory

Dislocation theory is a branch of solid state physics that relates the plastic properties of crystals to atomic structure (Taylor, 1934; Orowan, 1934; Polanyi, 1934; Koehler, 1941; Cottrel, 1964; Kovacs and Zsoldos, 1973). Although it is mainly concerned with mechanical properties, dislocation theory contributes to the understanding of other properties of solids; e.g. chemical properties such as crystal growth, surface catalysis, diffusion and chemical reactions in crystals; and physical properties such as carrier lifetimes in semi-conductors, magnetic coercetivity and dielectric breakdown. Instead of working with real laws of interatomic force, derived from quantum mechanics, some ideal models of crystals in which the forces are represented by simple analytic formulae are widely used (Cottrel, 1964; Hull, 1975; Nabarro, 1979; Hirth and Lothe, 1982). Therefore, the strain field of a dislocation has a long range, and so can be discussed rigorously from simple elasticity theory. Several of the important properties of dislocations, e.g. self-energy, long-range interactions, can thus be deduced reliably.

Dislocation theory has also been related to the fracture behaviours of materials (Lardner, 1974; Comninou, 1977b; Chang and Ohr, 1981). This dissertation is to investigate the fracture behaviour of layered materials by employing the dislocation theory.

In this chapter, the edge dislocation theory is reviewed. After some fundamentals about dislocation theory are introduced, the focus is put on the interactions between crack and dislocation: the effect of crack on dislocation is investigated by analyzing the force on

dislocation; the effect of dislocation on crack is examined by analyzing the changes of stress intensity factor at crack tip.

4.1 Plastic flow and dislocations

4.1.1 Plastic flow in crystals

When single crystals of many materials are stressed above their yield strength they are often observed to undergo plastic deformation which is concentrated as slip on a few parallel planes (Figure 4-1). The planes on which the deformation occurs are called slip-planes. When a group of slip-planes become active within the same neighbourhood of the crystal, they are often said of form a slip-band. The slip-planes are usually crystal planes on which the atoms are closest packed (e.g. {111} plane in face centered cubic crystal and {110} in body centered cubic crystal), regardless of the orientation of the applied stress. Furthermore, the direction of slip within the slip-plane is always crystallographic, no matter what the direction of the shear stress on the slip plane. In the plastic deformation of a polycrystal, each grain behaves as a separate single crystal, slipping on one or more sets of crystal planes, but with the additional constraint that the slip displacements in adjacent grains have to be continuous across the grain boundary between them. Thus, in detail, the plastic flow of polycrystal is considerable more complicated than that of single crystals, although basically it is the same process.

The elementary slip process is illustrated in Figure 4-2 for a simple cubic crystal, where intersections of pairs of line represent atoms. The two halves of the crystal slide relative to one another on the plane SS' (slip plane). In this simplest process the amount of

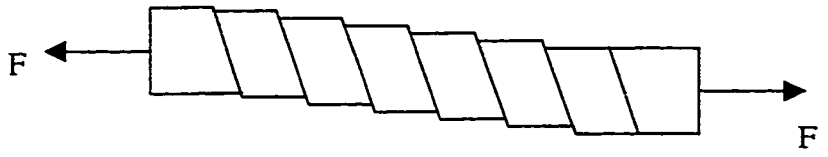

Figure 4-1 Plastic deformation of single crystal under tension.

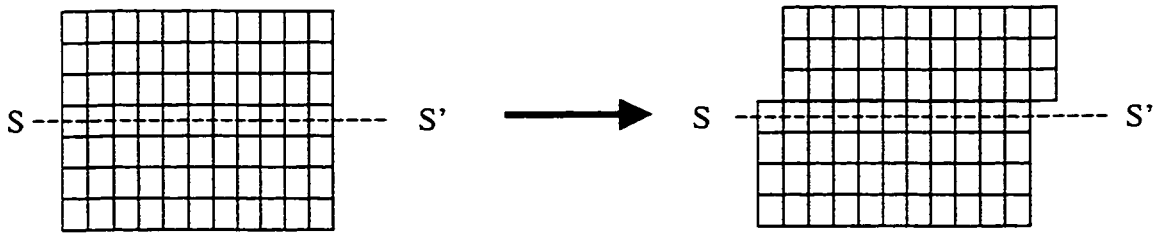

Figure 4-2 Elementary slip process in cubic crystal.

slip is one lattice spacing. In practice, slip can and does occur through many lattice spacings on the same slip plane, leading to visible steps on external surfaces, but such multiple slip corresponds to many repetitions of the above basic process (Lardner, 1974).

The simplest hypothesis for the slip mechanism shown in Figure 4-2 is that slip occurs over the whole plane at once. This process requires that bond breakage across the slip plane occurs simultaneously. But the yield stress based on this model is several orders of magnitude higher than the experimental values of yield stress of the crystal. This discrepancy was not explained until the dislocation theory was established.

4.1.2 Dislocations in crystal

A dislocation is a lattice line defect that defines the boundary between slipped and unslipped portions of the crystal (Hertzberg, 1996). Two basically different dislocations can be identified: edge dislocation and screw dislocation.

The edge dislocation, shown in Figure 4-3, was proposed by Taylor (1934), Orowan (1934) and Polanyi (1934) to explain the discrepancy between the theoretical yield stress and experimental value, as discussed above. The edge dislocation is defined by the edge of the extra half plane of atoms. This extra half plane wedged into the top half of the crystal. As a result, the upper part of the crystal is compressed, while the region below the dislocation experiences dilatation. Note the symbol $\perp$ is used to denote the edge dislocation. The horizontal line denotes the slip plane and the vertical line denotes the extra half plane. Burgers (1939) advanced the description of the screw dislocation shown in Figure 4-4. The screw dislocation is generated by displacement of one part of the crystal

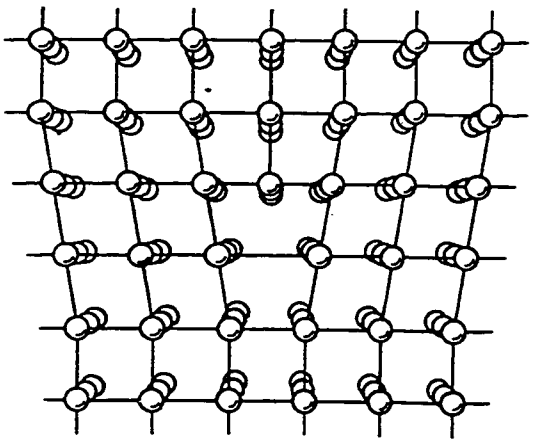

Figure 4-3 An edge dislocation in a simple cubic crystal.

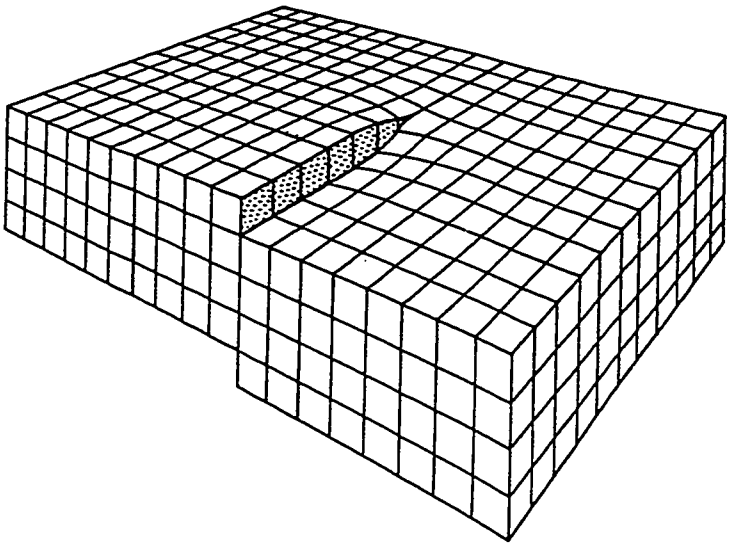

Figure 4-4 A screw dislocation in a simple cubic crystal.

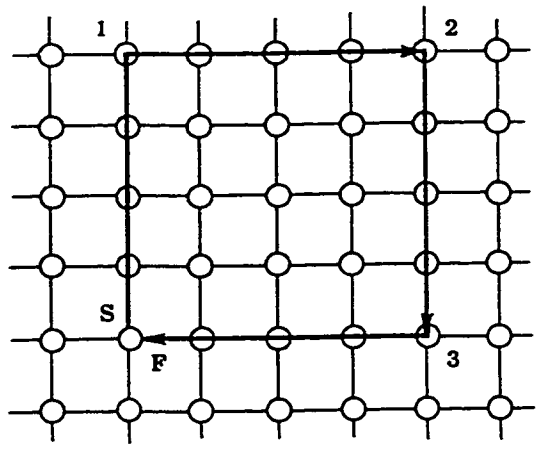

(a)

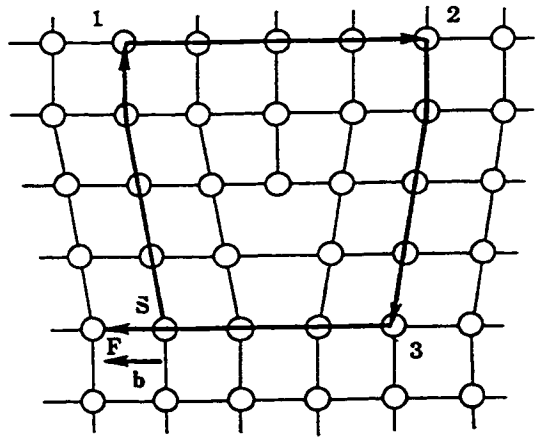

(b)

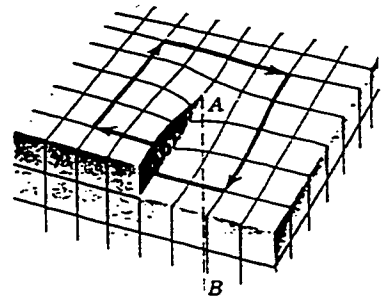

(c)

Figure 4-5 Burgers circuits. (a) In a perfect reference crystal, (b) in a real crystal with edge dislocation and (c) in a real crystal with screw dislocation.

relative to the other.

In dislocation theory, Burgers circuit is used to describe the movement of a dislocation. The Burgers circuit is a series of atom-to-atom steps along lattice vectors that generated a closed loop about any location in the lattice. In a perfect lattice, the Burgers circuit beginning at S and progressing an equal and opposite number of lattice vectors in the horizontal and vertical directions will return to its starting position. When this occurs, the lattice constrained within the circuit is considered perfect (Figure 4-5(a)). When an edge dislocation is present in the lattice, the circuit does not close (Figure 4-5(b). The vector needed to close the Burgers circuit (SF) is called the Burgers vector $\bar{\mathbf{b}}$ of the dislocation and represents both the magnitude and direction of slip of the dislocation. The Burgers circuit and Burgers vector for screw dislocation are shown in Figure 4-5(c). It should be noted that the orientation of $\bar{\mathbf{b}}$ with respect to the dislocation line is different for two types of dislocations. For the edge dislocation, $\bar{\mathbf{b}}$ is oriented normal to the line defect (the extra half plane). For the screw dislocation, $\bar{\mathbf{b}}$ is parallel to the line defect (line AB in Figure 4-5(c)).

4.1.3 Explanation of plastic flow in crystal

Using the dislocation movement model shown in Figure 4-6, the lower yield stress of material can be explained. As the dislocation line moves through the crystal, bond breakage across the slip plane occurs consecutively rather than simultaneously as was necessary in the perfect lattice. The end result of the movement of the dislocation is the same as shown in Figure 4-2: the upper half of the cubic has been translated relative to the

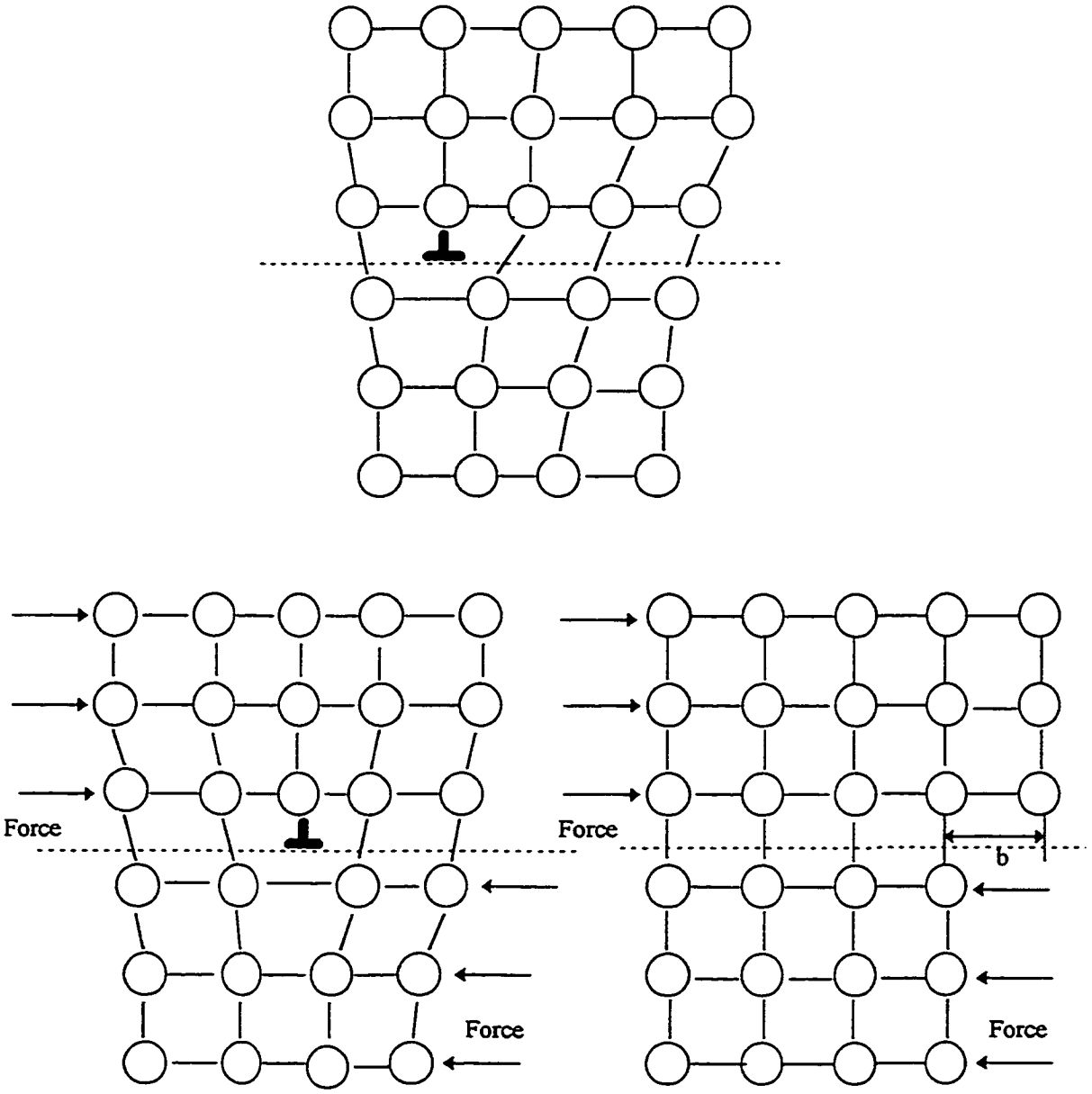

Figure 4-6 Edge dislocation movement in crystal.

bottom half by an amount equal to the magnitude of the Burgers vector $\bar{\mathbf{b}}$. The major difference is the fact that it takes much less energy to break one bond at a time than all the bonds at once. So, one may reconcile the large errors between theoretical and experimental yield stresses by considering the presence of dislocations in the crystals that were examined. In practice, dislocation has been observed in materials by various experimental methods and is the internal defect of the material (Doner et al., 1974; Hirth and Lothe, 1982). The plastic behaviour of crystal is due to the movement of the dislocations within the crystal.

4.2 Elastic behaviour of edge dislocation in a homogeneous isotropic medium

The mathematical work that eventually contributed to dislocation theory was developed earlier than the physical phenomena that led to the discovery of dislocations. To qualitatively address dislocation theory, the approaches developed by Volterra (1907) in treating the elastic behaviour of a cut homogeneous isotropic cylinder is extensively used. For edge dislocation (symbol as $\perp$), the treatment is done by considering a hollow edge dislocation along the axis of a circular cylinder with inner and outer radii r_o and R, respectively (Figure 4-7).

The edge dislocation can be produced from a perfect cylinder by shear displacements in the x direction across the xz glide plane, and has a positive Burges vector $\bar{\mathbf{b}}$. The xz plane is called the slip plane and the x direction is the slip direction of the dislocaiton.

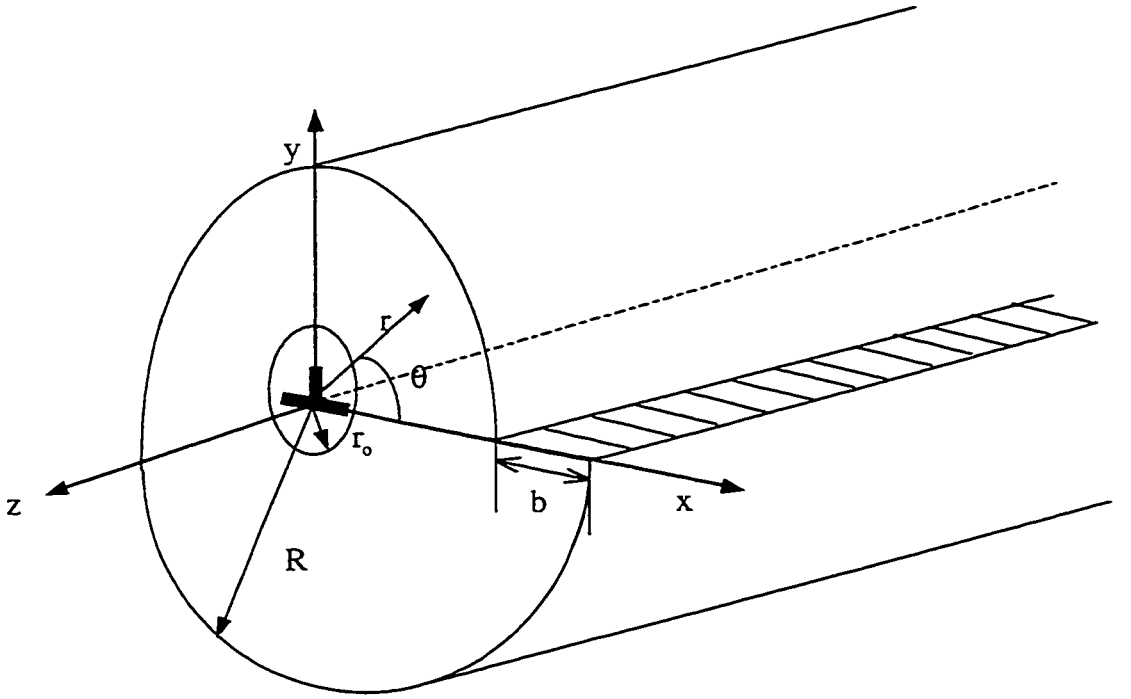

Figure 4-7 An edge dislocation modelling with cylinder.

4.2.1 Elastic field

Classical elastic approach can be used to solve the stresses and strains for the edge dislocation illustrated in Figure 4-7. The material parameters are: μ is the shear modulus, ν is the Poisson's ratio. In plane strain deformation, the only stresses to be determined are the normal stresses σ_{xx}, σ_{yy} (note that $\sigma_{zz} = \nu(\sigma_{xx} + \sigma_{yy})$), and the shear stress σ_{xy}. In polar coordinates r, θ, z, the stresses are σ_{rr}, $\sigma_{\theta\theta}$ and $\sigma_{r\theta}$. The elastic equations for plane deformation are satisfied by any solution of the biharmonic equation

$$\nabla^4 \Omega = 0, \tag{4.1}$$

and Ω is the Airy stress function. The stresses are

$$\sigma_{xx} = \frac{\partial^2 \Omega}{\partial y^2}, \ \sigma_{yy} = \frac{\partial^2 \Omega}{\partial x^2}, \ \sigma_{yy} = -\frac{\partial^2 \Omega}{\partial x \partial y}, \tag{4.2}$$

or

$$\sigma_{rr} = \frac{1}{r}\frac{\partial \Omega}{\partial r} + \frac{1}{r^2}\frac{\partial^2 \Omega}{\partial \theta^2}, \ \sigma_{\theta\theta} = \frac{\partial^2 \Omega}{\partial r^2}, \ \sigma_{r\theta} = -\frac{\partial}{\partial r}\left(\frac{1}{r}\frac{\partial \Omega}{\partial \theta}\right). \tag{4.3}$$

Considering the free-surface boundary conditions of $\sigma_{rr} = \sigma_{r\theta} = 0$ on both $r = r_o$ and $r = R$, and the x direction displacement of b, stresses can be expressed as

$$\sigma_{rr} = \sigma_{\theta\theta} = -D\sin\theta / r, \sigma_{r\theta} = D\cos\theta / r, \tag{4.4}$$

and

$$\sigma_{xx} = -D\frac{y(3x^2 + y^2)}{(x^2 + y^2)^2}, \ \sigma_{yy} = D\frac{y(x^2 - y^2)}{(x^2 + y^2)^2}, \ \sigma_{xy} = D\frac{x(x^2 - y^2)}{(x^2 + y^2)^2}. \tag{4.5}$$

Here $D = \mu b / 2\pi(1-\nu)$ and b is the magnitude of the Burgers vector $\vec{b}$.

4.2.2 Self-energy

The strain energy per unit length of dislocation between two cylindrical surfaces of radius r_o and R about an edge dislocation in an infinite medium is

$$W_o = \int_{r_o}^{R} r dr \int_0^{2\pi} d\theta [\frac{1}{2\mu}\sigma_{xy}^2 + \frac{1}{2E}(\sigma_{xx}^2 + \sigma_{yy}^2 - 2\nu\sigma_{xx}\sigma_{yy} - \sigma_{zz}^2)], \qquad (4.6)$$

and yields

$$W_o = \frac{\mu b^2}{4\pi(1-\nu)} \ln \frac{R}{r_o}. \qquad (4.7)$$

In dislocation terminology, r_0 is defined as the effective core size of dislocation. It can be seen that the energy W_o diverges as $R \to \infty$ or $r_o \to 0$. The divergence with R shows the energy depends on the size of the crystal. In practice, R is a finite value. For the case of one dislocation in a crystal, an approximate choice for R is the shortest distance from the dislocation to the free surface. Because of the logarithmic dependence, the energy is insensitive to the precision of choice of a value of R (Hirth and Lothe, 1982). The divergence with r_o arises from the inadequacy of linear elasticity theory to deal with the severe lattice distortion near the core of the dislocation. Thus the treatment leading to Equation (4.7) is restricted to the matter outside a cylinder of radius $r_o \sim b$, where linear elasticity theory should apply (Hirth and Lothe, 1982). The total energy is obtained by adding an energy term of misfit for the matter inside the core cylinder. For the case of glide dislocations in close-packed structures the core energy is about ~ 0.1 to 0.05 μb^2, thus the core energy can be neglected in practice when it is compared to the total energy calculated by Equation (4.7) by setting $r_o = b$.

4.2.3 Forces on dislocation

Peach and Koehler (1950) analysed the forces exerted on dislocations in homogeneous media. Consider a dislocation line Γ (mixed with edge component and screw component) having a Burgers vector $\bar{\mathbf{b}}$. Let $\mathbf{d}\bar{\mathbf{l}}$ be a line element of the dislocation in the direction shown in Figure 4-2. The dislocation is immersed in a stress field by the tensor $\tilde{\sigma}$

$$\tilde{\sigma} = \begin{pmatrix} \sigma_{xx} & \sigma_{xy} & \sigma_{xz} \\ \sigma_{xy} & \sigma_{yy} & \sigma_{yz} \\ \sigma_{xz} & \sigma_{yz} & \sigma_{zz} \end{pmatrix}. \tag{4.8}$$

The force exerted on the unit length dislocation is

$$\bar{\mathbf{f}} = -\bar{\mathbf{n}} \times (\bar{\mathbf{b}} \cdot \tilde{\sigma}) \tag{4.9}$$

where $\bar{\mathbf{n}}$ is the unit vector and $\mathbf{d}\bar{\mathbf{l}} = \bar{\mathbf{n}}\, dl$.

Taking an edge dislocation with Burgers vector $\bar{\mathbf{b}}$ as an example, if the resolved shear stress on the slip plane is denoted as $\bar{\tau}$ and the angle between these two directions is θ, the magnitude of the force is $\tau b \cos\theta$.

The force on dislocation can also be derived from the work done by Eshelby (1951, 1956), who was the first to associate an energetic force on an elastic defect with a conserved integral of elasto-static field quantities over a surrounding surface (or a contour for two dimensional (2D) fields). His concern was with "any source of internal stress, such as an inclusion or dislocation whose motion translated an incompatible and possible singular field along with its core".

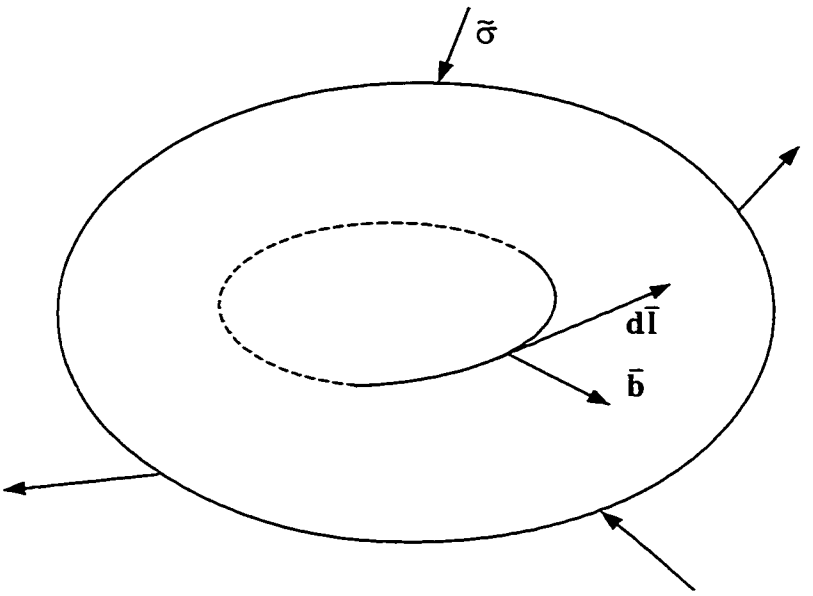

Figure 4-8 Dislocation in infinite homogeneous media.

4.3 Edge dislocation in crack-free bimaterials system

For an edge dislocation embedded in a bimaterial media, forces on edge dislocation include the Peach-Koehler type force due to external load as discussed previously, and the image force due to the bonded interface. Because the Peach-Koehler force can be solved for different boundary conditions by the traditional mechanics approach, we only consider here an edge dislocation in the two bonded semi-infinite plane without external loading as shown in Figure 4-9. Therefore, only the image force will be discussed in this section.

Employing Airy stress function, Head (1953), Dundurs and Sendeckyj (1967) and Dundurs (1969) solved the image force for an edge dislocation with Burgers vector parallel and normal to the bonded interface, respectively. The results are reviewed in following sections. Note that the subscripts 1 and 2 to other symbols are used here for reference to the two regions denoted as two materials in Figure 4-9.

4.3.1 Image force on edge dislocation with Burgers vector normal to interface

The Airy stress functions for a dislocation with Burgers vector b_x (normal to the interface) are (Dundurs, 1969)

$$\Omega_x^{(1)} = -\frac{2\mu_1 b_x}{\pi(\kappa_1+1)(1-\beta^2)}[(1-\beta^2)r_1 \log r_1 \sin\theta_1 + (\beta^2-\alpha)r_2 \log r_2 \sin\theta_2 - (1-\alpha)\beta r_2\theta_2 \cos\theta_2 - (\beta-\alpha)(1+\beta)c(\sin 2\theta_2 - 2c\frac{\sin\theta_2}{r_2})] \tag{4.10}$$

for region 1 and

$$\Omega_x^{(2)} = -\frac{2\mu_1 b_x(1-\alpha)}{\pi(\kappa_1+1)(1-\beta^2)}[r_1 \log r_1 \sin\theta_1 + \beta(r_1\theta_1 \cos\theta_1 + 2c\theta_1)] \tag{4.11}$$

for region 2, where c is the distance from the dislocation to the interface.

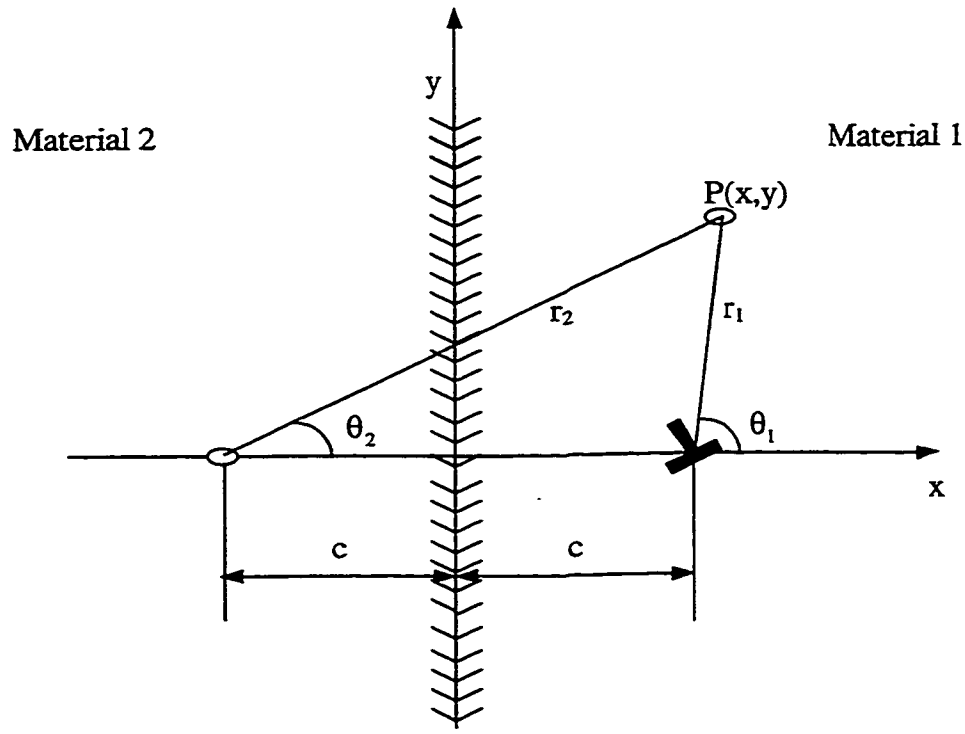

Figure 4-9 Edge dislocation in bimaterial media with bonding interface.

It was indicated that (Dundurs and Sendeckyj, 1967), the force tending to move the dislocation on the slip plane by glide is

$$f_{glide} = b_x(\tau_{xy1})\Big|_{\substack{x=c\\y=0}} \tag{4.12}$$

where τ_{xy1} is the shearing stress in material 1 produced by the image term in Equations (4.10) and (4.11), i.e., terms containing r_2 and θ_2. From Equation (4.2), the stresses are

$$\sigma_{xx1} = 0, \sigma_{yy1} = 0, \tau_{xy1} = -\frac{\mu_1(\beta^2-\alpha)b_x}{\pi(\kappa_1+1)(1-\beta^2)c}. \tag{4.13}$$

and the glide force is

$$f_{glide} = \frac{\mu_1 b_x^2\ (\beta^2-\alpha)}{\pi c(\kappa_1+1)(1-\beta^2)} \tag{4.14}$$

4.3.2 Image force on edge dislocation with Burgers vector parallel to interface

For Burgers vector b_y (parallel to the interface) (Dundurs, 1969)

$$\begin{aligned}\Omega_y^{(1)} = \frac{2\mu_1 b_y}{\pi(1+\kappa_1)(1-\beta^2)}[&(1-\beta^2)r_1\log r_1\cos\theta_1 + (\beta^2-\alpha)r_2\log r_2\sin\theta_2 \\ &+(1-\alpha)\beta r_2\theta_2\sin\theta_2 - (\beta-\alpha)(1+\beta)c(2\log r_2 - \cos 2\theta_2 + 2c\frac{\cos\theta_2}{r_2})]\end{aligned} \tag{4.15}$$

for region 1 and

$$\Omega_y^{(2)} = \frac{2\mu_1 b_y(1-\alpha)}{\pi(\kappa_1+1)(1-\beta^2)}[r_1\log r_1\cos\theta_1 - \beta(r_1\theta_1\sin\theta_1 + 2c\log r_1)] \tag{4.16}$$

for region 2. The stresses in material 1 produced by the image term are

$$\sigma_{xx1} = \frac{\mu_1(\beta^2-\alpha)b_y}{\pi(\kappa_1+1)(1-\beta^2)c}, \sigma_{yy1} = -\frac{\mu_1(\beta^2-\alpha)b_y}{\pi(\kappa_1+1)(1-\beta^2)c}, \tau_{xy1} = 0. \tag{4.17}$$

The forces tending to move the dislocation on the slip plane by glide and climb are

$$f_{glide} = \frac{\mu_1 b_y^2 (\beta^2 - \alpha)}{\pi c(\kappa_1 + 1)(1-\beta^2)},$$
$$f_{climb} = -\frac{\mu_1 b_y^2 (\beta^2 - \alpha)}{\pi c(\kappa_1 + 1)(1-\beta^2)}. \quad (4.18)$$

The above equations show that the forces become very small when c is larger than a critical length scale, which means that the image forces are restricted in a small area near the interface.

4.4 Dislocation in cracked materials system

In cracked materials system, the interaction between crack and dislocation should be considered (see Figure 4-10). Two aspects will be addressed in this section: the effect of crack on dislocation and the effect of dislocation on crack. The former effect is to block dislocation emission or to promote dislocation emission. The latter can be shielding (decreasing stress intensity factor) or anti-shielding (increasing stress intensity factor) effect on crack.

4.4.1 Effect of crack on dislocation

Employing dislocation model, Bilby et al. (1963) firstly defined the plastic zone at a crack tip in homogeneous media by a continuous distribution function of screw dislocations coplannar with the crack. The effect of crack on dislocation is to look at the conditions for dislocation initiation and movement in a cracked component.

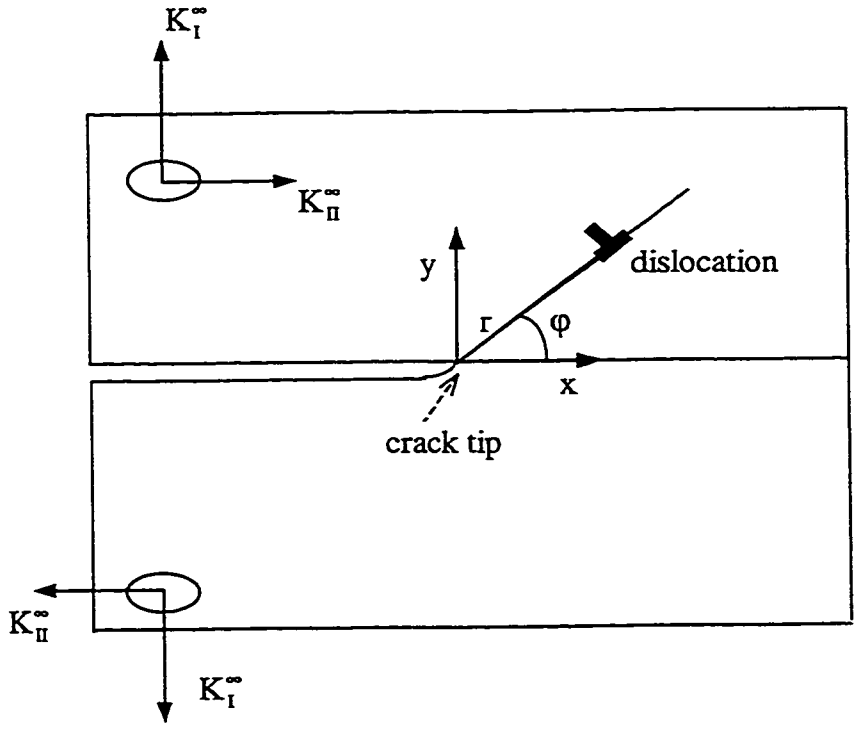

(a)

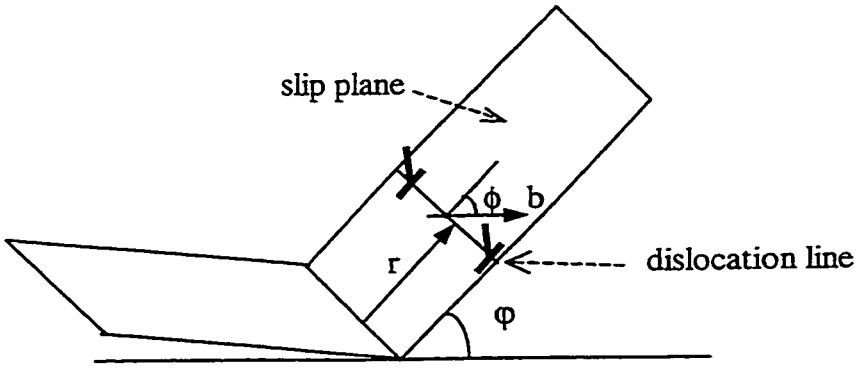

(b)

Figure 4-10 Interaction between crack and dislocation. (a) Illustration of crack and dislocation; (b) Orientation of slip plane and dislocation on slip plane.

Rice and Thomson (1974) and Thomson (1986) analysed the forces on an edge dislocation near a crack tip in homogeneous media. Three parts contribute the total force on the dislocation: force due to the applied load (Peach-Koehler type force), image force due to the crack surface and the ledge force due to the ledge left behind as the dislocation is formed at the crack tip.

Conserved integrals of the Eshelby (1951, 1956) type representing energetic forces on dislocations and cracks were reviewed and related to invariant transformations by Rice (1985). Applications were discussed based on path independence for 2D integrals of J and M type and on the Maxwell reciprocity satisfied by energy forces. Such concepts have been used to get the result for the image force drawing a dislocation to a V-notch tip and to a bicrystal interface, and to develop the full 2D interaction effects between a crack tip and a nearby dislocation in a crystal of general anisotropy.

Employing elastic potential functions, Lin and Thomson (1986) examined the interaction between dislocation and crack in homogeneous solid (Figure 4-11). The effect of crack on dislocation was analyzed by considering the force on dislocation. The total force on dislocation with Burgers vector $\vec{b}$ is

$$f = \frac{\mu b^2}{2(1-\nu)\sqrt{2\pi r}} + b[K_I \vartheta_1(\varphi) + K_{II} \vartheta_2(\varphi)] \tag{4.19}$$

where $\vartheta_1(\varphi) = \frac{1}{2}\sin\varphi\cos\frac{\varphi}{2}$, $\vartheta_2(\varphi) = \cos\frac{3\varphi}{2} + \frac{1}{2}\sin\varphi\sin\frac{\varphi}{2}$ and b is the magnitude of the Burgers vector.

For dislocation in bimaterial system with an interfacial crack, the total force on the dislocation was explicitly expressed by Beltz and Rice (1992) as

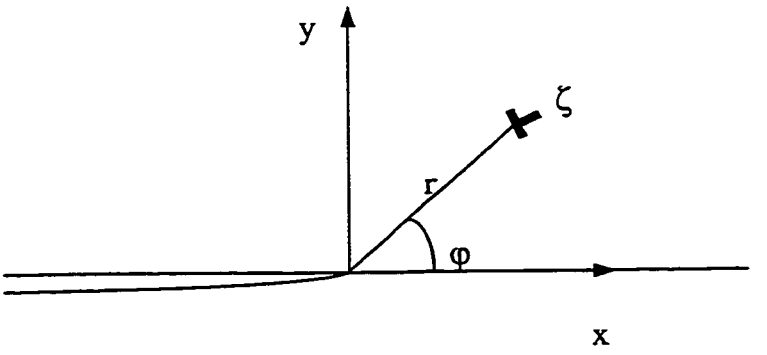

Figure 4-11 Coordinate system for crack and dislocation.

$$f = -\frac{\mu_1 b^2}{4\pi r}\left[\frac{\cos^2\phi}{1-\mu_1} + \sin^2\phi\right] + \frac{b}{\sqrt{r}}\left[\mathrm{Re}(Kr^{i\varepsilon})\Sigma^{I}_{r\varphi} + \mathrm{Im}(Kr^{i\varepsilon})\Sigma^{II}_{r\varphi} + K_{III}\Sigma^{III}_{r\varphi}\right], \qquad (4.20)$$

where μ_1 is the shear modulus of the material in which the dislocation is embedded, K is the interface stress intensity factor, r is the distance from the crack tip, ϕ is the orientation of the Burgers vector in the slip plane (Figure 4-10) and $\Sigma^{j}_{r\varphi}$ ($j = I, II, III$) are angular functions defined in Equation (3.21) by setting $\theta = \varphi$. Re and Im denote the real part and imaginary part of the complex variable, respectively.

4.4.2 Effect of dislocation on crack

The fracture behavior of a crack screened by dislocations has been widely analyzed (Chang and Ohr, 1981; Thomson and Sinclair, 1982; Rice 1985). The effect of dislocation on crack is denoted as the shielding or anti-shielding effect in terms of modify crack tip field by changing stress intensity factor.

In homogeneous solid, the effect of a group of dislocations on crack was examined by Lin and Thomson (1986). For one single dislocation, the effect can be expressed by

$$K = K^{\infty} - k^{D} \qquad (4.21)$$

where K^{∞} ($K^{\infty} = K_I^{\infty} + iK_{II}^{\infty}$) is the far field stress intensity factor of the loaded crack, and $k^{D} = k_I^{D} + ik_{II}^{D}$. k^{D} is the contribution from the dislocation located at ζ ($\overline{\zeta}$ is the complex conjugate) in complex Z plane as

$$k^{D} = \frac{\mu}{2i(1-\nu)}\left\{\frac{b}{\sqrt{2\pi\zeta}} + \frac{b}{\sqrt{2\pi\overline{\zeta}}} + \frac{\pi\overline{b}(\zeta - \overline{\zeta})}{(2\pi\overline{\zeta})^{3/2}}\right\} \qquad (4.22)$$

where μ is the shear modulus, ν the Poission's ratio, b is the magnitude of the Burgers vector with $b = b_1 + ib_2$ and $\bar{b}$ is the conjugate of b. In coordinate system illustrated in Figure 4-11, $\zeta = r\cos\varphi + i\sin\varphi$ and

$$k_I^D = k_{I1}^D \frac{\mu b_1}{\sqrt{2\pi r}} + k_{I2}^D \frac{\mu b_2}{\sqrt{2\pi r}},$$

$$k_{II}^D = k_{21}^D \frac{\mu b_1}{\sqrt{2\pi r}} + k_{22}^D \frac{\mu b_2}{\sqrt{2\pi r}} \tag{4.23}$$

where

$$k_{mn}^D = \frac{1}{1-\nu}\begin{bmatrix} \frac{1}{2}\sin\varphi\cos\frac{3\varphi}{2} & \cos\frac{\varphi}{2} + \frac{1}{2}\sin\varphi\sin\frac{3\varphi}{2} \\ \cos\frac{\varphi}{2} - \frac{1}{2}\sin\varphi\sin\frac{3\varphi}{2} & \frac{1}{2}\sin\varphi\cos\frac{3\varphi}{2} \end{bmatrix} \quad (m, n = 1,2). \tag{4.24}$$

In a bimaterial system with a crack at the interface, the dislocation shielding effect can be deduced from Suo's work (1989). The stress intensity factor, k, contributed by dislocation shielding on the interfacial crack is

$$k = -\sqrt{2\pi}\{(1+\Lambda)\bar{B}(\bar{\zeta})^{\frac{1}{2}-i\varepsilon} + (1+\Pi)[\bar{B}\zeta^{\frac{1}{2}-i\varepsilon} + B(\zeta-\bar{\zeta})(-\frac{1}{2}-i\varepsilon)\zeta^{\frac{3}{2}-i\varepsilon}]\}, \tag{4.25}$$

where $B = \frac{\mu}{\pi i(1+\kappa)} b$ and $\bar{B}$ is the complex conjugate of B. The Burgers vector, $b = b_1 + ib_2$, is located at ζ in the complex Z plane (Figure 4-11). Here, $\kappa = 3-4\nu$ for a plane strain problem and $\kappa = (3-\nu)/(1+\nu)$ for plane stress, where μ and ν are the shear modulus and Poisson's ratio of the material where the dislocation exists. Λ and Π are defined by

$$\Lambda = \frac{\alpha+\beta}{1-\beta} \text{ and } \Pi = \frac{\alpha-\beta}{1+\beta}. \tag{4.26}$$

Here, α, β are Dundurs' parameters. ε is the oscillatory singularity index defined in Equation (3.19).

If $\beta = 0$, then $\varepsilon = 0$, and $\Lambda = \Pi = \alpha$. k can then be simplified as

$$\begin{aligned} k &= -\sqrt{2\pi}\{(1+\alpha)\overline{B}(\overline{\zeta})^{-\frac{1}{2}} + (1+\alpha)[\overline{B}\zeta^{-\frac{1}{2}} + B(\zeta-\overline{\zeta})(-\frac{1}{2})\zeta^{-\frac{3}{2}}]\} \\ &= (1+\alpha)k^0 \end{aligned} \tag{4.27}$$

where

$$k^0 = \begin{Bmatrix} k_1^0 \\ k_2^0 \end{Bmatrix} = \begin{Bmatrix} k_{11}\dfrac{\mu b_1}{\sqrt{2\pi r}} + k_{12}\dfrac{\mu b_2}{\sqrt{2\pi r}} \\ k_{21}\dfrac{\mu b_1}{\sqrt{2\pi r}} + k_{22}\dfrac{\mu b_2}{\sqrt{2\pi r}} \end{Bmatrix} \tag{4.28}$$

and k_{mn} (m, n = 1,2) is defined in Equation (4.24). This confirms that k^0 for dislocation shielding in bimaterial is the same as that in the corresponding homogeneous materials (Lin and Thomson, 1986).

4.4.3 Energy consideration in bimaterial system with dislocation and crack

For a single dislocation in bimaterial in the presence of an interfacial crack, the energy includes the dislocation self-energy, interaction energy between the dislocation and the interfacial crack and the ledge energy due to the new created surface around the crack tip.

For a dislocation located at r along the slip plane from the interface crack tip (see Figure 4-10), it was suggested by Rice and Thomson (1974) that the self energy for a dislocation ahead of a semi-infinite crack is the same as a dislocation near a free surface, and can be evaluated as the work done by dragging the dislocation against its image force along the slip plane from the interface crack tip to the current location r,

$$W_d'(r) = \frac{\mu b^2}{4\pi(1-\nu)} \ln \frac{r}{r_{effective}}, \tag{4.29}$$

where $r_{effective}$ is the effective core radius to initiate a dislocation near the interfacial crack tip. An approximate value of $r_{effective}$ is b, the magnitude of the Burgers vector.

The interaction energy between the dislocation and the interface crack tip is the work done by the resolved crack tip gliding force to drive the dislocation from the interface crack tip to its current location r_i,

$$W'_k(r) = \int_0^r \sigma_{r\varphi} b dr, \tag{4.30}$$

where $\sigma_{r\varphi}$ is the crack tip shear stress for interfacial crack and can be deduced from Equations (3.20) and (3.21). Since, for most materials combinations, β is very small, we take $\beta = 0$ (so $\varepsilon = 0$) as the assumption for the present case. The angular functions $\Sigma^{I}_{r\varphi}$ and $\Sigma^{II}_{r\varphi}$ in Equation (3.21) (setting $\theta = \varphi$) can be simplified such that

$$\sigma_{r\varphi} = \frac{1}{\sqrt{2\pi r}} [K_1 \sin\frac{\varphi}{2}\cos^2\frac{\varphi}{2} + K_2(\cos\frac{3\varphi}{2} + \cos\frac{\varphi}{2}\sin^2\frac{\varphi}{2})], \tag{4.31}$$

where K_1 and K_2 are, respectively, the mode I and mode II components of interface stress intensity factor without dislocation emission, and $K = K_1 + iK_2$. So the interaction energy can be simplified as

$$\begin{aligned} W'_k(r) &= \int_0^r \sigma_{r\varphi} b dr \\ &= -\frac{2b\sqrt{r}}{\sqrt{2\pi}} [K_1 \sin\frac{\varphi}{2}\cos^2\frac{\varphi}{2} + K_2(\cos\frac{3\varphi}{2} + \cos\frac{\varphi}{2}\sin^2\frac{\varphi}{2})]. \end{aligned} \tag{4.32}$$

Due to the dislocation emission, one ledge is left behind at the crack tip, the ledge energy

for this ledge is

$$W'_L = b\gamma\,, \tag{4.33}$$

where γ is the surface energy of the middle layer material.

These energy terms will be used in Chapter 6 to investigate the fracture behavior of metal/ceramic layered materials after some modifications are made.

Chapter 5

Ductile versus Brittle Behavior of Metal/Ceramic Layered Materials

The ductile versus brittle behavior in metal/ceramic layered materials is examined in this chapter in terms of the competition between atomic decohesion and dislocation nucleation at the interfacial crack tip. A model of one metal layer sandwiched between ceramic layers is presented, and a straight line edge dislocation is assumed to emit from the crack tip at the lower interface. Considering the image force due to the upper interface, the total force on the emitted dislocation is obtained, from which the critical energy release rate for dislocation emission, G_{disl}, is expressed as a function of the metal layer thickness. The role of the length scale (thickness) on G_{disl} is analyzed and compared with the previous work done by Rice et al. (1990). The results show that ductile versus brittle behavior is controlled by the metal layer thickness, through the image force from the upper interface and the mode mixity in terms of the atomic phase angle (Rice et al. 1990). When the thickness is larger than a critical value, transition from ductile to brittle is insensitive to the metal layer thickness.

5.1 Introduction

Although some experiments and models are recommended for analyzing the fracture behavior of layered materials from the macroscopic viewpoint (Hutchinson and Suo, 1992), the atomic groundwork on the ductile versus brittle behavior of the layered materials, which will be addressed here in terms of the competition between dislocation

emission from the crack tip and brittle cleavage of the interface crack, has not been accomplished.

Historically, ductile versus brittle behavior of materials has attracted the attention of both researchers and engineers. In a cracked component, if the failure mechanism is due the atomic bond breakage at the crack tip, the behavior of such material is referred to as brittle. On the other hand, due to the stress singularity at crack tip, plasticity is likely produced around the crack tip. If this occurs, the behavior of such material is denoted as ductile. Based on the review in Chapter 4, dislocation is the physical mechanism to induce plasticity in materials. Therefore, the ductile behavior of the material is judged by the condition for dislocation nucleation at the crack tip.

In practice, even though a failure may appear macroscopically to be cracklike, from microscopic standpoint, the cleavage crack tip will be blunt instead of sharp. On the other hand, a crack showing considerable ductility may consist of a sharp underlying cleavage crack surrounded by large numbers of dislocations. Concerning propagation, the crack takes the form of an expanding blunt notch, rounded hole or advances by brittle cleavage. To understand these types of behavior, the mechanism behind the ductile versus brittle behavior should be examined.

One earlier systematic approach to analyze the ductile versus brittle behavior was proposed by Kelly et al. (1967). This approach assumes the cleavage dominance criterion is given as

$$\sigma^{max}/\tau^{max} > \sigma_0/\tau_0 \tag{5.1}$$

where σ^{max} refers to the maximum stress in the tensile direction on the atom bonds at the crack tip, τ^{max} is the maximum shear stress, while σ_0 and τ_0 are the theoretical tensile and shear strength of the bonds between atoms in the material, respectively.

From the energy perspective, Rice and Thomson (1974) treated the ductile versus brittle question by assuming: (a) an atomically sharp crack is postulated; (b) the ductile versus brittle behavior is controlled by the criterion for the spontaneous emission of dislocations from the sharp cleavage crack. The crack is loaded normal to its plane (mode I) so that the Griffith criterion, $G = 2\gamma$ (G is the energy release rate, γ is the true surface energy of the crack plane) can be used to examine the stability of the sharp crack tip against emission of a blunting dislocation in terms of the force equilibrium. The concept of an activation energy (U_{act}), proposed in the three-dimensional analysis, is the work required to nucleate a metastable loop of dislocation from the tip of the crack, thus blunting the crack. If the activation energy is positive, the work required for dislocation nucleation is greater than that needed to form new surfaces via crack advance. If the energy for brittle cleavage is satisfied, the crack tends to advance in a brittle manner. On the other hand, if the activation energy is negative, the crack will blunt via dislocation nucleation before the critical Griffith conditions could be attained at the tip.

An alternative approach was proposed by Manson (1979) to analyze the ductile versus brittle behavior of materials. As the crack is loaded, the stress intensity factor, K, was examined to compare two values: a K corresponding to the Griffith load for a propagating crack, or one corresponding to a load at which dislocation nucleation is possible. The techniques developed by Manson (1979) were used (Wang and Anderson,

1991; Beltz and Wang, 1992) to solve the bicrystal problems in terms of G_{cleave}, the energy release rate for cleavage, and G_{disl}, the energy release rate associated with the emission of a single dislocation on a slip plane emanating from the crack tip. The basic conclusion is illustrated on Figure 5-1. If $G_{disl} < G_{cleave}$, a dislocation is spontaneously emitted, thus blunting the crack tip from further increases in applied loading; if $G_{disl} > G_{cleave}$, the crack propagates in a brittle manner in terms of atomic decohesion.

To avoid the uncertainty due to the effective core size assumption for the emitted dislocation in the above approaches, Rice et al. (1992) and Beltz and Rice (1992) solved the elasticity problem of a traction-free crack, with a Peierls-type stress versus displacement relation being satisfied as a boundary condition along a slip plane ahead of the crack tip.

Recently, Mao and Evans (1997) investigated the influence of blunting on crack growth at oxide/metal interfaces of layered materials in terms of a superdislocation. However, the fundamental work associated with the dislocation nucleation at the crack tip has not been done.

The primary purpose of this chapter is to examine the condition for ductile behavior in layered materials in the presence of an interfacial crack (Li and Mao, 1998a). Because of the fine scale of the layered material, the condition for ductile behavior is that for dislocation nucleation at the crack tip. A dislocation is assumed to exist in the middle layer, and the forces exerted on the dislocation are analyzed. Based on force equilibrium, the critical interface stress intensity factor is obtained. Thus, the critical energy release rate for dislocation emission from the crack tip can be expressed clearly. In layered materials,

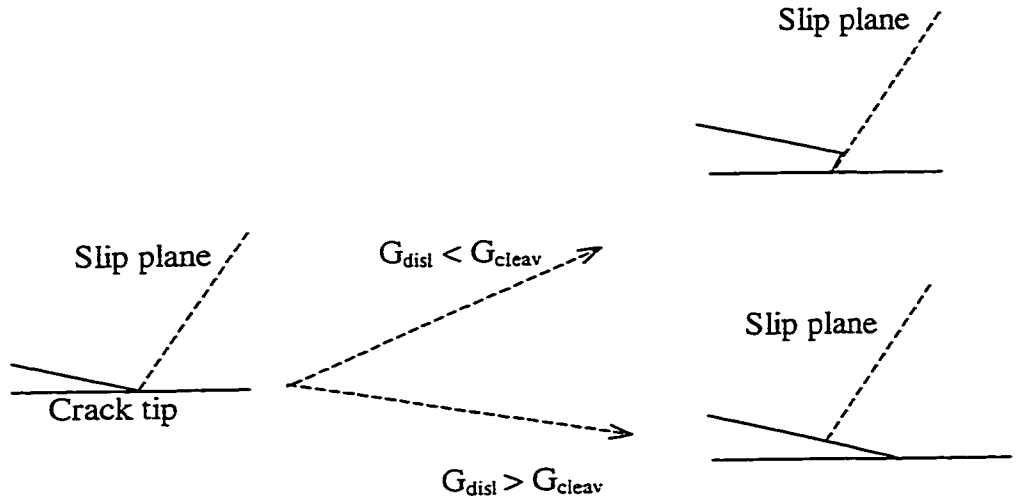

Figure 5-1 Atomic competition between dislocation emission and cleavage decohesion.

the middle layer plays a key role through the image force from the interface and the mode mixity. The effect of the length scale (layer thickness) on G_{disl} is analyzed using a bending sandwich specimen. Some results are compared to the work done by Rice et al. (1990).

5.2 Layered model

A layered model introduced here is shown in Figure 5-2. A thin layer of metal is sandwiched in a homogeneous body of ceramic. Ceramic is taken to be isotropic and no dislocation within it. The plasticity in the metal layer is modeled with dislocations embedding into it. The crack lies at the lower interface coincident with the x-axis with the tip at the origin. A dislocation is emitted from the crack tip on a slip plane which intersects the crack front with angle φ. The asymptotic problem for the semi-infinite interfacial crack will be considered as plane strain or plane stress. The crack tip field of the homogeneous problem (no metal layer and dislocation presenting) is prescribed as the far field which is characterized by the mode I and mode II stress intensity factors, K_I and K_{II}, induced by the loads on the reference homogeneous model. The interfacial crack tip field is characterized by a different set of interface stress intensity factors, $K = K_1 + iK_2$.

5.3 Ductile behavior of layered material

If dislocation can nucleate at the crack tip, the behavior of the layered material is ductile. In this section, the condition for the dislocation nucleation will be investigated by analyzing the force on the dislocation. This force analyzing approach has been used to examine the ductile behaviors of a homogeneous material (Rice and Thomson, 1974) and

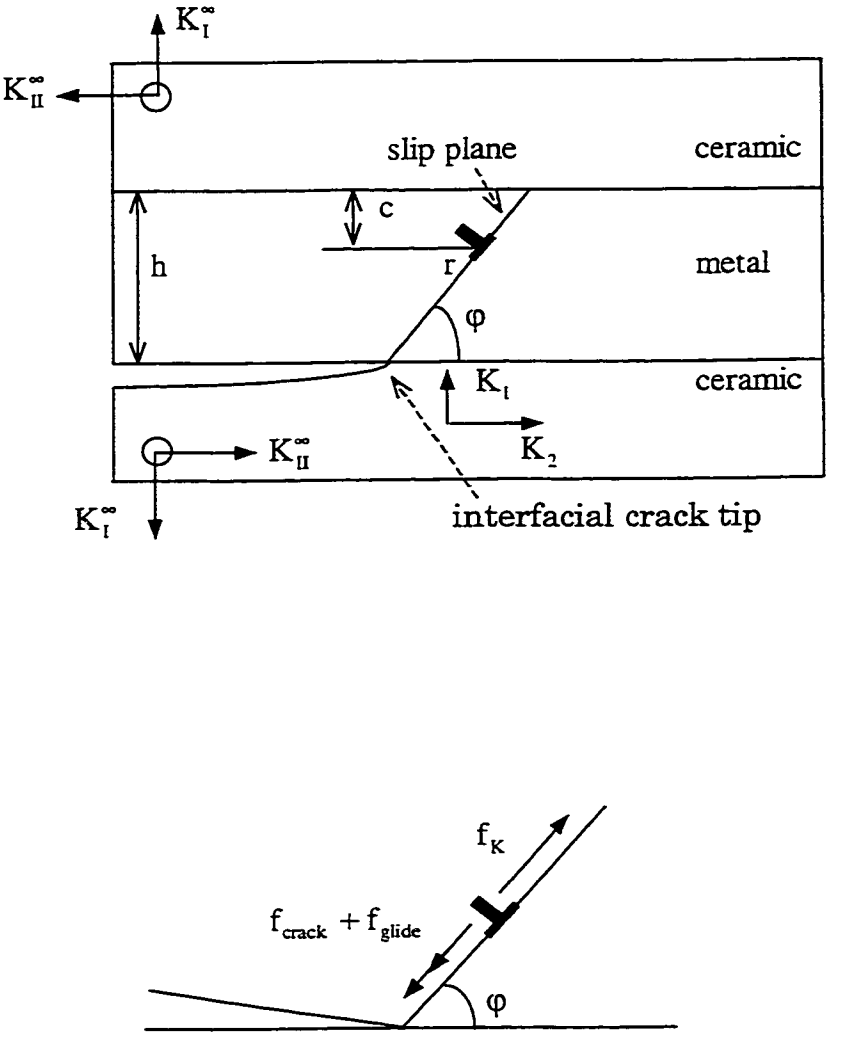

Figure 5-2 Dislocation emission in layered material and forces on dislocation.

bimaterial (Rice et al., 1990).

5.3.1 Force analysis

The forces on the dislocation in the layered model include three components: the force due to the external load, f_K, the image force due to the stress-free crack, f_{crack}, and the image force due to the upper and lower bonded interfaces, f_{glide} (this force makes the dislocation glide on the slip plane). The image forces draw the dislocation back to the crack tip, and the stress due to the external load tends to expel the dislocation away from the crack tip. The equivalent position r_c can be derived from the balance of the total forces. The force due to the external load is straightforward. Although Anderson and Li (1993) proposed a solution for screw dislocation in layered materials (which implied a mode III problem), the image forces for edge dislocation in layered materials by considering both the interface crack and bonded interfaces have not been solved (Hirth, 1998). To qualitatively estimate the effect of the layer thickness, we ignore the couple effect between interface crack and upper interface, and take a simple approach by superimposing two cases directly: the image force due to the interfacial crack without upper interface; and the image force due to the upper bonded interface without interfacial crack, which is modeled as one edge dislocation in two bonded semi-infinite media.

(1) Image force due to the interface crack

The image force due to the interfacial crack in the absence of the upper interface, $f_{crack.}$ was introduced by Rice et al. (1990) and Beltz and Rice (1992), and was summarized

in Chapter 3 as

$$f_{crack} = -\frac{\mu_1 b^2}{4\pi r}\left[\frac{\cos^2\phi}{1-\nu_1} + \sin^2\phi\right] \tag{5.2}$$

where b is the magnitude of the dislocation Burgers vector, ϕ is the angle between the Burgers vector and the direction normal to the dislocation line as shown in Figure 4-10.

(2) Image force due to the upper interface

The image force due to the upper bonded interface is simplified as a plane solution for an edge dislocation near the interface between two isotropic, perfectly bonded semi-infinite bodies, as shown in Figure 4-9. The problems for the dislocation Burgers vectors parallel and normal to the interface have been solved and introduced in Chapter 3. But the general solution for a dislocation with an angle to the interface is not given, and this will be analyzed in detail as follows.

For an edge dislocation with a slip plane angle φ to the interface, its Burgers vector b_e can be expressed as $b_e = b_x + ib_y$ in the coordinate system in Figure 4-9, and the corresponding Airy stress functions are

$$\Omega^{(1)} = \Omega_x^{(1)} + \Omega_y^{(1)} \tag{5.3}$$

for region 1 and

$$\Omega^{(2)} = \Omega_x^{(2)} + \Omega_y^{(2)} \tag{5.4}$$

for region 2. Here Ωs are defined in section 4.2.1. From Equation (4.2), the stresses on the dislocation are

$$\sigma_{xx} = \frac{\mu_1(\beta^2-\alpha)b_y}{\pi(\kappa_1+1)(1-\beta^2)c}, \sigma_{yy} = -\frac{\mu_1(\beta^2-\alpha)b_y}{\pi(\kappa_1+1)(1-\beta^2)c}, \tau_{xy} = -\frac{\mu_1(\beta^2-\alpha)b_x}{\pi(\kappa_1+1)(1-\beta^2)c}. \quad (5.5)$$

Combined with

$$b_y = b_e \cos\varphi, \qquad b_x = -b_e \sin\varphi, \quad (5.6)$$

the resolved shear stress along the slip plane is

$$\begin{aligned}\tau &= -(\cos^2\varphi - \sin^2\varphi)\tau_{xy} + \sin\varphi\cos\varphi(\sigma_{xx}-\sigma_{yy}) \\ &= \frac{\mu_1(\beta^2-\alpha)b_e\sin\varphi}{\pi(\kappa_1+1)(1-\beta^2)c}.\end{aligned} \quad (5.7)$$

The normal stress perpendicular to the slip plane is

$$\begin{aligned}\sigma &= -\tau_{xy}\sin 2\varphi + \sigma_{xx}\sin^2\varphi + \sigma_{yy}\cos^2\varphi \\ &= -\frac{\mu_1(\beta^2-\alpha)b_e\cos\varphi}{\pi(\kappa_1+1)(1-\beta^2)c}.\end{aligned} \quad (5.8)$$

Substituting Equations (5.7) and (5.8) into the Equation (4-12), the glide force for dislocation is

$$f_{glide} = \frac{\mu_1 b_e^2 (\beta^2-\alpha)\sin\varphi}{\pi c(\kappa_1+1)(1-\beta^2)}. \quad (5.9)$$

The above equation shows that the glide force becomes very small when c is larger than a critical value, which indicates that the image force is localized in a small area near the interface. Also, the value of f_{glide} includes the term $\frac{\beta^2-\alpha}{1-\beta^2}$, which means that f_{glide} is controlled by the combination of two different materials. If $\frac{\beta^2-\alpha}{1-\beta^2}<0$, $f_{glide}<0$, which means the force tends to draw the dislocation to the interface; when $\frac{\beta^2-\alpha}{1-\beta^2}>0$,

$f_{glide} > 0$, that is, the dislocation will be expelled away the interface. For general bimaterial system in Figure 4-9 with metal as material 1 and some sample data in Table 3-1, $\alpha < 0$, $\beta << 1$, so $f_{glide} > 0$, the image force will expel the dislocation along the upper interface to the crack in Figure 5-2.

(3) Peach-Koehler force due to external loading

In the layered material, the Peach-Koehler force on the dislocation located in the metal layer is due to the stress around the interfacial crack tip. With the interface stress intensity factor, $K = K_1 + iK_2$, for layered materials defined by Suo and Hutchinson (1989), the shear stress along the slip plane can be obtained from Equation (3.20). The Peach-Koehler force due to the external load is

$$f_K = \frac{b_e}{\sqrt{2\pi r}}[\mathrm{Re}(Kr^{i\varepsilon})\Sigma^{I}_{r\varphi} + \mathrm{Im}(Kr^{i\varepsilon})\Sigma^{II}_{r\varphi}]. \tag{5.10}$$

Here, $\Sigma^{I}_{r\varphi}$ and $\Sigma^{II}_{r\varphi}$ are defined in Equation (3.21) by setting $\theta = \varphi$, Re and Im denote the real part and imaginary part of a complex variable, respectively.

5.3.2 Ductile behavior

The total force on the dislocation emerging from the interfacial crack is composed of a linear combination of the image forces and the Peach-Koehler force. The total force on the emitted dislocation is

$$
\begin{aligned}
f_{total} &= f_{crack} + f_{glide} + f_K \\
&= -\frac{\mu_1 b^2}{4\pi r}\left[\frac{\cos^2\phi}{1-\nu_1} + \sin^2\phi\right] - \frac{\mu_1 b^2(\beta^2-\alpha)\cos^2\phi\sin\varphi}{\pi(\kappa_1+1)(1-\beta^2)(h-r\sin\varphi)} \\
&\quad + \frac{b\cos\phi}{\sqrt{2\pi r}}\left[\mathrm{Re}(Kr^{i\varepsilon})\Sigma^{I}_{r\varphi} + \mathrm{Im}(Kr^{i\varepsilon})\Sigma^{II}_{r\varphi}\right]
\end{aligned}
\tag{5.11}
$$

where $b_e = b\cos\phi$ and $h = c + r\sin\varphi$ are utilized. For a positive b, these forces oppose one another. The net force is illustrated in Figure 5-3.

According to Equation (5.11), there is always an attractive force for sufficiently small values of r. This is because of the different functional dependence of the image and K-field forces on r. Thus, on the basis of purely elastic effects, a crack will always be mechanically stable against the spontaneous emission of a dislocation. But for values of r smaller than the core size of the dislocation, the elastic approximation breaks down (Thomson, 1986). Assuming that r_c is a measure of the effective core size, and r_0 is the distance for which $f_{total} = 0$. If the zero of Equation (5.11) occurs for values $r_0 < r_c$, emission will occur spontaneously. This means that if $f_{total} > 0$ for $r_0 < r < r_c$, then the repulsive force is dominant and facilitates formation of the dislocation. On the other hand, if $r_0 > r_c$, the net force is attractive, which will restrain dislocation emission, and the crack propagates by brittle cleavage.

Setting r_0 equal to the effective core size r_c, from the discussion above, an equation is obtained for values of K^{tip}_{disl} which must be exceeded in order to emit a dislocation. Setting $f_{total} = 0$ yields

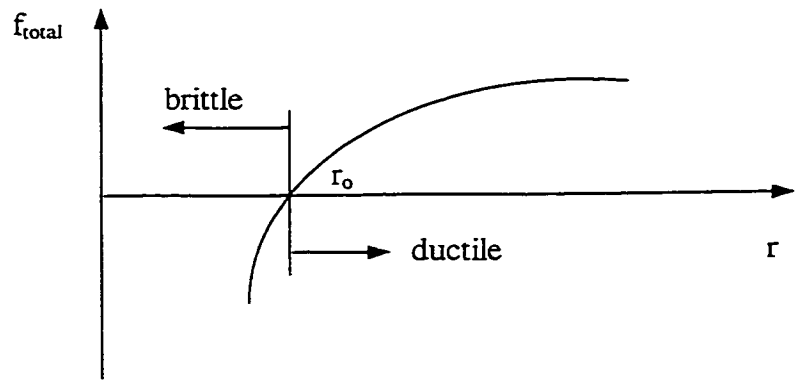

Figure 5-3 Total force on emitted dislocation. The criterion for ductile versus brittle transition is shown in terms of the effective core size r_c.

$$\frac{b\cos\phi}{\sqrt{2\pi r_c}}[\mathrm{Re}(K_{disl} r_c^{i\varepsilon})\Sigma^{I}_{r\varphi} + \mathrm{Im}(K_{disl} r_c^{i\varepsilon})\Sigma^{II}_{r\varphi}] =$$

$$\frac{\mu_1 b^2}{4\pi r_c}[\frac{\cos^2\phi}{1-\nu_1} + \sin^2\phi] + \frac{\mu_1 b^2(\beta^2-\alpha)\cos^2\phi\sin\varphi}{\pi(\kappa_1+1)(1-\beta^2)(h-r_c\sin\varphi)}. \qquad (5.12)$$

In terms of the atomic scale phase angle Ψ' (Rice et al., 1990), the critical energy release rate G_{disl} for dislocation emission is deduced from Equation (3.26) and Equation (5.12) as

$$G_{disl} = \frac{\mu_1 b^2}{(1-\nu_1)(1-\alpha)r_c}\{\frac{[\cos\phi + (1-\nu_1)\sin\phi\tan\phi] + [\frac{4r_c(1-\nu_1)(\beta^2-\alpha)\cos\phi\sin\varphi}{(\kappa_1+1)(1-\beta^2)(h-r_c\sin\varphi)}]}{4\sqrt{\pi}\cosh\pi\varepsilon(\Sigma^{I}_{r\varphi}(\varphi)\cos\Psi' + \Sigma^{II}_{r\varphi}(\varphi)\sin\Psi')}\}^2 \qquad (5.13)$$

which yields a criterion for emission of a dislocation in layered material.

5.3.3 Application of ductile criterion

Equation (5.13) is employed here to analyze a sample layered material, in which a film of copper is bonded to sapphire on both sides, as shown in Figure 5-4. This configuration is similar to the model analyzed by Rice et al. (1990). A notched bottom sapphire layer induces the crack at the interface between the sapphire and the copper layer.

As mentioned by Rice et al. (1990), the atomic scale phase angle Ψ' is related to the crack tip phase angle Ψ^{tip} of the interface stress intensity factor K by

$$\Psi' = \Psi^{tip} - \varepsilon\ln(L/b) \qquad (5.14)$$

where L is a characteristic length (e.g., layer thickness, crack length), and b is the magnitude of the Burgers vector $\vec{b}$.

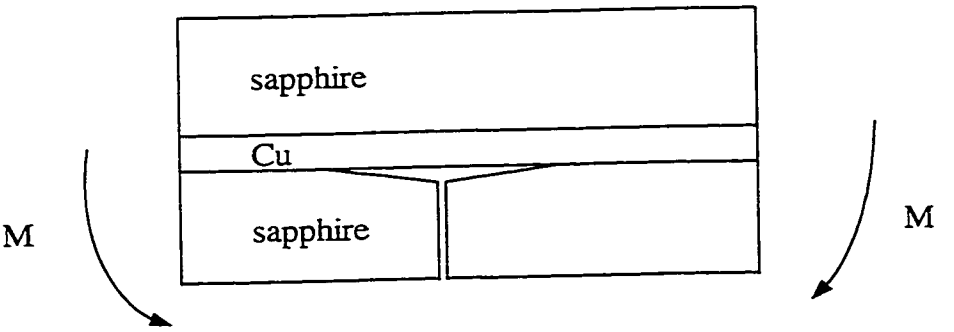

Figure 5-4 Bending layered material.

For the bending layered material in Figure 5-4, $\alpha = -0.47$, $\beta = -0.096$, L is chosen as the layer thickness h of the copper film, b and Ψ^{tip} are 0.15 nm and -39° as suggested by Rice et al. (1990). Ψ' is a function of the layer thickness. It can be seen from Equation (5.13), that the effect of layer thickness h on G_{disl} is through both Ψ' and image force term due to the upper interface.

The role of the thickness is examined for two applications: Cu is treated as isotropic; and Cu is bonded to sapphire with a $(001)_{Cu}$ interface, and $[\bar{1}10]$ cracking direction. In the following calculations, G_{disl} is evaluated with $\mu = 5.0 \times 10^{10}\ N/m^2$, $r_c/b = 1$, $\nu = 0.3$, and $\phi = 60^\circ$ for Cu.

For isotropic Cu, G_{disl} for different slip systems, defined in terms of the angles ϕ and φ, is presented in Figure 5-5. With the minimum G_{disl} representing the probable slip system, it can be seen that the Peach-Koehler driving force is the principal factor determining which slip system is likely to operate. The effect of the layer thickness is to slightly increase G_{disl} and shift the probable slip system.

For the application with a $(001)_{Cu}$ interface, and a $[\bar{1}10]$ cracking direction, the effect of the atomic scale phase angle Ψ' is shown on Figure 5-6. In this type of crystal, the $\{111\}$ slip planes intersect with the crack tip at $\varphi = 54.7^\circ$ and $\varphi = 125.3^\circ$. The results for both slip systems are presented on Figure 5-6. G_{disl} is minimum around $\Psi' = -77^\circ$, that is, for a slip system with $\varphi = 125.3^\circ$ and $\phi = 60^\circ$, the external load which results in an atomic scale phase angle of -77° promotes dislocation emission. In Figure 5-6, the dashed line is the result obtained by Rice et al. (1990), in which there is no image force due to the

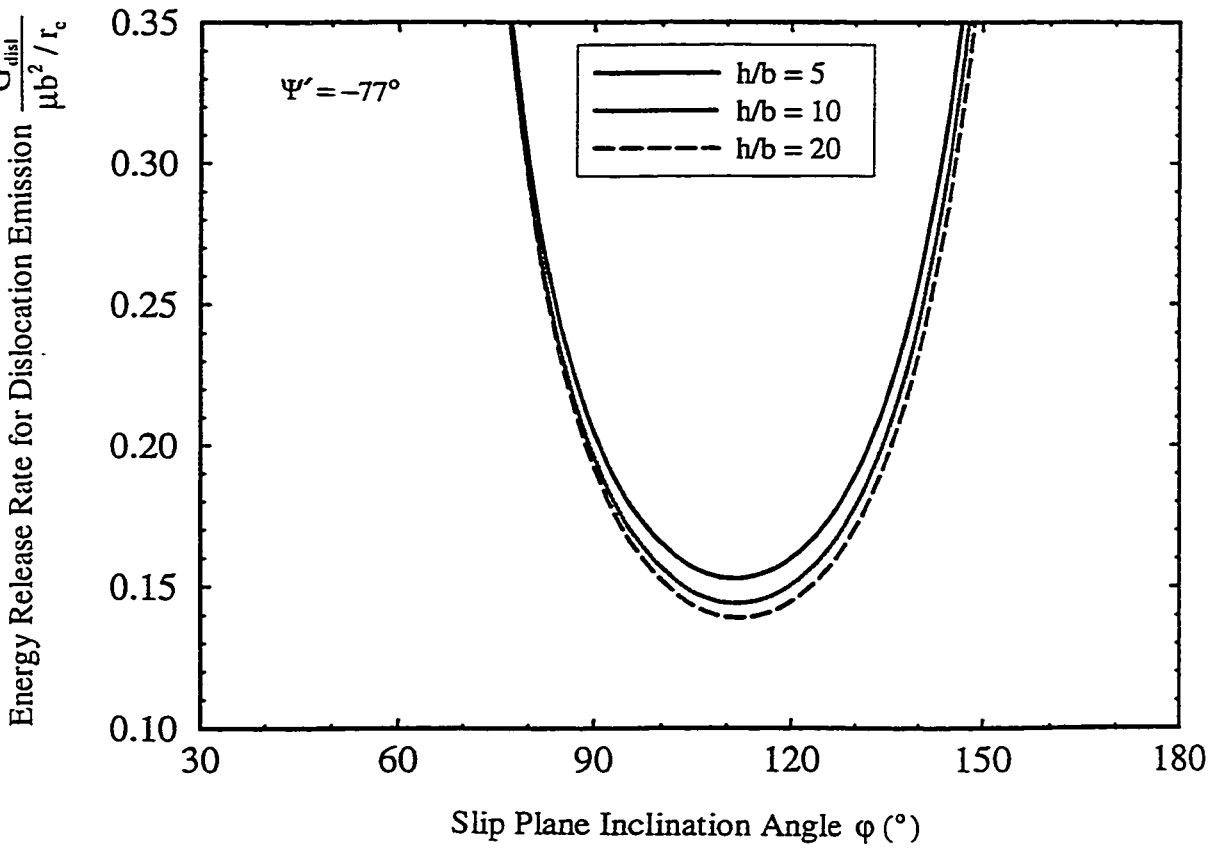

Figure 5-5 The critical G_{disl} for dislocation emission versus slip system inclination angle.

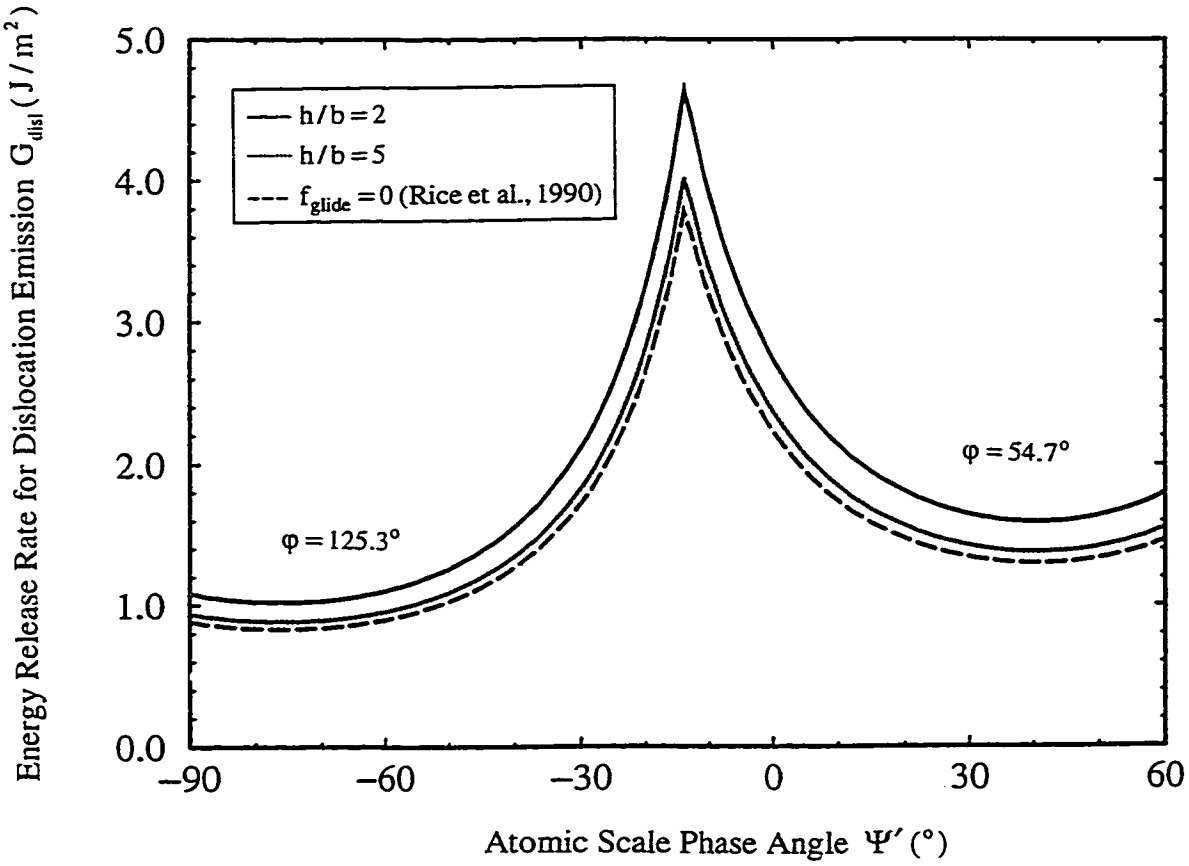

Figure 5-6 The critical G_{disl} for dislocation emission versus atomic scale phase angle.

upper interface (f_{glide}=0). It can be seen that the effect of image force due to the upper interface (shown as solid line and dotted line in Figure 5-6), is obvious only when h is very small (e.g., $h/b = 5$). Detailed results showing the relationship between h and G_{disl} are provided in Figure 5-7 (the dashed line denotes the result by Rice et al. (1990)). G_{disl} is controlled by h through the image force f_{glide} (expressed in Equation (5.9)) and the atomic scale phase angle Ψ' (expressed in Equation (5.14)). With $\varphi = 125.3°$, it can be concluded that G_{disl} is insensitive to h when h is beyond a critical value (e.g., $\frac{h}{b\sin\varphi} = 30$). In practice, the metal layer thickness is at the order of micron, therefore, the results based on bimaterial (Rice et al., 1990) can be a good approximation. On the other hand, if the metal layer is in the regime of nanometer, the image force due to the upper interface should be considered and the results provided in this chapter can be used for predictions.

5.4 Brittle behavior of layered material

If there is no dislocation nucleation at the crack tip, rather the crack tip atomic bond breakage occurs, the behavior of the layered material is referred to as brittle. G_{cleav}, the critical energy release rate for interfacial crack cleavage (atomic bond breakage), is generally used to investigate the criterion for brittle behavior and can be calculated by (Rice and Wang, 1989; Wang and Anderson, 1991)

$$G_{cleav} = 2\gamma_{int} \tag{5.15}$$

where $2\gamma_{int}$ is the reversible work to separate, against atomic cohesive forces, the interface along which the crack grows. For layered materials with an interfacial crack, the

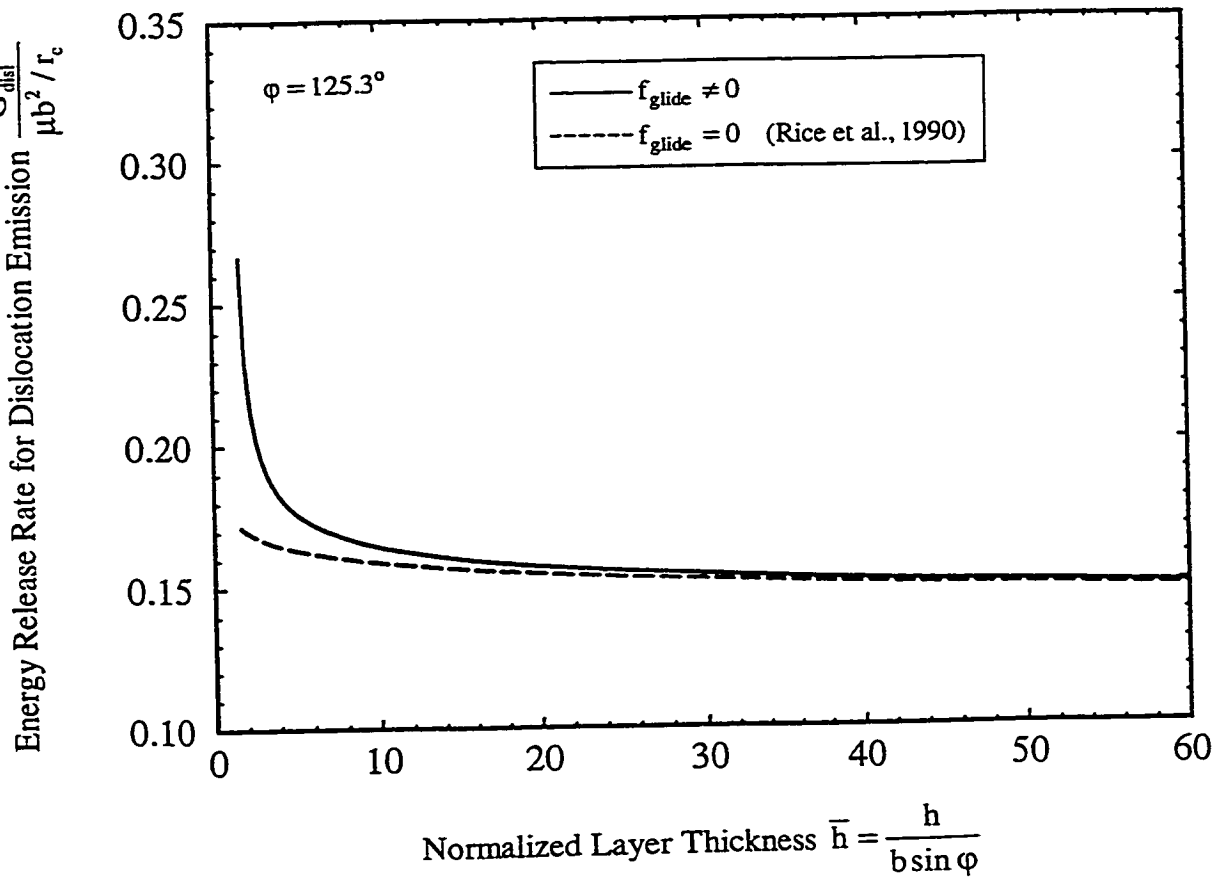

Figure 5-7 G_{disl} for dislocation emission versus layer thickness.

results for bimaterial can be used because only the property of the interface is concerned to calculate G_{cleav}. Some example values of G_{cleav} were obtained experimentally (Wang and Anderson, 1991; Beltz and Wang, 1992).

5.5 Ductile versus brittle behavior of layered materials

Comparing Equation (5.13) with Equation (5.15), the ductile versus brittle behavior criterion is

$$G_{disl} < G_{cleav} \text{ ductile,} \tag{5.16a}$$

$$G_{disl} > G_{cleav} \text{ brittle.} \tag{5.16b}$$

Therefore, the ductile versus brittle behavior of the layered material is determined by the two values of critical energy release rate, G_{disl} and G_{cleav}. For the previous bending material sample, the values of G_{cleav} can be obtained from the work done by Beltz and Wang (1992) and are between 5.0 J/m^2 and 8.0 J/m^2. The values of G_{disl} are shown in Figure 5-6 and are generally below 5.0 J/m^2 (it can be expected to get higher value when $\frac{h}{b} \to 0$). It indicates that dislocation can easily emit in the sapphire/copper/sapphire material and the behavior of the metal/ceramic layered material is ductile in most cases.

Chapter 6

Interfacial Toughening in Metal/Ceramic Layered Materials

A dislocation shielding model is employed in this chapter to analyze the interfacial toughening in metal/ceramic layered materials in terms of dislocation plasticity. The dislocation emission in cracked layered materials is investigated. A group of emitted dislocations will pile up against the bonded interface and concentrate in a small area near the bonded interface. Superdislocation assumption is employed to look at the shielding effect of this group of dislocations. The interfacial crack tip field is modified and crack propagation is investigated in detail under mixed mode loading condition. The effects of length scale (metal layered thickness) and interfacial strength are examined. It is demonstrated that thicker metal layer, stronger interface and more mode II loading component are preferable for higher toughness.

6.1 Introduction

Layered materials mixed with different materials are widely used because of their optimal properties, which traditional materials cannot achieve, e.g. high strength with high toughness, corrosion-resistance. Recently, thin layered materials especially are required in micro-electrical components, such as computer chips, electrical packaging, and micro-actuator. Defects in these layered materials will decay the performance significantly. Many analytical and experimental research (Evans and Dalgleish, 1992; Turner and Evans, 1996) have been done to investigate the mechanical and thermal performance of the layered

materials. Interfacial crack initiation and propagation in metal/ceramic layered materials will be investigated in this chapter. The typical length scale of the metal layer thickness is in the order of micrometer. Dislocation shielding model is employed here to analyze the toughening mechanism of layered materials.

6.2 Background

Although comprehensive research on interfacial crack induced problem could be traced to Williams (1959), results for interfacial crack are accumulated recently (Comninou, 1977; Cherepanov, 1979; Rice, 1987; Hutchinson et al., 1987; Rice, 1988; Hutchinson and Suo, 1992; Embury et al., 1996). This trend is mainly due to the industry requirements, especially from computer-associated fields. Both properties and structures require high-density, high-performance design, which makes thin layered materials widely available. Micro-cracks or defects are frequently generated on the interface during fabrication processes and grow to critical size, causing interfacial failure. Although analytical models (Shih and Asaro, 1988; Rice et al., 1990; Bose and Ponte Castaneda, 1992; Tvergarrd and Hutchinson, 1993, 1994 and 1996; Liang and Liechti, 1995) and numerical simulations such as FEM analysis (McMeeking, 1977; Wei and Hutchinson, 1996) have been employed to estimate the "elastic-plastic" stress profile as well as the macroscopic "plastic" zone near an interfacial crack tip, conventional macromechanics is not appropriate to analyze the performance of these thin layered materials. Because of the confined space in these thin layered materials, the plasticity in the metal layer should be analyzed by considering the behavior of each individual dislocation.

Dislocation theory has long been used to investigate the plastic and fracture behaviors of materials (see Chapter 4). Recently, a superdislocation model has been used to analyze the fracture behavior of the crack (Lii et al., 1990; Lubarda et al., 1993). Hsia et al. (1994) used superdislocation model to analyze the cleavage due to dislocation confinement in layered materials under mode I loading condition. The crack was assumed within the metal layer, and fracture mechanics approaches are those for homogeneous material. However, in practice, the crack is likely generated at the interface in the layered material. To overcome this limitation, Mao and Evans (1997) analyzed the interfacial crack initiation and propagation in metal/ceramic layered materials employing the similar superdislocation model as Hsia et al. (1994). Although the experimental result is from mixed mode loading condition (Figure 6-1), Mao and Evans (1997) only established a model for mode I condition. Even though an interfacial crack was assumed, the fracture parameters to describe the interfacial crack were approximated by those for homogeneous material.

This chapter aims to analyze the toughening mechanism in metal/ceramic layered materials by overcoming the limitations mentioned above (Mao and Li, 1998; Li and Mao, 1998b). Interfacial crack fracture mechanics will be used to investigate the interfacial crack initiation and propagation in metal/ceramic layered material subject to mixed mode (mode I + mode II) loading condition. Superdislocation approach, similar to Mao and Evans (1997), is used to investigate the fracture toughness of the metal/ceramic layered material. The roles of the metal layer thickness and mode mixity (in term of phase angle) on the fracture toughness will be examined in detail.

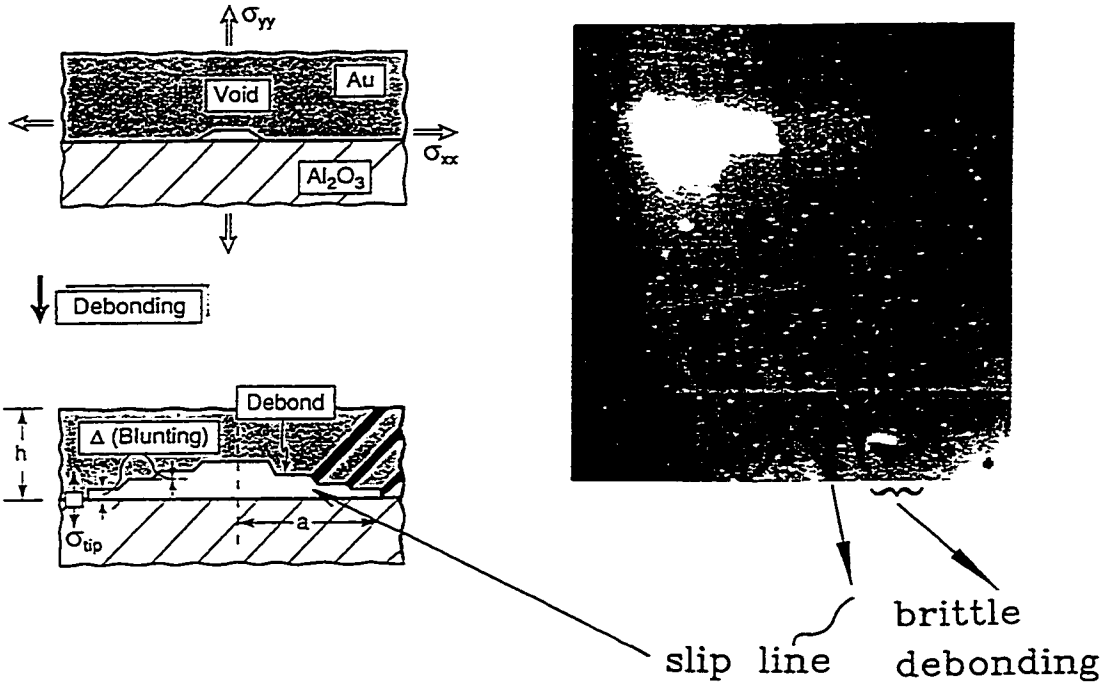

Figure 6-1 A schematic of the small debonding extension process along Al_2O_3/Au interface under atomic force microscope.

6.3 Dislocation model in metal/ceramic layered materials

A model of metal/ceramic layered material is shown in Figure 6-2. It is assumed that metal layer has dislocation plasticity and ceramic layers are elastic with no dislocation plasticity. The middle metal layer thickness is h and associated materials parameters are: shear modulus μ, Poisson's ratio ν, Burgers vector $\bar{\mathbf{b}}$ and surface energy γ. The energy needed for a single dislocation emission from crack tip is assumed to be much smaller than the interface cleavage fracture energy (as the case described in Chapter 5). Subject to loading, a cluster of dislocations will emit from the crack tip and move along a slip plane in the metal at an angle φ to the interface crack plane, until pile up against the upper interface. The i'th emitted dislocation is located on the slip plane at h_i from the crack tip, and leading emitted dislocation can travel a maximum distance $h_\varphi = h/\sin\varphi$, as shown in Figure 6-2. As shown in Figure 6-3, for FCC metal with [100] plane on the interface and [111] as the slip plane, φ is 70.5°; for BCC metal with [100] plane on the interface and [110] as the slip plane φ is 45°.

The emitted dislocations have two effects on the crack tip. Firstly, if the burgers vector has a component normal to the crack plane, the emitted dislocations blunt the crack tip and a ledge is generated as shown in Figure 6-4. The blunting reduces the stress concentration at the crack tip such that it is more difficult to reach the decohesive tensile strength of the interface. Secondly, the interaction forces between the crack and the emitted dislocations will result in crack tip shielding, giving rise to crack tip stress intensity lower than the far field applied stress intensity.

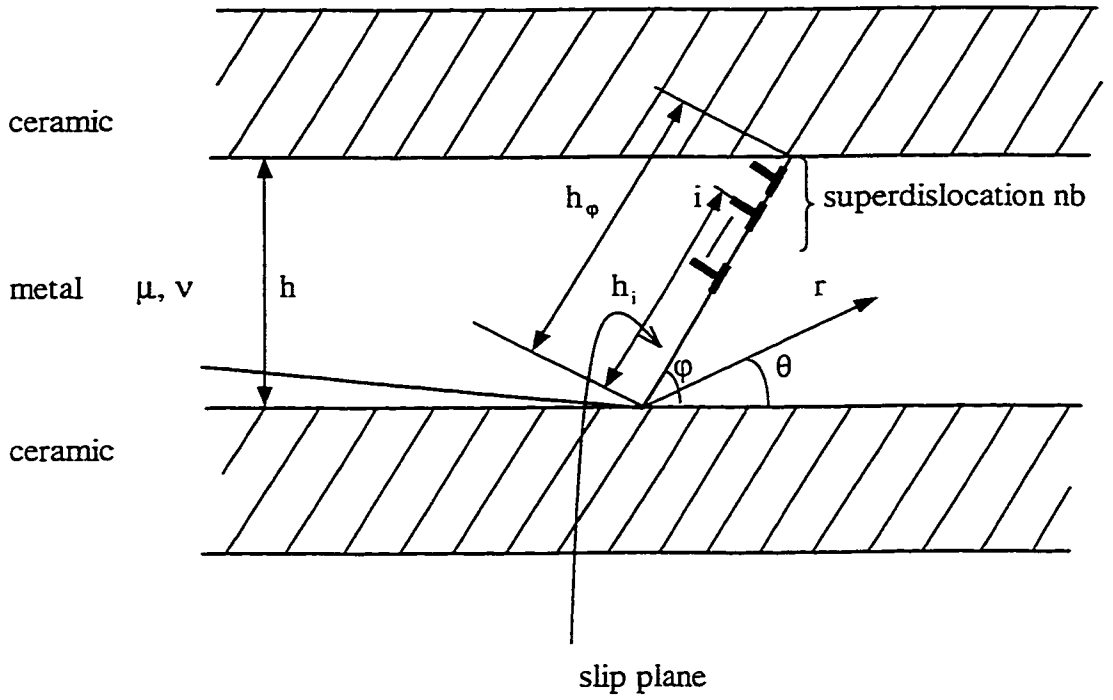

Figure 6-2 Ceramic/metal/ceramic layered material model with an interface crack.

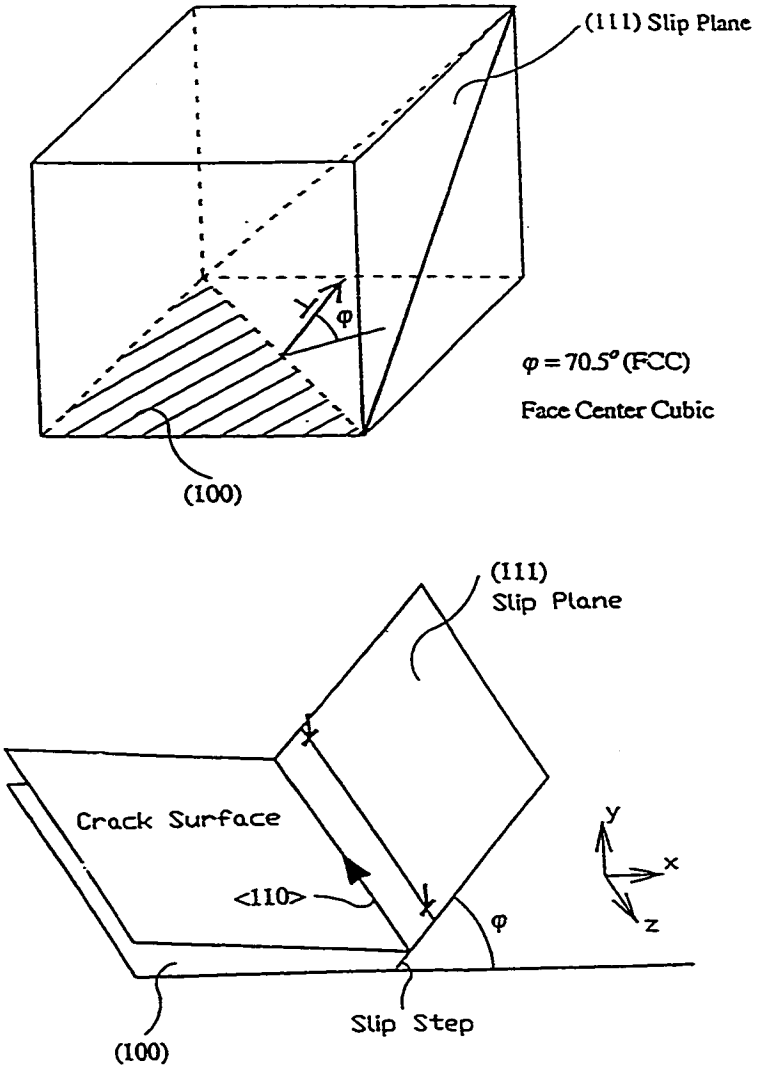

Figure 6-3 Slip system for FCC metal.

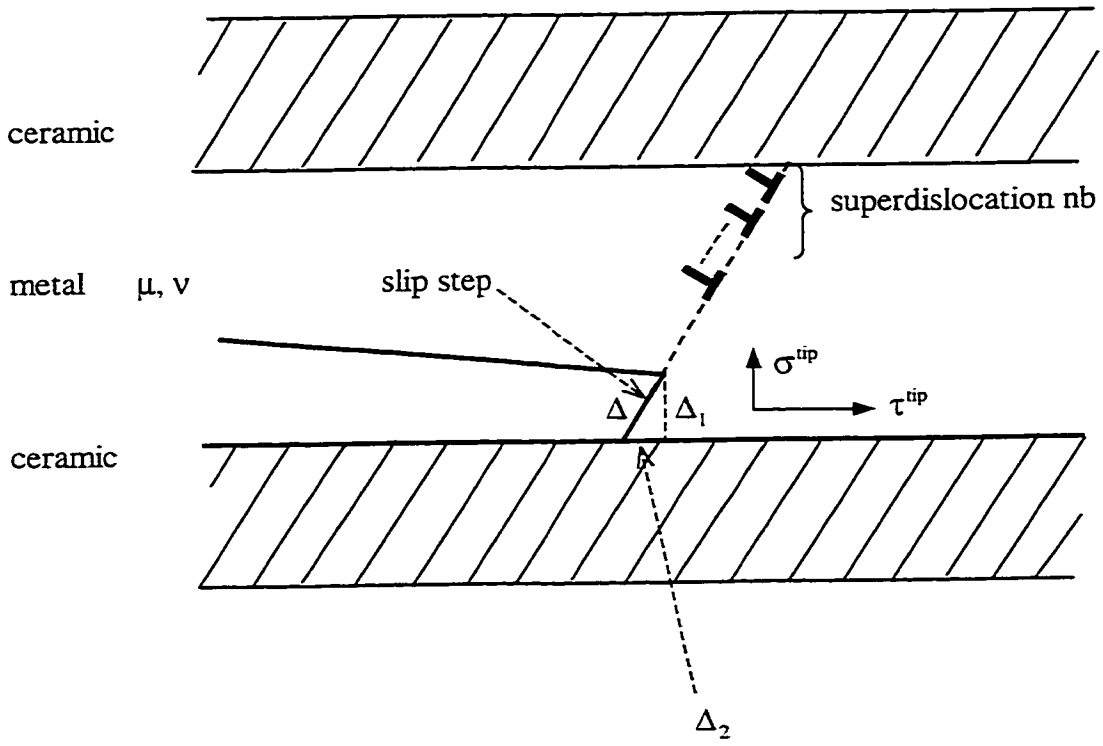

Figure 6-4 Slip step and crack tip stress at the blunting crack tip.

6.3.1 Dislocation emission and equilibrium number of emitted dislocations

From the results in Chapter 5, the required energy to emit dislocation from crack tip is very small compared to the energy to debond the interface ($G_{disl} < G_{cleav}$), such that the energy barrier for dislocation emission from crack tip can be ignored. But in a layered material, dislocations emitted from the interface crack tip are blocked by the upper interface, sending a back stress to the crack tip to impede further dislocation emission. For a given applied load and layer thickness, there is an equilibrium number of dislocations in the pile-ups. Once the equilibrium number is reached, emission of additional dislocations is prevented by the back stress, which hinders further blunting of the crack tip.

The similar approach proposed by Hsia et al. (1994) is employed here to analyze each energy term in such dislocation embedded layered material. The energy for single dislocation was presented in Chapter 4, and the energy for dislocation cluster is analyzed then.

6.3.1.1 Energy for single dislocation in layered materials

For single dislocation in layered materials the in presence of interfacial crack, the energy includes the dislocation self-energy, interaction energy between dislocation and interface crack and the ledge energy due to the new created surface around crack tip. All these energy terms are analyzed in Chapter 4. Therefore, those results in Chapter 4 are used here by considering the role of the upper interface.

Consider a dislocation located at $r = h_i$ along the slip plane from the interface crack tip (see Figure 6-3). The self energy of the dislocation is

$$W_d'(h_i) = \frac{\mu b^2}{4\pi(1-\nu)} \ln \frac{h_i}{r_{crack}}, \tag{6.1}$$

where r_{crack} is the effective core radius to initiate a dislocation near the interfacial crack tip. The interaction energy between the dislocation and the interfacial crack tip $K^{tip'}$ field is

$$\begin{aligned} W'_k(h_i) &= \int_0^{h_i} \sigma_{r\theta} b dr \\ &= -\frac{2b\sqrt{h_i}}{\sqrt{2\pi}} [K_1^{tip'} \sin\frac{\theta}{2}\cos^2\frac{\theta}{2} + K_2^{tip'}(\cos\frac{3\theta}{2} + \cos\frac{\theta}{2}\sin^2\frac{\theta}{2})]. \end{aligned} \tag{6.2}$$

where $\sigma_{r\theta}$ is the crack tip shear stress for interfacial crack defined in Equation (4-31). It is remarked here that $K^{tip'}$ is the interface stress intensity factor before dislocation emission and $K^{tip'}$ is described in Equation (3.36).

The ledge energy for a single dislocation is

$$W'_L = b\gamma, \tag{6.3}$$

where γ is the surface energy of the metal.

6.3.1.2 Energy for dislocation cluster in layered materials

As mentioned by Hsia et al. (1994). The strength of the local stress and strain field associated with the dislocation can be expressed as

$$\sigma_{mn}(h_l) = \frac{\mu b}{2\pi(1-\nu)r_l} S_{mn}(\theta_l), \ \varepsilon_{mn}(h_l) = \frac{b}{2\pi r_l} E_{mn}(\theta_l), \quad (m,n = r,\theta) \tag{6.4}$$

where local polar coordinates (r_l, θ_l) are centered at $r = h_l$. The forms of angular variations S_{mn} and E_{mn} do not depend on h_l. They are documented in the dislocation theory literature, such as the book by Hirth and Lothe (1982). For a group of n dislocations (denoted here as dislocation cluster), Equation (6.4) can be rewritten as

$$\sigma_{mn} = \frac{\mu b}{2\pi(1-\nu)} \sum_{l=1}^{n} \frac{1}{r_l} S_{mn}(\theta_l), \ \varepsilon_{mn} = \frac{b}{2\pi r} \sum_{q=1}^{n} \frac{1}{r_q} E_{mn}(\theta_q), \tag{6.5}$$

so the self energy for the dislocation cluster is

$$W_d = \frac{1}{2} \int_V \sigma_{mnj} \varepsilon_{mn} dV = \frac{\mu b^2}{8\pi^2(1-\nu)} \sum_{l=1}^{n} \sum_{q=1}^{n} \int_V \frac{1}{r_l r_q} S_{mn}(\theta_l) E_{mn}(\theta_q) dV, \tag{6.6}$$

and W_d consists of the dislocation self-energy and the interaction energy between dislocations.

The interaction energy between the dislocation cluster and the interfacial crack tip field, W_k, is obtained by the superposition of $W'_K(h_i)$ in Equation (6.2),

$$W_k = -\frac{2b}{\sqrt{2\pi}} [K_1^{tip'} \sin\frac{\theta}{2}\cos^2\frac{\theta}{2} + K_2^{tip'}(\cos\frac{3\theta}{2} + \cos\frac{\theta}{2}\sin^2\frac{\theta}{2})] \sum_{l=1}^{n} \sqrt{h_l}. \tag{6.7}$$

The Ledge energy for the dislocation cluster, W_L, is the superposition of W'_L.

$$W_L = nb\gamma. \tag{6.8}$$

The total energy of the system, W_T, is

$$W_T(K_1^{tip'}, K_2^{tip'}, n) = W_d + W_K + W_L. \tag{6.9}$$

The equilibrium condition requires that

$$\frac{\partial W_T}{\partial n} = 0 \tag{6.10}$$

which determines the number of dislocations that are emitted from the interfacial crack tip under an equilibrium condition. This number is the measurement of the blunting at crack tip and the dislocation plasticity involved into the layered materials.

6.3.2 Superdislocation approach

Even for dislocations perfectly aligned in a single slip system, the calculation for their equilibrium spacing is cumbersome. As pointed out by Lin and Thomson (1986), the mutual interaction between the dislocations is in general not one-dimensional. The similar approach in Hsia et al. (1994) is employed here to circumvent this difficulty. The approximation is outlined below. If the dislocations are located at

$$h_i = h_\varphi - \delta_i \qquad (i = 1,\ldots,n) \tag{6.11}$$

where δ_i is the distance between the i'th dislocation and the upper interface on the slip plane. The dislocation cluster can be treated as one dislocation provided that each δ_i $(i = 1,\ldots,n)$ are much smaller than h_φ. This special dislocation is referred to as superdislocation with the magnitude of Burgers vector as the sum of those for each individual dislocation in the dislocation cluster. For modelling as a superdislcoation, each h_i (i = 1,...,n) of the dislocation cluster is taken as h_ϕ.

After using a superdislocation with strength nb to substitute the group of n dislocation, the energy terms for the dislocation cluster can be calculated on this superdislocation. Using the same mathematical approach as that proposed by Hsia et al. (1994), W_d and W_K for the superdislocation are derived from Equations (6.6) and (6.7) as

$$W_d = \frac{\mu(nb)^2}{4\pi(1-\nu)}\left(\ln\frac{h_\phi}{r_0} - 1\right), \tag{6.12}$$

$$W_k = -\frac{nb}{\sqrt{2\pi}}\left[K_1^{tip}\sin\theta\cos\frac{\theta}{2} + 2K_2^{tip}\cos\frac{\theta}{2}\left(1-3\sin^2\frac{\theta}{2}\right)\right]\sqrt{h_\phi}. \tag{6.13}$$

where r_0 is the effective core radius of the superdislocation as defined in Hsia et al. (1994).

The ledge energy for the superdislocation is the same as that expressed in Equation (6.8). Substituting Equations (6.8), (6.12) and (6.13) into Equation (6.10), the equilibrium emitted dislocation number is

$$n = \frac{2\pi(1-\nu)}{\ln \bar{h}}\left[\bar{K}_1^{tip^*}\sqrt{\frac{\bar{h}}{2\pi}}g_1(\varphi) + \bar{K}_2^{tip^*}\sqrt{\frac{\bar{h}}{2\pi}}g_2(\varphi) - \bar{\gamma}\right] \tag{6.14}$$

where $g_1(\varphi) = \sin\varphi\cos\frac{\varphi}{2}$, $g_2(\varphi) = 2\cos\frac{\varphi}{2}\left[1-3\sin^2\frac{\varphi}{2}\right]$, $\bar{h} = h_\varphi / b = h/(b\sin\varphi)$, $(\bar{K}_1^{tip^*}, \bar{K}_2^{tip^*}) = (K_1^{tip^*}, K_2^{tip^*})/(\mu\sqrt{b})$ and $\bar{\gamma} = \gamma/(\mu b)$. The value of $\bar{\gamma}$ ranging from 0 to 0.2 for most metals (Hsia et al., 1994).

To describe the ratio of the $\bar{K}_2^{tip^*}$ to $\bar{K}_1^{tip^*}$, phase angle Ψ^{tip^*} at crack tip is defined here as

$$\tan\Psi^{tip^*} = \frac{\bar{K}_2^{tip^*}}{\bar{K}_1^{tip^*}}. \tag{6.15}$$

Considering Equations (3.26) and (6.15), Equation (6.14) can be rewritten as

$$n = \frac{\sqrt{2\pi\bar{h}\bar{G}}(1-\nu)}{\ln \bar{h}}\left|\cos\Psi^{tip^*}\right|\left[g_1(\varphi) + \tan\Psi^{tip^*}g_2(\varphi)\right] - \frac{2\pi(1-\nu)}{\ln \bar{h}}\bar{\gamma} \tag{6.16}$$

where $\bar{G} = G\Big/\frac{1-\beta^2}{E_*}\mu^2 b$ and E_* is defined in Equation (3.25) in which metal is the material 1 and ceramic is the material 2. From above equation, it can be seen that n is a function of loading, layer thickness, slip system of the metal and the surface energy. Equilibrium dislocation numbers for different loads with two different layer thickness (Taking FCC Au as metal layer, $\varphi = 70.5°$. h is about 10 μm when $\bar{h} = 35000$, and h is about 100 nm when $\bar{h} = 350$) are shown in Figure 6-5(a) and 6-5(b), where the effects of $\bar{\gamma}$ on n are also illustrated. It can bee seen that n is not sensitive to $\bar{\gamma}$ when h is of the order

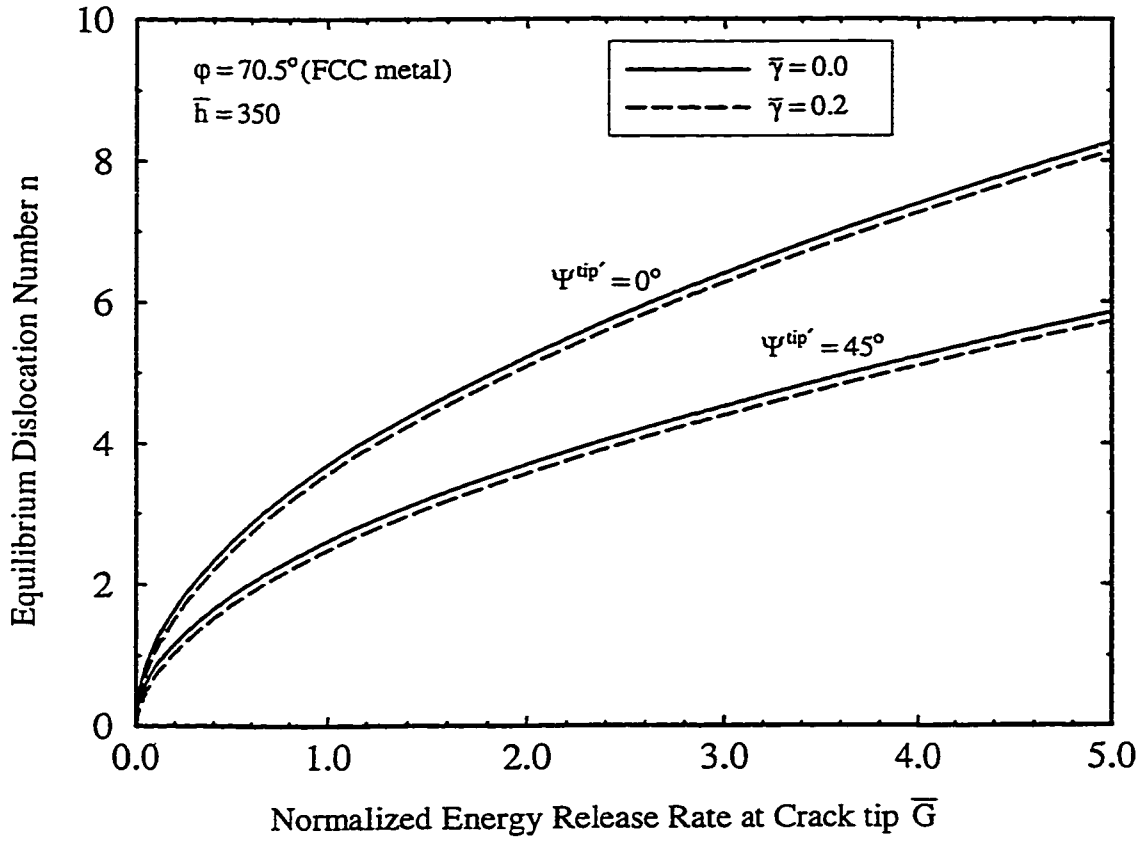

Figure 6-5(a) Equilibrium dislocation number for different loading conditions with metal layer thickness $\bar{h} = 350$ (0.1 μm for Au)

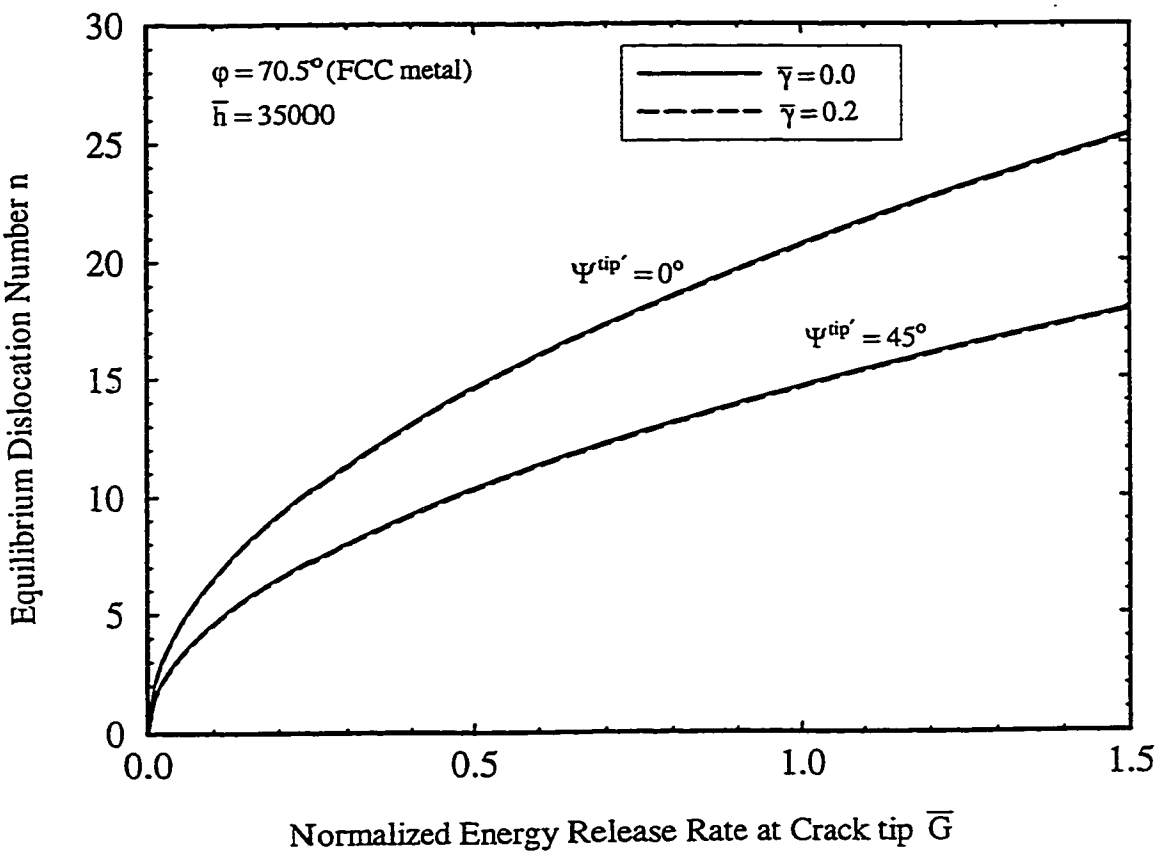

Figure 6-5(b) Equilibrium dislocation number for different loading conditions with metal layer thickness $\bar{h} = 35000$ (10 μm for Au).

of micrometer. Therefore, $\bar{\gamma}$ is taken as zero in the following analysis to simplify the computation without loss the accuracy. The phase angle (Ψ^{tip}) effect on such material system ($\varphi = 70.5°$) is also presented, which indicates that more mode I load ($\Psi^{tip} = 0$) will obtain more dislocations. The effect of metal layer thickness on the normalized equilibrium emitted dislocation number $n / \sqrt{2\pi\bar{\bar{G}}(1-\nu)}\left|\cos\Psi^{tip}\right|[g_1(\varphi) + \tan\Psi^{tip} g_2(\varphi)]$ is shown in Figure 6-6, indicating more dislocation can emit with thicker metal layer.

Equation (6.16) also indicates the relationship between n and material system in terms of φ. For different material, which means different slip plane angle φ, there exists a different critical phase angle corresponding to the maximum n. Because n is a measurement of the dislocation plasticity, the maximum n means highest dislocation plasticity. To extend this result to all materials, the relationship between the critical phase angle $\Psi_{critical}^{tip}$ and slip plane angle φ is derived from $\frac{\partial n}{\partial \Psi^{tip}} = 0$ as

$$\Psi_{critical}^{tip} = \tan^{-1}\left[\frac{g_1(\varphi)}{g_2(\varphi)}\right]. \tag{6.17}$$

The numerical results for Equation (6.17) are shown in Figure 6-7. Therefore, for any material, there is an optimum phase angle $\Psi_{critical}^{tip}$ to achieve the maximum plasticity; for a fixed phase angle, a specific material could be selected to get the maximum plasticity.

6.4 Dislocation shielding effect on crack tip field

The emitted dislocations will reduce the crack tip stress intensity as shielding effect, or to increase the crack tip stress intensity as anti-shielding effect. For shielding dislocations,

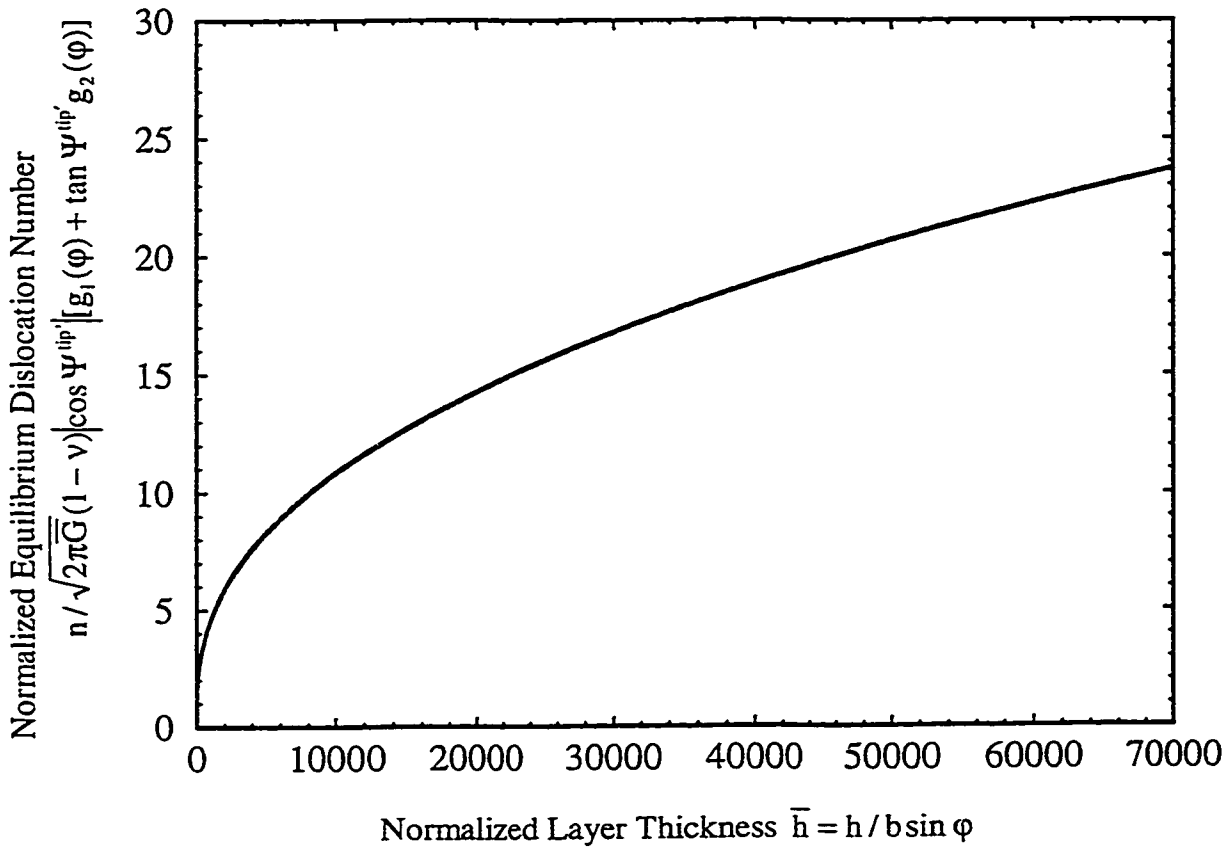

Figure 6-6 Normalized equilibrium dislocation number for different layer thickness.

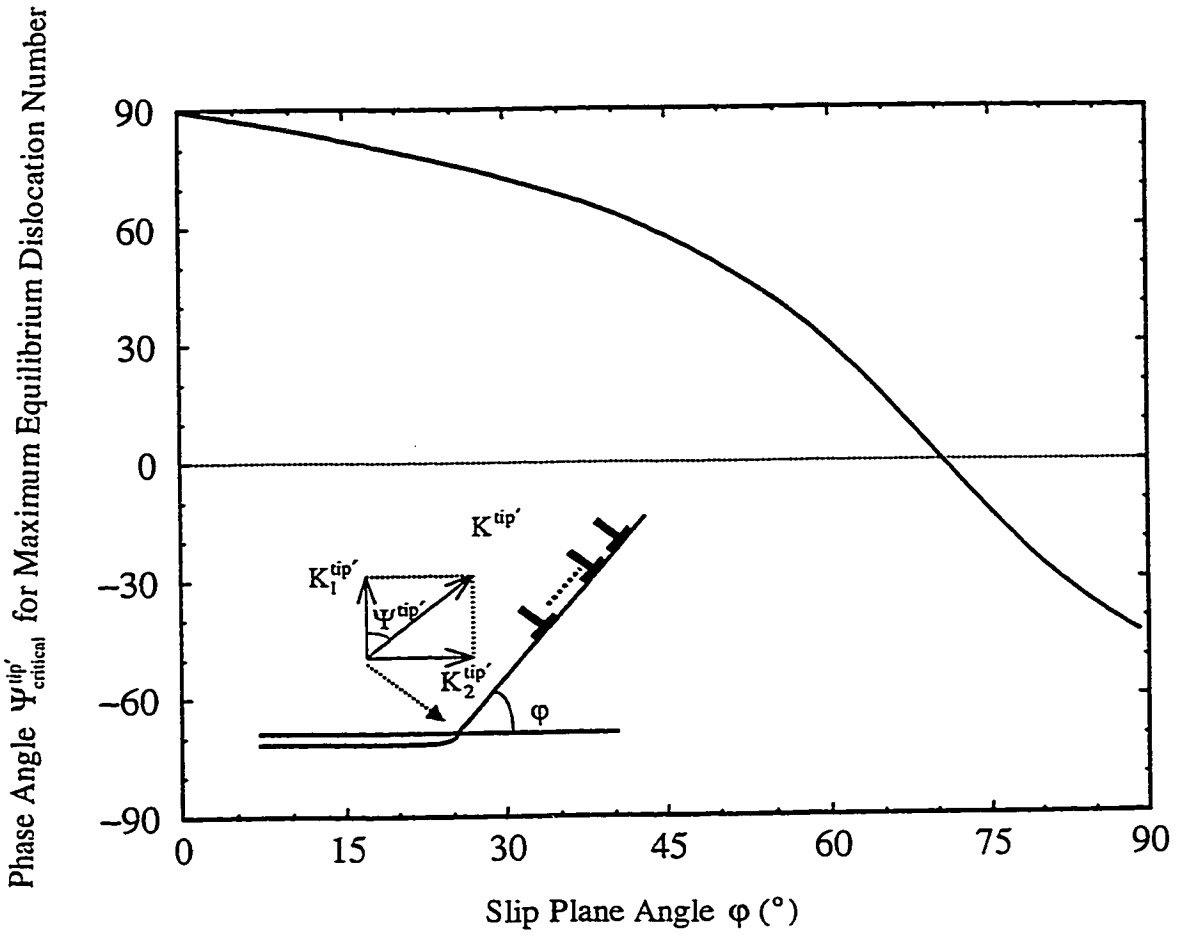

Figure 6-7 Optimal phase angle for maximum equilibrium dislocation number for different slip system.

the relationship between interface stress intensity factors at crack tip can be expressed by

$$\begin{bmatrix} K_1^{tip'} \\ K_2^{tip'} \end{bmatrix} = \begin{bmatrix} K_1^{tip} \\ K_2^{tip} \end{bmatrix} + \begin{bmatrix} k_1 \\ k_2 \end{bmatrix} \tag{6.18}$$

where the subscripts 1 and 2 denote the mode I and mode II components, respectively. K^{tip} is the stress intensity factor at the crack tip after dislocation shielding. The stress intensity factor k contributed from the superdislocation with strength nb is (details were given in Chapter 4)

$$\begin{bmatrix} k_1 \\ k_2 \end{bmatrix} = \frac{3n\mu\sqrt{b}}{2\sqrt{2\pi\bar{h}}\,(1-\nu)} \begin{bmatrix} f_1(\varphi) \\ f_2(\varphi) \end{bmatrix} \tag{6.19}$$

where $f_1(\varphi) = (1+\alpha)\sin\varphi\cos\frac{\varphi}{2}$, $f_2(\varphi) = \frac{1}{3}(1+\alpha)(2\cos\varphi\cos\frac{\varphi}{2} - \sin\varphi\sin\frac{\varphi}{2})$, and α is one of Durdurs parameters defined in Equation (3.15) with μ_1 and μ_2 as the shear moduli of metal and ceramic, respectively.

The phase angle Ψ^{tip} at the crack tip after dislocation emission is defined as

$$\tan\Psi^{tip} = \frac{K_2^{tip}}{K_1^{tip}}. \tag{6.20}$$

From Equations (6.14), (6.18), (6.19) and (6.20), the relationship between Ψ^{tip} and $\Psi^{tip'}$ is

$$\begin{bmatrix} \overline{K}_1^{tip} \\ \overline{K}_2^{tip} \end{bmatrix} = \begin{bmatrix} \lambda_{11}\overline{K}_1^{tip'} + \lambda_{12}\overline{K}_2^{tip'} + \overline{\gamma}_1 \\ \lambda_{21}\overline{K}_1^{tip'} + \lambda_{22}\overline{K}_2^{tip'} + \overline{\gamma}_2 \end{bmatrix}. \tag{6.21}$$

Here, $(\overline{K}_1^{tip}, \overline{K}_2^{tip}) = (\overline{K}_1^{tip}, \overline{K}_2^{tip})/(\mu\sqrt{b})$ and

$$\lambda_{11} = 1 - \frac{f_1(\varphi)g_1(\varphi)}{\ln\bar{h}}, \qquad \lambda_{12} = -\frac{f_1(\varphi)g_2(\varphi)}{\ln\bar{h}},$$

$$\lambda_{21} = -\frac{f_2(\varphi)g_1(\varphi)}{\ln \bar{h}}, \qquad \lambda_{22} = 1 - \frac{f_2(\varphi)g_2(\varphi)}{\ln \bar{h}},$$
$$\bar{\gamma}_1 = \frac{f_1(\varphi)\bar{\gamma}}{\sqrt{\bar{h}/2\pi}}, \qquad \bar{\gamma}_2 = \frac{f_2(\varphi)\bar{\gamma}}{\sqrt{\bar{h}/2\pi}}. \tag{6.22}$$

The phase angle Ψ^{tip} can be expressed as

$$\Psi^{tip} = \tan^{-1}\frac{\lambda_{21}\bar{K}_1^{tip'} + \lambda_{22}\tan\Psi^{tip}\bar{K}_1^{tip'} + \bar{\gamma}_1}{\lambda_{11}\bar{K}_1^{tip'} + \lambda_{12}\tan\Psi^{tip}\bar{K}_1^{tip'} + \bar{\gamma}_2}. \tag{6.23}$$

If $\bar{\gamma} = 0$,

$$\Psi^{tip} = \tan^{-1}\frac{\lambda_{21} + \lambda_{22}\tan\Psi^{tip'}}{\lambda_{11} + \lambda_{12}\tan\Psi^{tip'}}. \tag{6.24}$$

The results for Equation (6.24) are shown in Figure 6-8(a) & (b) for FCC and BCC metals, respectively. For a thin metal layer (e.g. $\bar{h} = 35$, $\varphi = 70.5°$, which means the layer thickness is 10 nm for Au), the difference is about several degree. On the other hand, the difference is not obvious for relative thicker layer (e.g. $\bar{h} = 35000$, $\varphi = 70.5°$, which means the layer thickness is 10 μm for Au). So, for all calculations and discussions in this chapter are based on $h \sim \mu m$ such that the phase angle at the crack tip after dislocation emission is taken as the same value as the phase angle at the crack tip before dislocation emission.

The second effect of the emitted dislocations is to create ledges at the crack tip such that the stresses ahead of the crack tip will be reduced. Slip step due to these ledges is shown in Figure 6-3. After n dislocations emit from the crack tip, the components of the slip step, Δ_1 and Δ_2 as shown in Figure 6-3, are given by

$$\Delta_1 = \Delta\sin\varphi, \quad \Delta_2 = \Delta\cos\varphi. \tag{6.25}$$

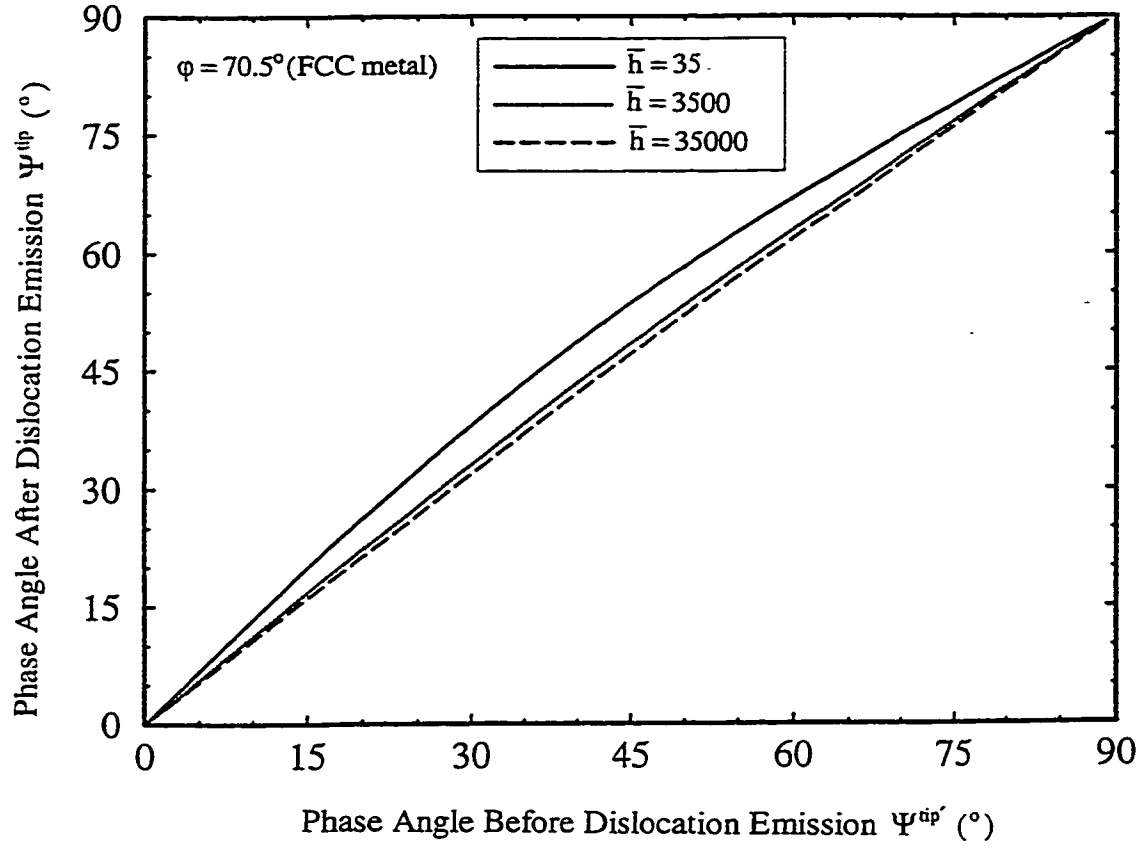

Figure 6-8(a) Difference between interfacial crack tip phase angle before dislocation emission and after dislocation emission in FCC metal ($\varphi = 70.5°$).

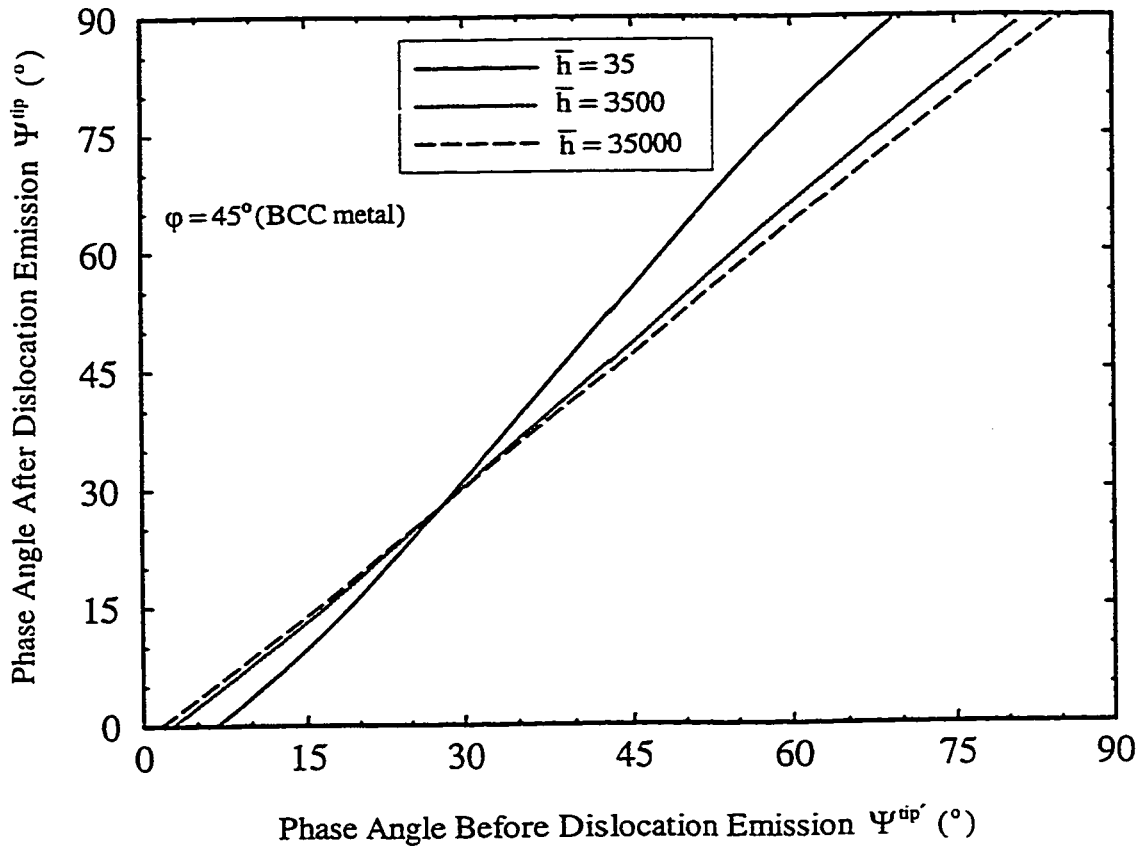

Figure 6-8(b) Difference between interfacial crack tip phase angle before dislocation emission and after dislocation emission in BCC metal ($\varphi = 45°$).

Here $\Delta = nb$. For simplicity, the blunted crack tip is approximated by a notch with radius of Δ. Therefore, the crack tip tensile stress σ^{tip} and shear stress τ^{tip} after dislocation emission can be expressed as (Tada et al., 1985)

$$\begin{aligned} \sigma^{tip} &= 2\sqrt{2/\pi}\, K_1^{tip} / \sqrt{\Delta_1}, \\ \tau^{tip} &= 2\sqrt{2/\pi}\, K_2^{tip} / \sqrt{\Delta_2}. \end{aligned} \tag{6.26}$$

Taking into account of Equations (6.16), (6.18) and (6.19) and $\bar{\gamma} = 0$, the stress can be expressed as

$$\left(\frac{\sigma^{tip}}{\mu}\right)^2 = \frac{4\sqrt{2\pi\bar{G}\cos^2\Psi^{tip}}}{\pi(1-\nu)\sin\varphi \ln\bar{h}\sqrt{\pi\bar{h}}}[g_1(\varphi) + g_2(\varphi)\tan\Psi^{tip}]\left[\frac{\ln\bar{h}}{g_1(\varphi) + g_2(\varphi)\tan\Psi^{tip}} - \frac{3f_1(\varphi)}{2}\right]^2,$$

$$\frac{\tau^{tip}}{\mu} = \frac{\sigma^{tip}}{\mu}\tan\Psi^{tip}\sqrt{\tan\varphi}. \tag{6.27}$$

Here $\bar{G} = G \Big/ \frac{1-\beta^2}{E_*}\mu^2 b$ and G is defined in Equation (3.26).

Figure 6-9(a) shows the relationship between the crack tip stresses and the loading for FCC metal and BCC metal, respectively. Even though the loading increase results in more crack tip blunting, the crack tip stress still increases. It can be seen that the shear stress is much higher than the tensile stress and the stress level for FCC metal is higher than that for BCC metal with same loading phase angle Ψ^{tip}. The phase angle effect is shown in Figure 6-9(b). If the external loading manner changes from mode I ($\Psi^{tip} = 0°$) to mode II ($\Psi^{tip} = 90°$), the crack tip shear stress increase dramatically though the tensile stress decrease in the mean time. The metal layer thickness effects are presented in Figure 6-9(a) and (b) as well, which indicate that a higher stress level can be obtained for a thinner metal layer.

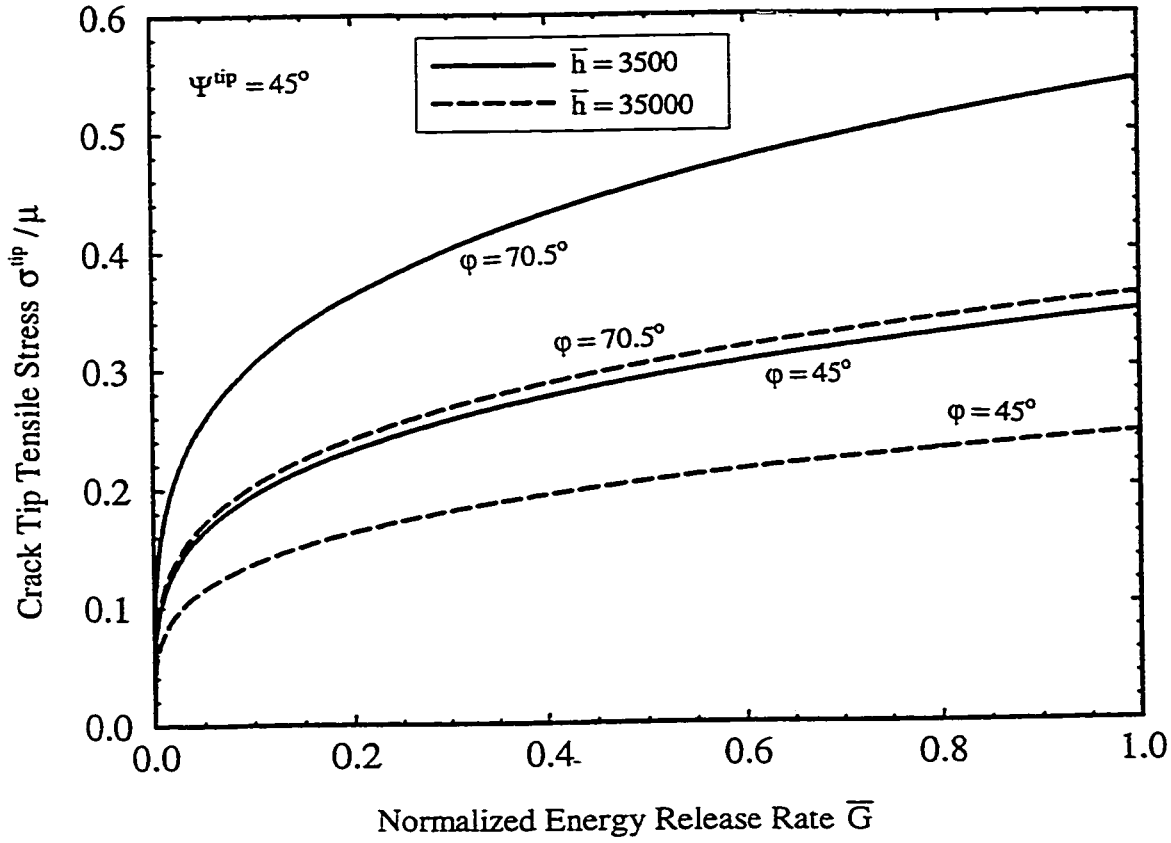

Figure 6-9(a) Effects of loading on interfacial crack tip stresses for FCC and BCC metals.

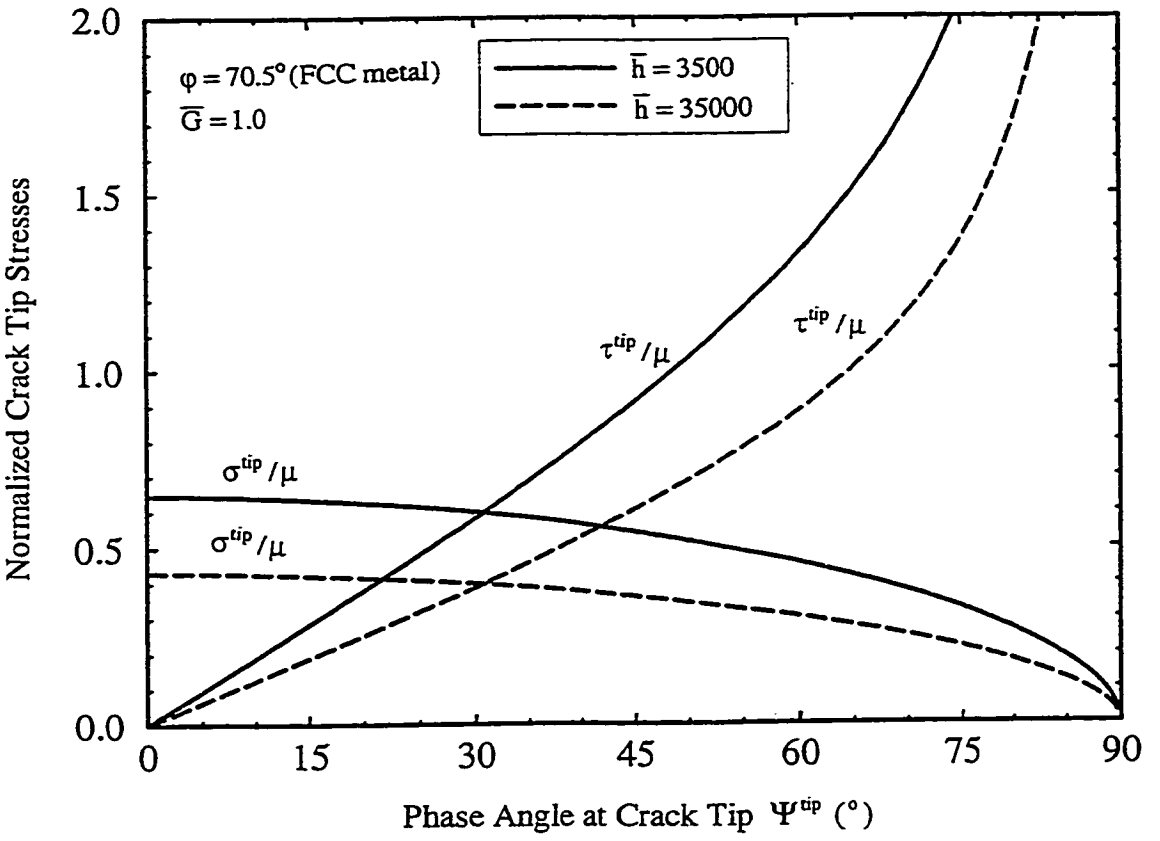

Figure 6-9(b) Effects of loading phase angle on interfacial crack tip stresses for FCC metals.

6.5 *Dislocation shielding effect on interfacial crack propagation*

The emitted dislocations will reduce the interface stress intensity factor at the crack tip such that more energy is required for crack initiation and propagation on the interface. This part will investigate this shielding effect in detail.

6.5.1 *Interface separation hypothesis under mixed mode loading*

Dislocations emitted from the crack tip will pile-up against the upper interface. This prevents the further emission of dislocations and impedes the blunting of the crack tip. Continuous loading will only increase the crack tip stresses. It is assumed that interface separation will occur when the combination of the tensile and shear stresses at the interfacial crack tip reaches a critical value. This separation hypothesis is expressed as

$$(\frac{\sigma^{tip}}{\sigma_b})^2 + (\frac{\tau^{tip}}{\tau_b})^2 = 1 \tag{6.28}$$

where σ_b and τ_b are the tensile strength and shear strength of the interface. Assuming that

$$\lambda = \sigma_b / \tau_b \tag{6.29}$$

and combining with Equations (6.20), (6.25) and (6.26), the interface separation condition can be expressed as

$$\sigma^{tip^2} + \lambda^2 (\frac{\tan \Psi^{tip}}{\sqrt{\cot \varphi}})^2 \sigma^{tip^2} = \sigma_b^2 \tag{6.30}$$

or

$$\sigma^{tip} = \frac{\sigma_b}{f\sqrt{\sin \varphi}} \tag{6.31}$$

where $f = [\frac{1}{\sin\varphi} + \lambda^2 \frac{\tan^2 \Psi^{tip}}{\cos\varphi}]^{\frac{1}{2}}$.

6.5.2 Critical dislocation number

When the separation condition in Equation (6.31) is satisfied, no more dislocation can emit from the crack tip and interface debonding tends to occur. The dislocation number at this point is defined as the critical dislocation number for crack initiation, and is denoted by n^*. n^* can be derived from Equations (6.14), (6.28), (6.29) and (6.31). If $\bar{\gamma} = 0$, n^* can be simplified as

$$n'(\bar{\sigma}_b, \Psi^{tip}, \bar{h}) = [\frac{(1-\nu)\bar{\sigma}_b \pi \sqrt{\bar{h}} [g_1(\varphi) + \tan\Psi^{tip} g_2(\varphi)]}{2f[\ln \bar{h} - \frac{3}{2}[f_1(\varphi)g_1(\varphi) + f_2(\varphi)g_2(\varphi)]]}]^2 . \tag{6.32}$$

It can be derived from Equation (6.32) that the larger n' is, the higher fracture toughness will be, since n^* provides crack tip shielding and blunting. The critical dislocation numbers from Equation (6.32) are shown in Figure 6-10 with $\Psi^{tip} = 0°$. It can be seen that the critical dislocation number increases dramatically when the combination of $\bar{h}$ and $\bar{\sigma}_b$ increases. Compared to equilibrium dislocation number n which is the available dislocations in the material without interface debonding, n' is the actual dislocation number that the layered material can achieve. Once n' is attained, the interface debonding will occur.

6.5.3 Interfacial crack initiation toughness Γ_i

Once crack tip stresses satisfy the separation condition expressed in Equation (6.31),

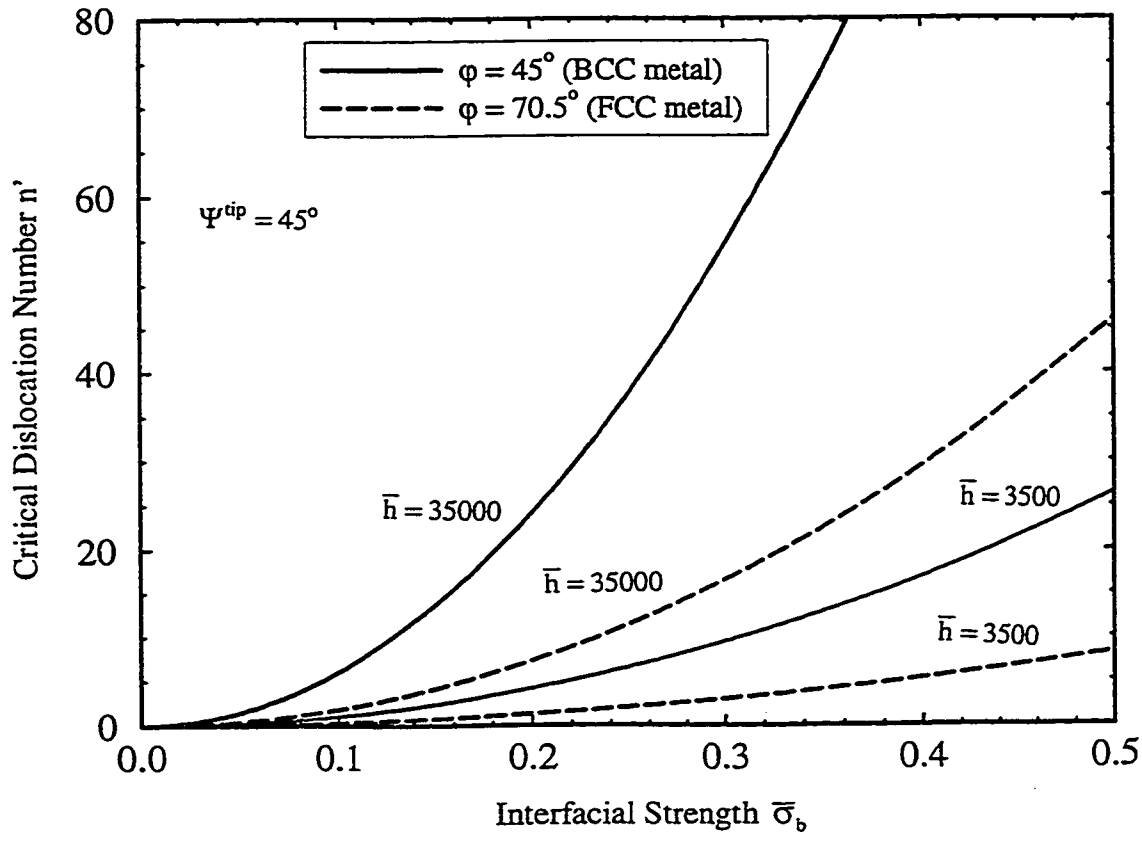

Figure 6-10 Critical dislocation number *n*'.

the interface debonding occurs. The far field applied stress intensity under this condition is then the fracture toughness of the layered material. In the present model, the far field applied stress intensity is the same as the stress intensity before dislocation emission (Suo and Hutchinson, 1989). Therefore, with the separation condition expressed by Equation (6.31), and Equations (3.26), (6.18) and (6.19), the interfacial crack initiation toughness Γ_i under mixed mode is

$$\Gamma_i(\Psi^{tip}, \bar{h}, \bar{\sigma}_b, \lambda) = \frac{1}{E_*}\mu^2 b\{[\frac{\sqrt{n'}\bar{\sigma}_b}{2\sqrt{2/\pi f}} + \frac{3}{2}n'\frac{1}{(1-\nu)\sqrt{2\pi\bar{h}}}f_1(\varphi)]^2 + [\frac{\sqrt{n'}\bar{\sigma}_b \tan\Psi^{tip}}{2\sqrt{2/\pi f}} + \frac{3}{2}n'\frac{1}{(1-\nu)\sqrt{2\pi\bar{h}}}f_2(\varphi)]^2\} \tag{6.33}$$

where n' is the critical dislocation number shown in Equation (6.32).

Calculation results for Γ_i are shown in Figure 6-11(a), (b) and (c). Figure 6-11(a) is for FCC metal with $\varphi = 70.5°$ and Figure 6-11(b) is for BCC metal with $\varphi = 45°$. Larger fracture energy is needed for interface crack initiation if the interface is stronger, or the metal layer is thicker. It can been seen that more mode II component is preferable to inhibit interface crack initiation because more energy is required to overcome the higher fracture toughness of the layered material.

For the same loading (phase angle) and geometrical (metal layer thickness) conditions, the difference between FCC metal and BCC metal is shown in Figure 6-11(c) that BCC metal requires higher fracture energy.

The effects of ratio of loading are illustrated in Figure 6-12. It can be seen that more mode II component (Ψ^{tip} changes from 0° to 90°) will increase the fracture energy thus the layered material gets more toughness.

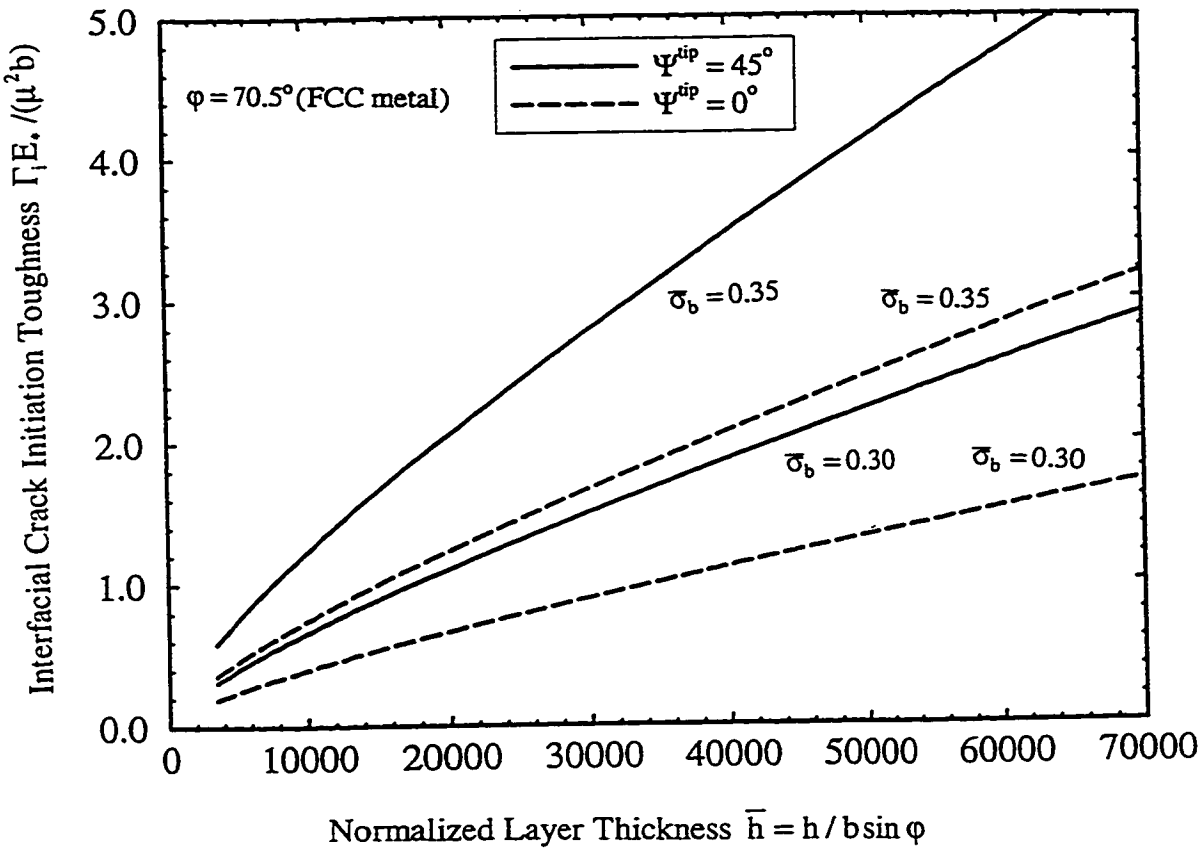

Figure 6-11(a) Interfacial crack initiation toughness for FCC metals ($\varphi = 70.5°$).

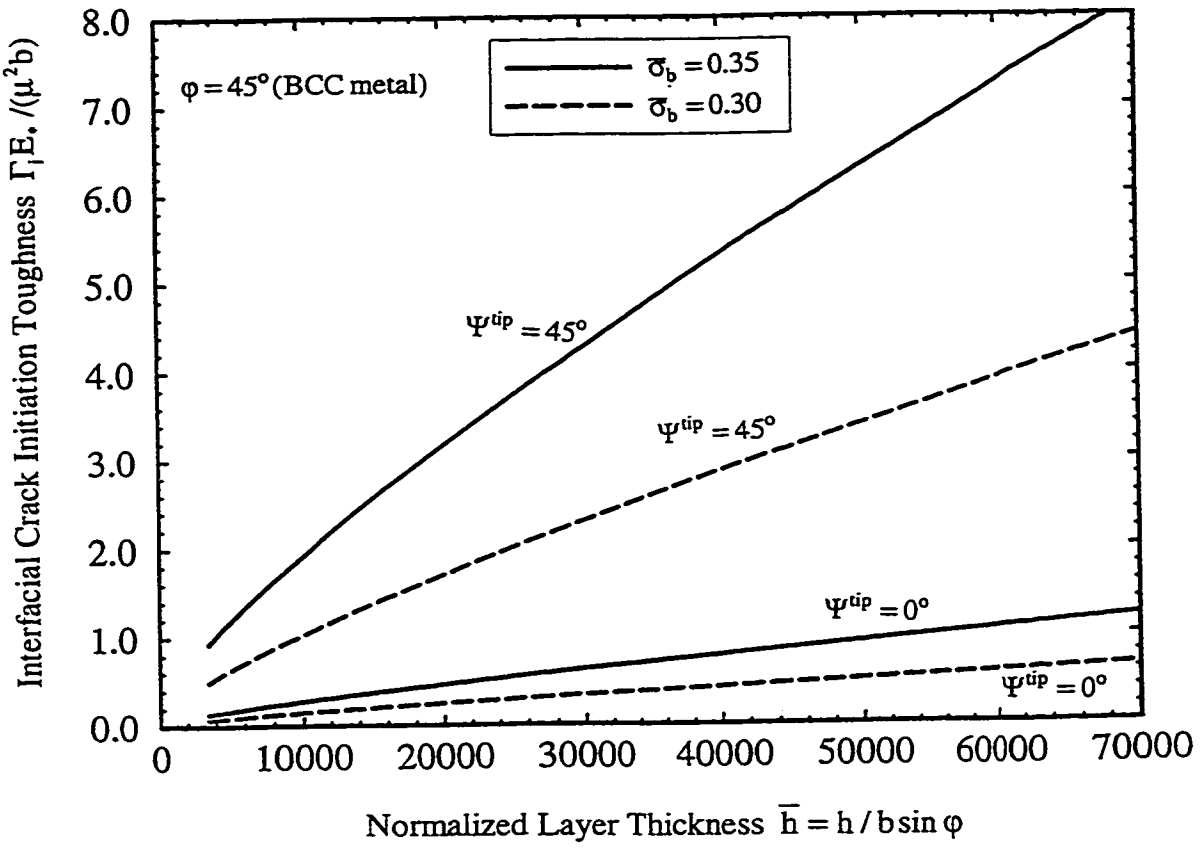

Figure 6-11(b) Interfacial crack initiation toughness for BCC metals ($\varphi = 45°$).

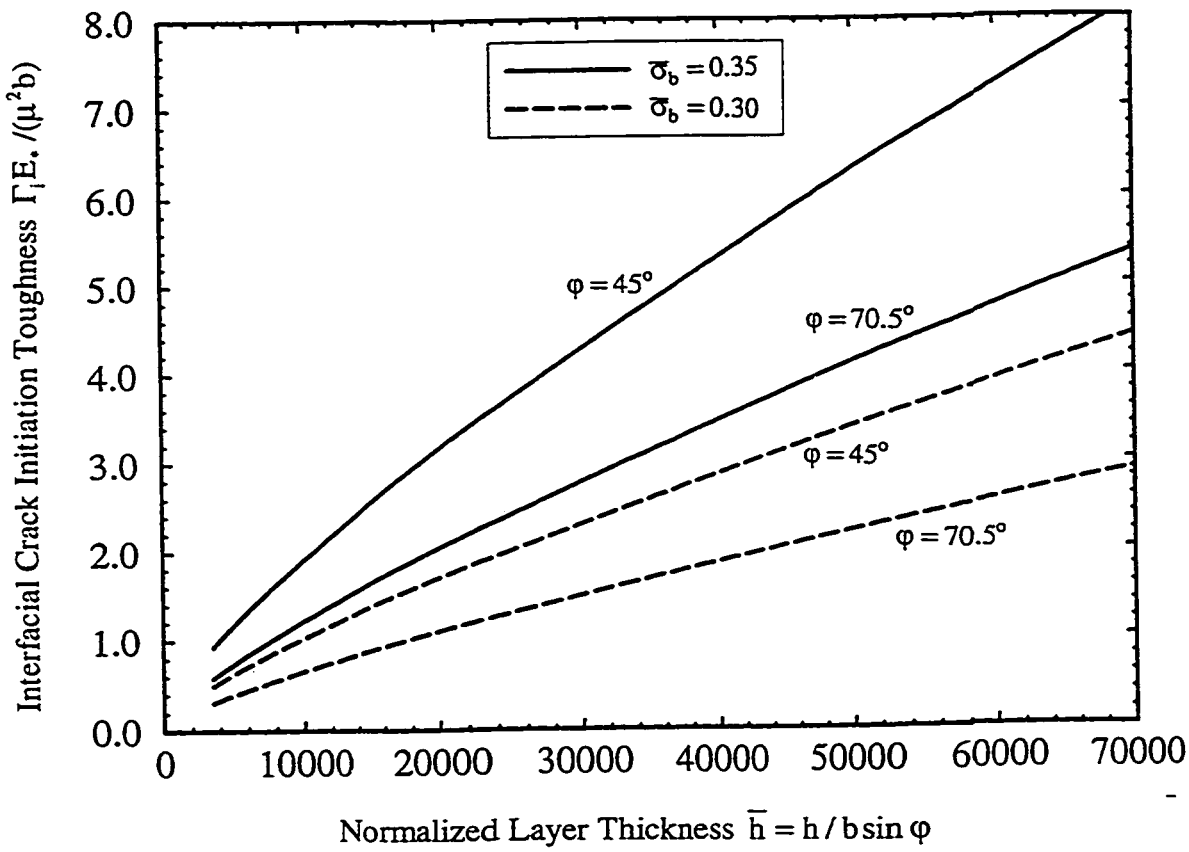

Figure 6-11(c) Comparison of interfacial crack initiation toughness between FCC metals and BCC metals.

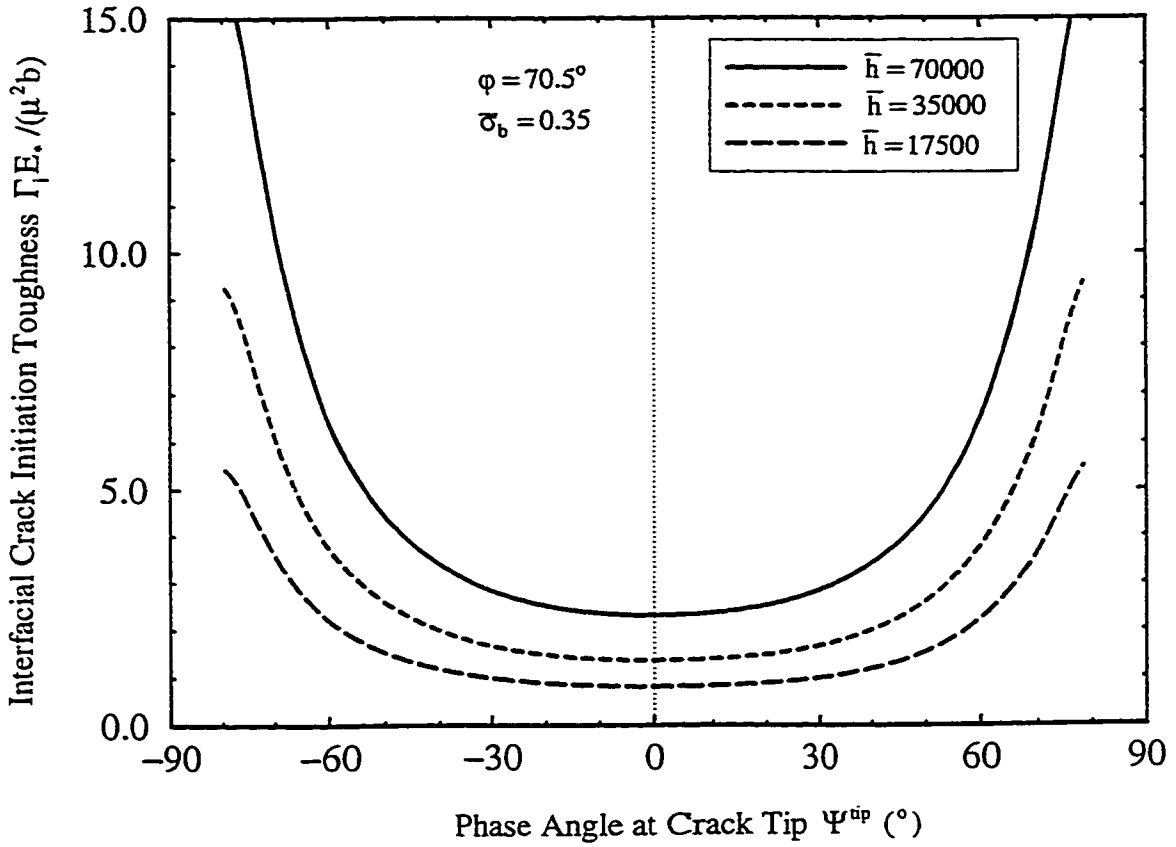

Figure 6-12 Effects of phase angle on interfacial crack initiation toughness.

6.5.4 Interfacial crack growth under mixed mode loading (resistance curve)

Atomic force microscopy (AFM) observations (Mao and Evans, 1997) have demonstrated that interfacial crack propagation in metal/ceramic layered material involves intermittent brittle debonding and plastic blunting through the activation of slip sources (see Figure 6-1). The process of the interfacial crack growth is approximated in this chapter by the procedure illustrated in Figure 6-13. It is assumed that dislocations are emitted from the interfacial crack tip and that the crack tip will be blunting. The interface ruptures when the separation condition in Equation (6.31) is satisfied. Once the interface rupture has occurred, subsequent crack propagation occurs in a repeating process, with an automatically sharp tip until interactions with other slip sources enable arrest by a new blunting event.

With the process illustrated in Figure 6-13, it is assumed that N superdislocations with the same strength, nb, are formed after the interfacial crack propagates a length of $\Delta a = L(N-1)$ as shown in Figure 6-14, where L is the crack advancement between two continuous slip steps. The location (r_i, φ_i) of the i'th superdislocation $(i = 1,2,...,N)$ in Figure 6-14 is governed by

$$\frac{iL}{\sin(\varphi_i - \varphi)} = \frac{h}{\sin\varphi_i \sin\varphi} \tag{6.34}$$

or

$$\left(\frac{h}{\sin\varphi_i}\right)^2 = (iL)^2 + \left(\frac{h}{\sin\varphi}\right)^2 - 2iL\frac{h}{\sin\varphi}\cos\varphi \ . \tag{6.35}$$

Rearranging Equation (6.35) to express φ_i in terms of iL/h and φ gives

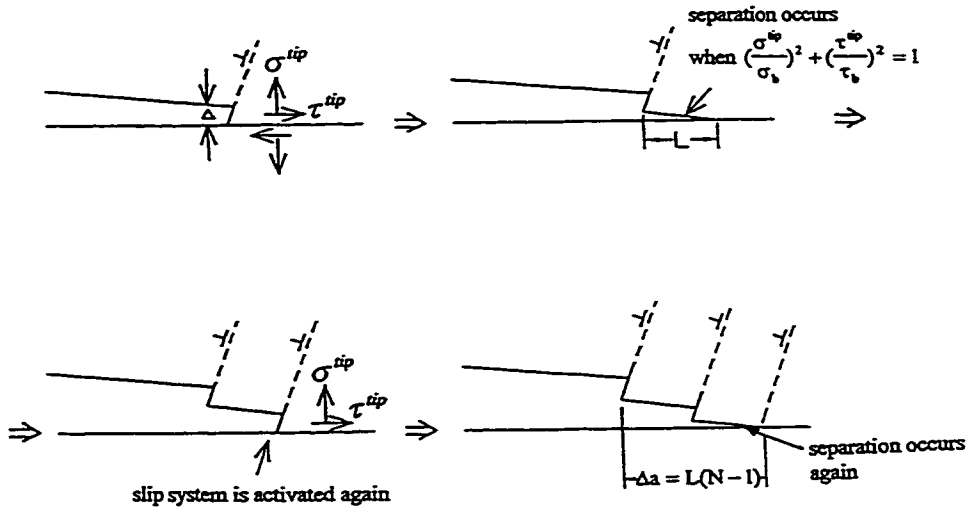

Figure 6-13 Interfacial crack propagation illustration in metal/ceramic layered material.

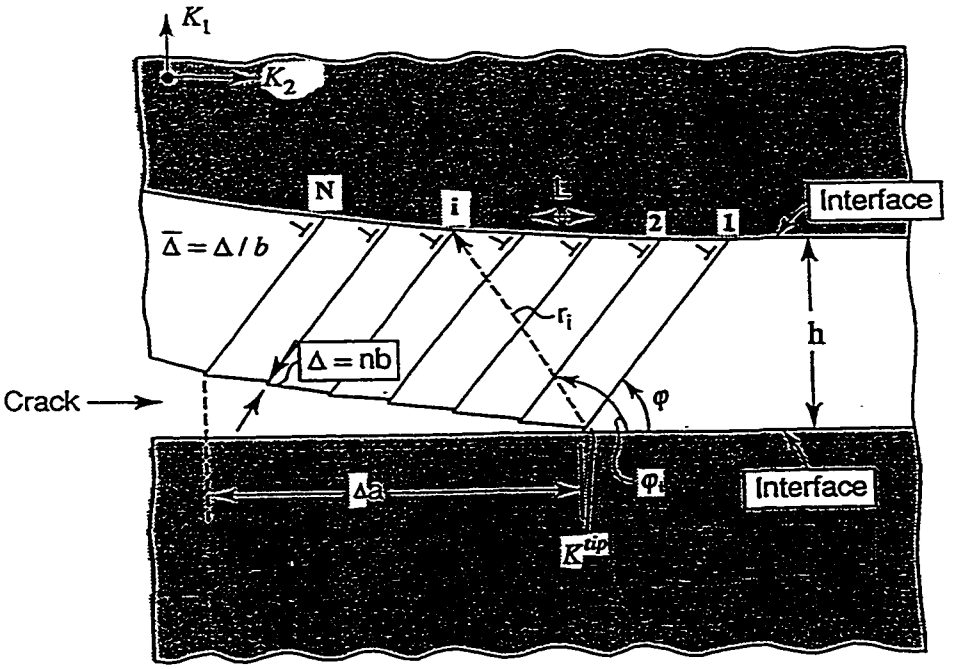

Figure 6-14 Superdislocation modeling for interfacial crack propagation process in metal/ceramic layered material.

$$\sin\varphi_i = \left[(iL/h)^2 + 1/\sin^2\varphi \;\; -2(iL/h)\cot\varphi\right]^{-1/2}. \tag{6.36}$$

This result is used in the text with the condition of $\sin\varphi \neq 0$.

For the i'th superdislocation located at (r_i, φ_i) with strength $b_1 + ib_2$, the shielding effect on the crack tip can be expressed as (details in Chapter 4)

$$k^i = \begin{bmatrix} k_1^i \\ k_2^i \end{bmatrix} = \frac{1+\alpha}{1-\nu}\begin{bmatrix} \frac{1}{2}\sin\varphi_i \cos\frac{3\varphi_i}{2}\frac{\mu b_1}{\sqrt{2\pi r_i}} + (\cos\frac{\varphi_i}{2} + \frac{1}{2}\sin\frac{\varphi_i}{2}\cos\frac{3\varphi_i}{2})\frac{\mu b_2}{\sqrt{2\pi r_i}} \\ \frac{1}{2}\sin\varphi_i \cos\frac{3\varphi_i}{2}\frac{\mu b_2}{\sqrt{2\pi r_i}} + (\cos\frac{\varphi_i}{2} - \frac{1}{2}\sin\frac{\varphi_i}{2}\cos\frac{3\varphi_i}{2})\frac{\mu b_1}{\sqrt{2\pi r_i}} \end{bmatrix}. \tag{6.37}$$

Considering $b_1 = \Delta\cos\varphi$, $b_2 = \Delta\sin\varphi$ and $r_i = \dfrac{h}{\sin\varphi_i}$, Equation (6.37) can be written as

$$k^i = \frac{\mu\Delta}{(1-\nu)\sqrt{h}}\delta k^i \tag{6.38}$$

where δk^i is the non-dimensional quantity

$$\delta k^i = \begin{bmatrix} \delta k_1^i \\ \delta k_2^i \end{bmatrix} = \frac{(1+\alpha)\sqrt{\sin\varphi_i}}{\sqrt{2\pi}}\begin{bmatrix} \frac{1}{2}\sin\varphi_i \cos\frac{3\varphi_i}{2}\cos\varphi + (\cos\frac{\varphi_i}{2} + \frac{1}{2}\sin\frac{\varphi_i}{2}\cos\frac{3\varphi_i}{2})\sin\varphi \\ \frac{1}{2}\sin\varphi_i \cos\frac{3\varphi_i}{2}\sin\varphi + (\cos\frac{\varphi_i}{2} - \frac{1}{2}\sin\frac{\varphi_i}{2}\cos\frac{3\varphi_i}{2})\cos\varphi \end{bmatrix}. \tag{6.39}$$

The values of δk^i are shown in Figure 6-15, where the negative values mean the anti-shielding effect of dislocation on crack tip. Δ is assumed to be constant during crack growth based on AFM observations (Mao and Evans, 1997), and $\Delta = n'b$. The total shielding effect from N superdislocations can be determined by

$$\begin{bmatrix} k_1 \\ k_2 \end{bmatrix} = \frac{\mu\Delta}{(1-\nu)\sqrt{h}}\begin{bmatrix} \delta k_1 \\ \delta k_2 \end{bmatrix} = \frac{\mu\Delta}{(1-\nu)\sqrt{h}}\begin{bmatrix} \sum_{i=1}^{N}\delta k_1^i \\ \sum_{i=1}^{N}\delta k_2^i \end{bmatrix}. \tag{6.40}$$

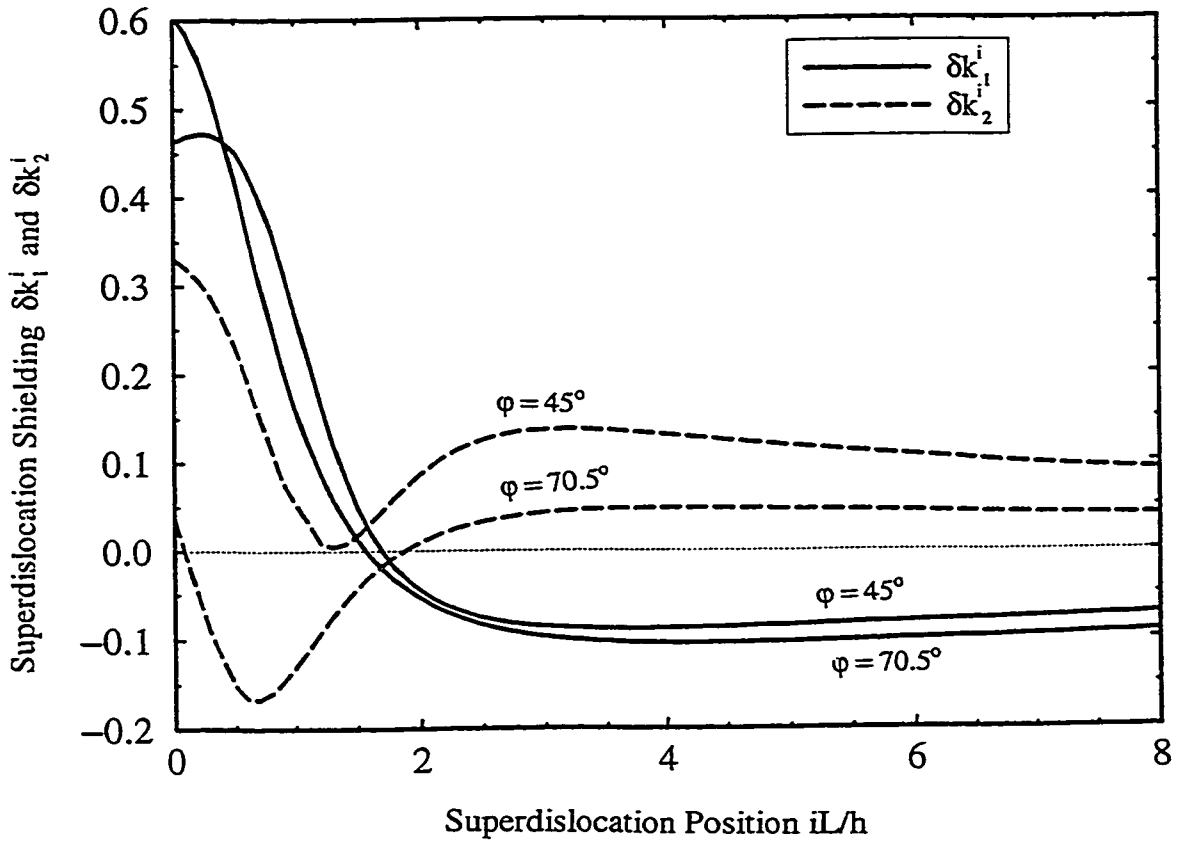

Figure 6-15 Superdislocation shielding effects.

Substituting Equations (6.40) and (6.18) into Equation (3.26), the fracture toughness during crack growth is given by

$$\Gamma_R = G_c = \frac{1}{E_*}\{[\frac{\sigma_b\sqrt{\Delta}}{2\sqrt{2/\pi}f} + \frac{\mu\Delta}{(1-\nu)\sqrt{h}}\delta k_1]^2 + [\frac{\sigma_b\sqrt{\Delta}}{2\sqrt{2/\pi}f}\tan\Psi^{tip} + \frac{\mu\Delta}{(1-\nu)\sqrt{h}}\delta k_2]^2\}. \quad (6.41)$$

The terms $\frac{\sigma_b\sqrt{\Delta}}{2\sqrt{2/\pi}f}$ and $\frac{\sigma_b\sqrt{\Delta}}{2\sqrt{2/\pi}f}\tan\Psi^{tip}$ in Equation (6.41) are the contributions to toughening from crack tip blunting, $\frac{\mu\Delta}{(1-\nu)\sqrt{h}}\delta k_1$ and $\frac{\mu\Delta}{(1-\nu)\sqrt{h}}\delta k_2$ are the contributions from dislocation shielding. The normalized fracture toughness for crack propagation is

$$\Gamma_R E_* /(\mu^2 b) = [\frac{\overline{\sigma}_b\sqrt{\overline{\Delta}}}{2\sqrt{2/\pi}f} + \frac{\overline{\Delta}}{(1-\nu)\sqrt{\overline{h}}}\delta k_1]^2 + [\frac{\overline{\sigma}_b\sqrt{\overline{\Delta}}}{2\sqrt{2/\pi}f}\tan\Psi^{tip} + \frac{\overline{\Delta}}{(1-\nu)\sqrt{\overline{h}}}\delta k_2]^2 \quad (6.42)$$

where $\overline{\Delta} = \Delta / b_*$. δk_1 and δk_2 will increase with crack extension and attain a constant value when a steady-state condition is reached.

Taking L/h = 0.1, the resistance curve is calculated for metal/ceramic layered material as shown in Figure 6-16. It can be seen that steady-state can be achieved when interfacial crack propagates a distance several times the middle metal layer thickness. The effect of layer thickness shown in Figure 6-16(a) indicates that thicker metal layer gets more toughening. For example, taking middle metal layer as gold, when h changes from 10 μm ($\overline{h} = 35000$) to 20 μm ($\overline{h} = 70000$), the interface toughness is doubled. Figure 6-16(b) shows that more toughness can be obtained through stronger interface, which is obvious because it requires more energy to overcome the interface strength barrier to debond the interface. The mode mixity (phase angle) effects are presented in Figures 6-16(c) and (d)

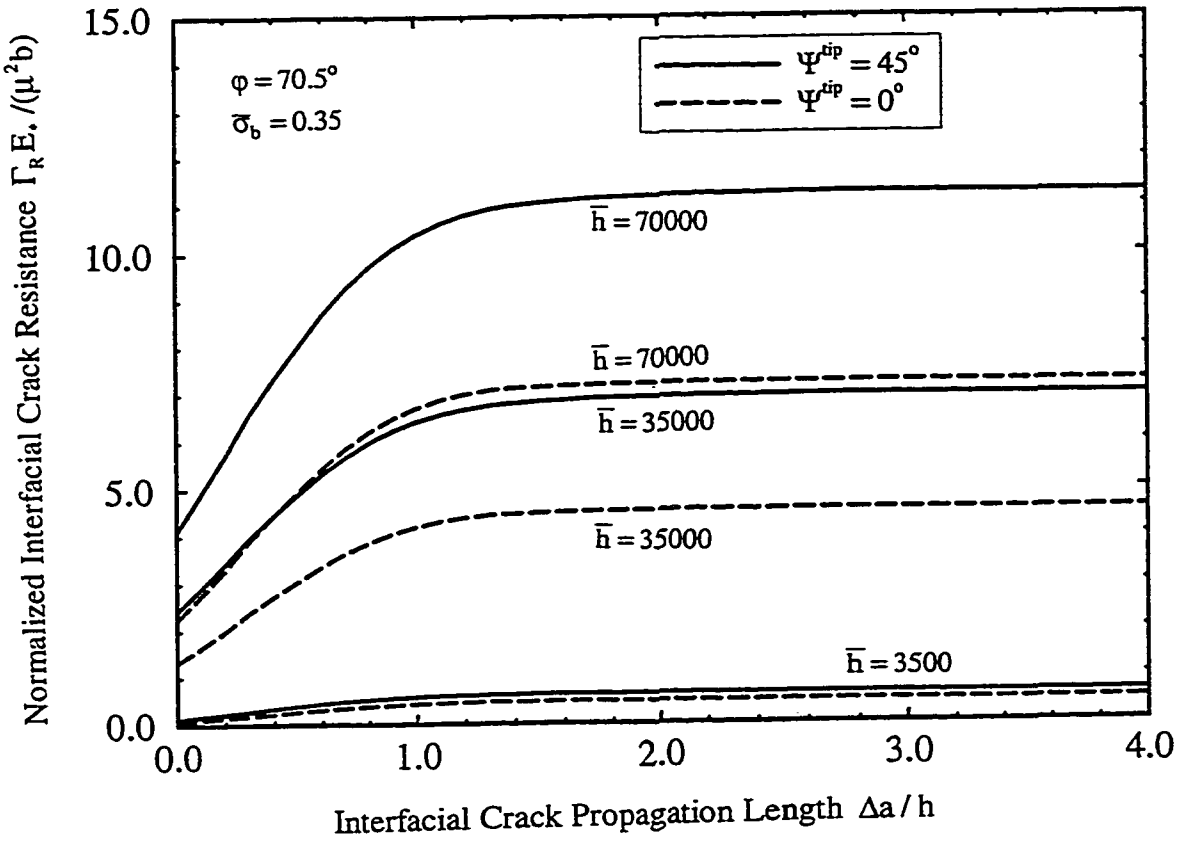

Figure 6-16(a) R-curves for layered materials: effects of middle layered thickness.

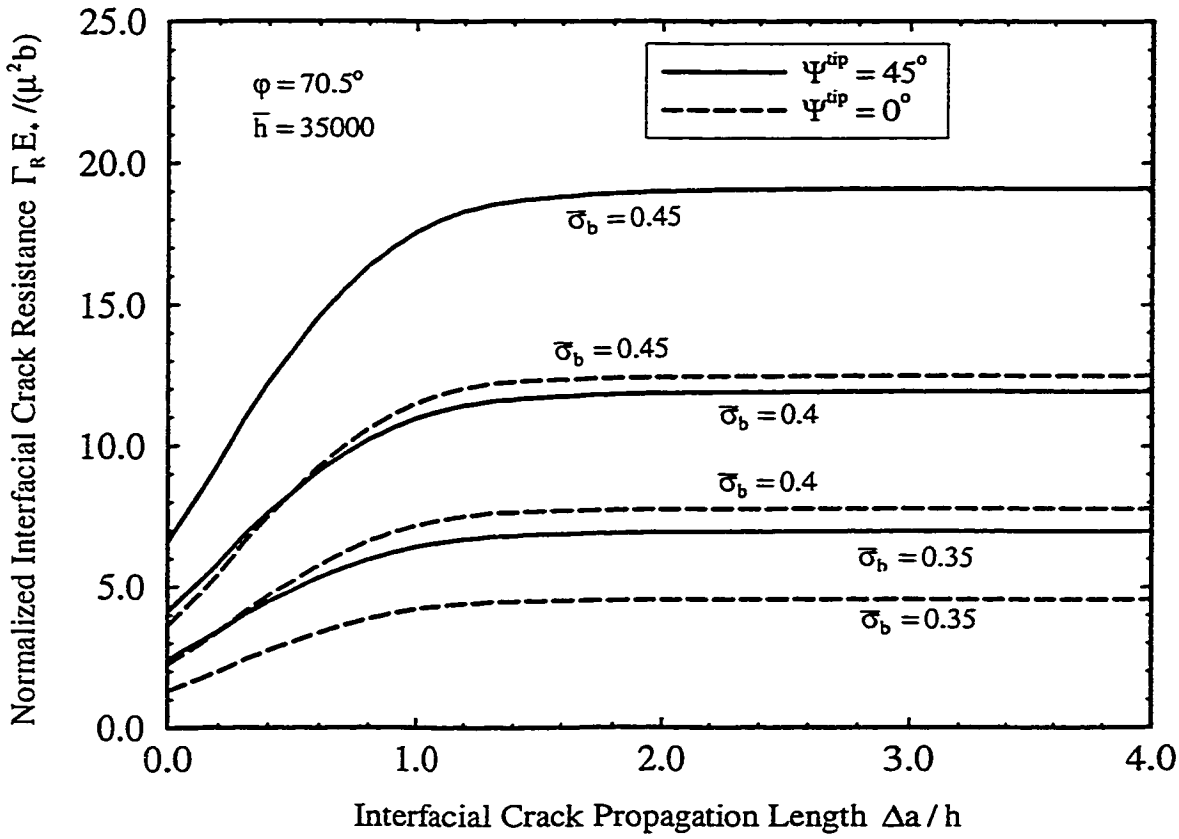

Figure 6-16(b) R-curves for layered materials: effects of interface strength.

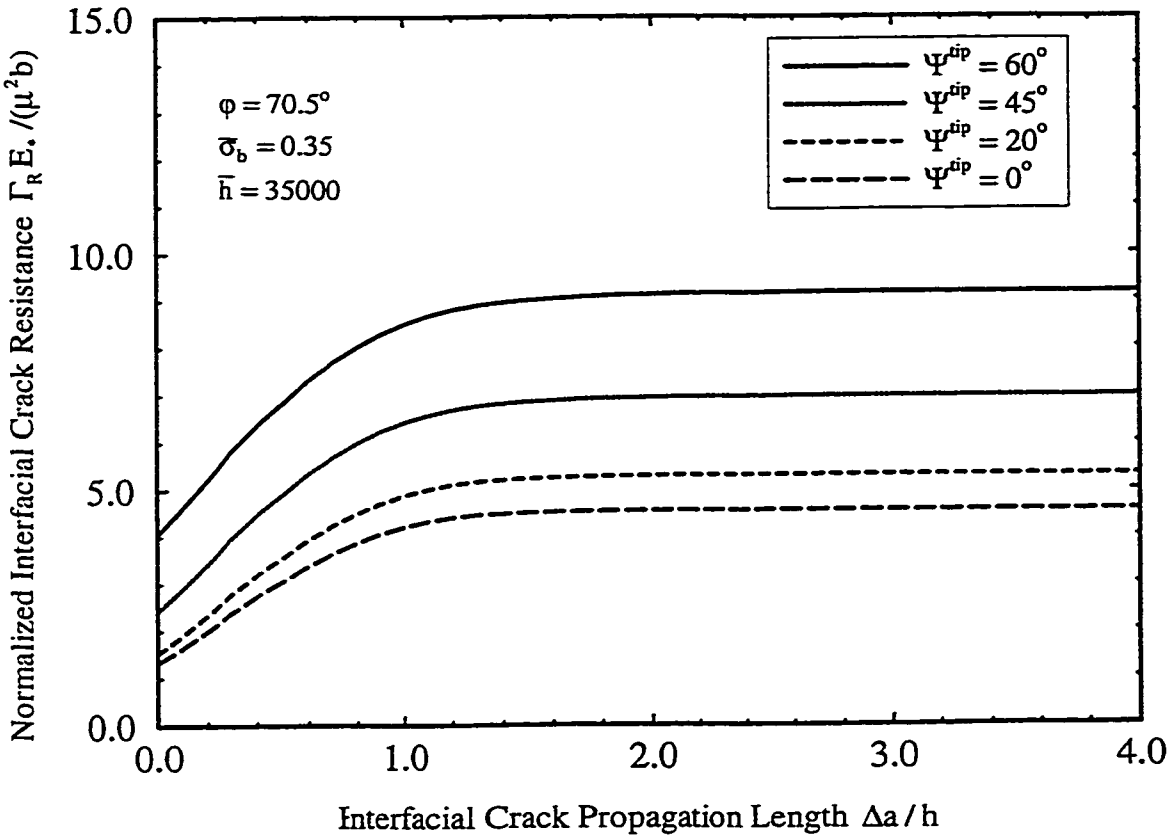

Figure 6-16(c) R-curves for layered materials: phase angle effects for FCC metal.

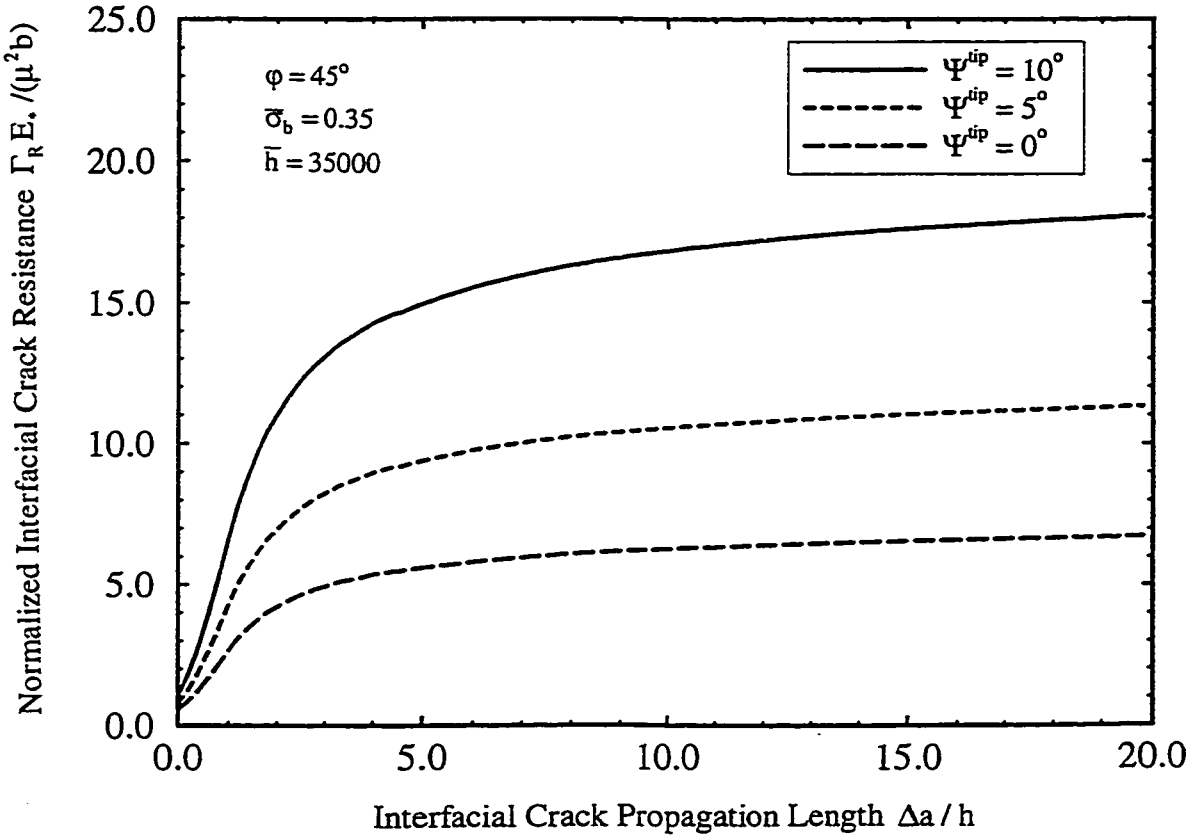

Figure 6-16(d) R-curves for layered materials: phase angle effects for BCC metals.

for FCC and BCC metal, respectively. Larger phase angle which means more mode II load component can get higher toughness, which is in accordance with other work (e.g. Tvergaard and Hutchinson, 1994).

The general effects of mode mixity on steady-state fracture toughness are illustrated in Figure 6-17. In Figure 6-17, the middle metal layer thickness is changed to compare the results. In summary, when the mode II load component increases, the interface fracture toughness gets higher value. In practice, if the layered material involves more mode II load condition, it is more difficult to get failure. On the other hand, pure mode I load condition will make the layered materials easy for failure.

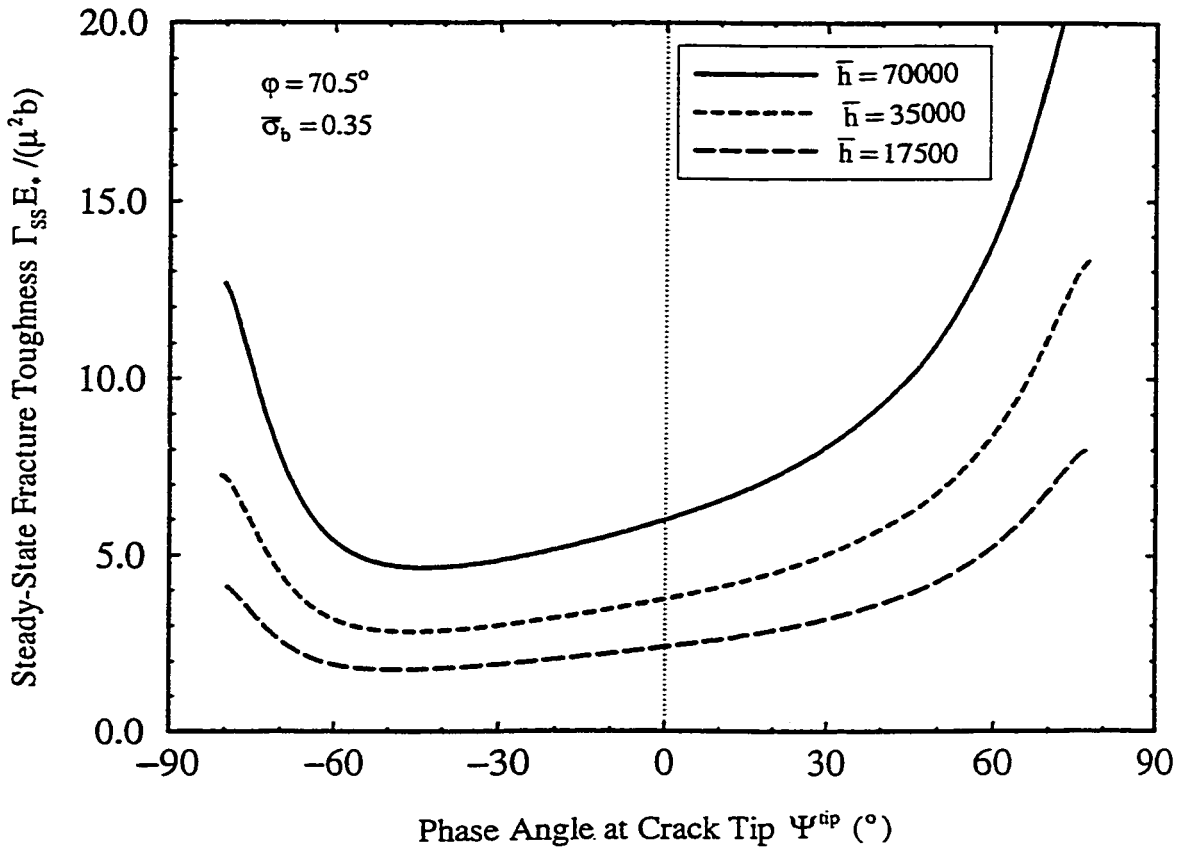

Figure 6-17 Effects of phase angle on steady-state toughness with change of middle metal layer thickness.

Chapter 7

Conclusions and Recommendations

7.1 Ductile versus brittle behavior of metal/ceramic layered materials

The criterion for ductile versus brittle behavior in layered materials has been investigated in terms of the dislocation emission and interface debonding in this dissertation. The results of this portion of work can be summarized as:

1. Based on the analysis of forces on the dislocation emitted from the interfacial crack tip, the critical energy release rate for dislocation emission, G_{disl}, has been obtained. This value provides the criterion to judge the ductile behaviour of the metal/ceramic layered material.
2. The length scale (thickness) controls G_{disl} through the image force due to the upper interface and the atomic scale phase angle. Calculations of G_{disl} have shown that G_{disl} is not sensitive to the length scale when the thickness exceeds a critical value (comparable to Burgers vector). The results based on bimaterial system (Rice et al., 1990; Beltz and Rice, 1992) are good approximations. On the other hand, for thin layered materials (e.g., nano-scale materials), the layer thickness will change the condition for ductile versus brittle transition significantly.
3. The calculations showed that the mode mixity has a significant effect on G_{disl}. For the example of the copper/sapphire layered material subject to bending, an mode mixity with phase angle of $-77°$ can get the minimum G_{disl}. The

maximum G_{disl} is under the mode mixity with phase angle of 0°, which indicates mode I condition.

4. The comparison of G_{disl} with G_{cleav} (the critical energy release rate for interfacial cleavage) has indicated that G_{disl} is less than G_{cleav} in the cases in which the metal layer thickness is above micrometer. Therefore, dislocation can easily nucleate and the behavior of the layered material is ductile.
5. To extend this work, a dislocation loop could be considered for three dimensional analysis, and G_{disl} can be obtained from an energy analysis (Wang and Anderson, 1991). To eliminate the uncertainty of the undefined effective dislocation core size r_c, another approach is to employ the Peierls-type stress-strain relationship for the emitted dislocation. This approach was proposed by Rice et al. (1992) to analyze the dislocation in homogeneous material, and by Beltz and Rice (1992) to investigate the dislocation behavior in bimaterial system.

7.2 Interfacial toughening in metal/ceramic layered materials

Interfacial toughening has been analyzed by considering dislocation plasticity in layered materials subject to mixed mode loading condition. Dislocation emission and shielding in metal/ceramic layered materials have been investigated in detail in the present study. The results of this portion of work can be concluded as:

1. It has been predicted that, for different material system, there always exists an

optimal loading condition to get the maximum equilibrium dislocation number, which indicates maximum plasticity involved in the material. However, this maximum equilibrium dislocation number cannot be reached when the interface is not so strong that interface debonding is inevitable.

2. The effect of these emitted dislocations is to modify the interfacial crack behavior. Employing discrete superdislocation concept, the dislocation plasticity in terms of dislocation blunting and shielding effects on crack tip field and interfacial crack propagation, has been analyzed. The results have indicated the dislocation plasticity significantly increases the interfacial crack fracture toughness.
3. A model of periodically enabling dislocation emission and interface debonding has been established to simulate the interfacial crack propagation process in metal/ceramic layered materials. Based on this model, the interfacial toughening for interfacial crack propagation has been examined. R-curves were obtained for FCC and BCC metals, and steady-state interfacial crack propagation has been predicated when the propagation length exceeds twice of the metal layer thickness.
4. The analytical model and numerical results have showed the strong dependence of interfacial crack fracture toughness on layer thickness and mode mixity.

For future work, experiments can be set up to examine the optimal loading phase angle for different materials system. Also, experiments are needed to obtain the interfacial toughness of the layered materials. For example, the experimental

methodology proposed by Turner and Evans (1996) can be implemented to compare the analytical results presented in this dissertation.

Bibliography

Aburatani, H., Harada, S., Uchino, K., Furuta, A. and Fuda, Y. (1994) Destruction mechanisms in ceramic multilayer actuators. Japanese J. Appl. Phys. **33**, 3091-3094.

Anderson, G. P., DeVries, K. L. and Williams, M. L. (1974) Mixed mode stress field effect in adhesive fracture. Int. J. of Fracture **10**, 565-583.

Anderson, P. M. and Li, C. (1993) Crack-dislocation modeling of ductile-to-brittle transitions in multilayered materials. Mat. Res. Soc. Symp. Proc. **308**, 731-736.

Anderson, P. M. and Li, C. (1995) Hall-Petch relations for multilayered materials. Nanostructured Materials **5**, 349-362.

Aoki, S., Kishimoto, K., Takeya, A. and Sakata, M. (1984) Effects of microvoids on crack blunting and initiation in ductile materials. Int. J. of Fracture **24**, 267-278.

Barnett, D. M. and Lothe, J. (1974) An image force theorem for dislocations in anisotropic bicrystals. J. Phys. F: Metal Phys. **4**, 1618-1635.

Beltz, G. E. and Freund, L. B. (1994) Analysis of the strained-layer critical thickness concept based on a Peierls-Nabarro model of a threading dislocation. Phil. Mag. **A69**, 183-202

Beltz, G. E. and Rice, J. R. (1992) Dislocation nucleation at metal-ceramic interfaces. Acta Metall. Mater. **40**, S321-S331.

Beltz, G. E. and Wang, J. S. (1992) Crack direction effects along copper/sapphire interfaces. Acta Metall. Mater. **40**, 1675-1683.

Bilby, B. A., Contrell, A. H. and Swinden, K. H. (1963) Proc. Roy. Soc. London **A272**, 304-1963.

Bose, K. and Ponte Castaneda, P. (1992) Stable crack growth under mixed-mode conditions. J. Mech. Phys. Solids **40**, 1053-1103.

Burgers, J. M. (1939) Proc. Kon. Ned. Akad. Wetenschap. **42**, 293, 378.

Cao, H. C. and Evans, A. G. (1989) An experimental study of the fracture resistance of bimaterial interface. Mechanics of Materials **7**, 295-305.

Chan, K. S. (1995) A fracture model for hydride-induced embrittlement. Acta Metall. Mater. **43**, 4325-4335.

Chang, S. J. and Ohr, S. M. (1981) Dislocation-free zone model of fracture. J. Appl. Phys. **52**, 7174-7181.

Charalambides, P. G., Lund, J., Evans, A. G. and McMeeking, R. M. (1989) A test specimen for determining the fracture resistance of bimaterial interfaces. J. Appl. Mech. **56**, 77-82.

Chen, Y. F. and Erdogan, F. (1996) The interface crack problem for a non-homogeneous coating bonded to a homogeneous substrate. J. Mech. Phys. Solids. **44.** 771-788.

Cherepanov, G. P. (1962) The stress state in a heterogeneous plate with slits (in Russian). Izvestia AN SSSR, OTN, Mekhan. i Mashin. **1**, 131-137.

Cherepanov, G. P. (1979) Mechanics of Brittle Fracture. McGraw-Hill, New York.

Chou, Y. T. (1966) Screw dislocations in and near lameller Inclusions. Phys. Stat. Sol. **17**, 509-516.

Chu, S. N. G. (1982) Screw dislocation in a two-phase isotropic thin film. J. Appl. Phys. **53**, 3019-3023.

Comninou, M. (1977a) A property of interface dislocations. Phil. Mag. **36**, 1281-1283.

Comninou, M. (1977b) The interface crack. J. Appl. Mech. **44**, 631-636.

Comninou, M. (1977c) Interface crack with friction in the contact zone. J. Appl. Mech. **44**, 780-781.

Cottrel, A. H. (1964) Theory of crystal dislocations. Gordon and Breach, New York.

De Graef, M., Dalgleish, B. J., Turner, M. R. and Evans, A. G. (1992) Interface between alumina and platinum: structure, bonding and fracture resistance. Acta Metall. Mater. **40**, S333-S344.

Doner, M., Chang, H. and Conard, H. (1974) Plastic flow and dislocation structure at small strains in OFHC copper deformed in tension, torsion and combined tension-torsion. J. Mech. Phys. Solids **22**, 555-573.

Dundurs, J. (1969) Elastic interaction of dislocation with inhomogeneties. In Mathematical theory of dislocations (ed. Toshio Mura), pp. 70-115. American Society of Mechanical Engineering, New York.

Dundurs, J. and Sendeckyj, G. P. (1967) Behavior of an edge dislocation near a bimetallic interface. J. App. Phys. **36**, 3353-3354.

Embury, J. D. and Hirth, J. P. (1994) On dislocation storage and the mechanical response of fine scale microstructures. Acta Metall. Mater. **42**, 2051-2056.

Embury, J. D., Freund, L. B., Needleman, A., Shih, C. F., Spaepen, F. and Suresh, S. (1996) Summary, J. Mech. Phys. Solids. **44,** 823-825.

England, A. H. (1965) A crack between dissimilar media. J. Appl. Mech. **32**, 400-402.

Erdogan, F., 1965. Stress distribution in bonded dissimilar materials with cracks. J. Appl. Mech. **32**, 403-410.

Erdogan, F. and Gupta, G. (1971) The stress analysis of multi-layered composites with a flaw. Int. J. Solids Structures **7**, 39-61.

Eshelby, J. D. (1951) The force on an elastic singularity. Phil. Trans. Roy. Soc. **A244**, 87-112.

Eshelby, J. D. (1956) The continuum theory of lattice defects. In Prog. Solid State Physics (ed. F. Seitz and D. Turnbull), pp. 79-114. Academic Press, New York.

Evans, A. G. and Dalgleish, B. J. (1992) The fracture resistance of metal-ceramic interfaces. Acta Metall. Mater. **40**, S295-S306.

Evans, A. G. and Hutchinson, J. W. (1989) Effects of non-planarity of the mixed mode fracture resistance of bimaterial interfaces. Acta Metall. Mater. **37**, 909-916.

Evans, A. G. and Hutchinson, J. W. (1995) The thermomechanical integrity of thin films and multilayers. Acta Metall. Mater. **43**, 2507-2530.

Evans, A. G., Ruhle, M., Dalgleish, B. J. and Charalambides, P. G. (1990) The fracture energy of bimaterial interfaces. Mater. Sci. Engng. **A126**, 53-64.

Finot, M. and Suresh, S. (1996) Small and large deformation of thick and thin-film multi-layers: effects of layer geometry, plasticity and compositional gradients. J. Mech. Phys. Solids **44**, 683-722.

Fleck, N. A., Hutchinson, J. W. and Suo. Z. (1991) Crack path selection in a brittle adhesive layer. Int. J. Solids Structures **27**, 1683-1703.

Freund, L. B. (1987) The stability of a dislocation threading a strained layer on a substrate. J. Appl. Mech. **54**, 553-557.

Furuta, A. and Uchino, K. (1993) Dynamic observation of crack propagation in piezoelectric multilayer actuators. J. Am. Ceram. Soc. **76**, 1615-16117.

Gautesen, A. K. and Dundurs, J. (1987) The interface crack in a tension field. J. Appl. Mech. **54**, 93-98.

Gautesen, A. K. and Dundurs, J. (1988) The interface crack under combined loading. J. Appl. Mech. **55**, 580-586.

Gong, X. and Suo, Z. (1996) Reliability of ceramic multilayer actuators: a nonlinear finite element simulation. J. Mech. Phys. Solids **44**, 751-770.

He, M. Y. and Hutchinson, J. W. (1989) Kinking of a crack out of an interface. J. Appl. Mech. **56**, 270-278.

Head, A. K. (1953) Edge dislocation in inhomogeneous media. Proc. Phys. Soc. London **B66**, 793-801.

Hertzberg, R. W. (1996) Deformation and fracture mechanics of engineering materials (4^{th} edition). John Wiley and Sons, New York.

Hirth, J. P. (1998) Private communication.

Hirth, J. P. and Lothe, J. (1982) Theory of Dislocations (2^{nd} edition). John Wiley and Sons, New York.

Hsia, K. J. and Argon, A. S. (1994) Experimental study of the mechanisms of the brittle-to-ductile transition of cleavage fracture in Si single crystals. Mater. Sci. Engng. **A176**, 110-111.

Hsia, K. J., Suo, Z. and Yang, W. (1994) Cleavage due to dislocation confinement in layered materials. J. Mech. Phys. Solids **42**, 877-896.

Huang, H. and Gerberich, W. W. (1992) Crack-tip dislocation emission arrangements for equilibrium - II, comparisons to analytical and computer simulation models. Acta. Metall. Mater. **40**, 2873-2881.

Hull, D. (1975) Introduction to dislocations. Pergamon, New York.

Hutchinson, J. W. and Suo, Z. (1992) Mixed mode cracking in layered materials. Adv. Appl. Mech. **29**, 63-191.

Hutchinson, J. W., Mear, M. E. and Rice. J. R. (1987) Crack paralleling an interface between dissimilar materials. J. Appl. Mech. **54**, 828-832.

Irwin, G. R. (1948) Fracture mechanics. In Fracturing of Metals, pp. 147-166. American Society for Metals, Cleveland.

Irwin, G. R. (1957) Relation of stresses near a crack to the crack extension force. In 9th International Congress of Applied Mechanics, pp. 245-254. Brussels.

Kamat, S. V. A., Hirth, J. P. and Carnahan, B. (1987) Image forces on screw dislocations in multilayer structures. Scripta Metall. **21**, 1587-1592.

Kelly, A., Tyson, W. and Conttrell, A. H. (1967) Ductile and brittle crystals. Phil. Mag. **15**, 567-586.

Kinloch, A. J. (1987) Adhesion and adhesives. Chapman and Hall, London.

Koehler, J. S. (1941) On the dislocation theory of plastic deformation. Phy. Rev. **60**, 397-410.

Kokini, K. and Takenchi, Y. R. (1995) Interface cracks in thermally loaded multilayer ceramic coatings. In Fracture Mechanics: 25th volume, ASTM STP 1220 (ed. F. Erodogan), pp. 177-190. American Society of Testing and Materials, Philaadelphia.

Kovacs, I. and Zsoldos, L. (1973) Dislocation and plastic deformation. Pergamon, Oxford.

Lardner, R. W. (1974) Mathematical theory of dislocation and fracture. University of Toronto Press.

Leung, D. K., He, M. Y. and Evans, A. G. (1995) The cracking resistance of Nanoscale layers and films. J. Mater. Res. **10**, 1693-1699.

Leung, D. K., Zhang, N. T., McMeeking, R. M. and Evans, A. G. (1995) Crack progression and interface debonding in brittle/ductile nanoscale multilayers. J. Mater. Res. **10**, 1958-1968.

Li, M. Z. and Mao. X. (1998a) Length scale (thickness) relationship of ductile versus brittle behavior at the interface in layered materials. Acta. Metall. Mater., submitted.

Li, M. Z. and Mao. X. (1998b) Interfacial toughening by dislocation shielding in metal/ceramic layered materials. Acta. Metall. Mater., submitted.

Liang, Y. M. and Liechti, K. M. (1995) Toughening mechanisms in mixed-mode interfacial fracture. Int. J. Solids Structures **32**, 957-978.

Liechti, K. M. and Chai, Y. S. (1992) Asymmetric shielding in interfacial fracture under in-plane shear. J. Appl. Mech. **59**, 295-304.

Liechti, K. M. and Hanson, E. C. (1988). Nonlinear effects in mixed-mode interfacial delaminations. Int. J. of Fracture **36**, 199-217.

Lii, M. J., Chen, X. F., Katz, Y. and Gerberich, W. W. (1990) Dislocation modeling and acoustic emission observation of alternating ductile/brittle events in Fe-3wt%Si crystals. Acta Metall. Mater. **38**, 2435-2453.

Lin, I. H. and Thomson, R. (1986) Cleavage dislocation emission and shielding for cracks under general loading. Acta Metall. Mater. **34**, 187-206.

Lubarda, V. A., Blume, J. A. and Needleman, A. (1993) An analysis of equilibrium dislocation distributions. Acta Metall. Mater. **41**, 625-642.

Majumdar, B. S. and Burns, S. J. (1983) A Griffith crack shielded by a dislocation pile-up. Int. J. of Fracture **21**, 229-240.

Malyshev, B. M. and Salganik, R. L. (1965) The strength of adhesive joints using the theory of cracks. Int. J. Fracture Mech. **5**, 114-128.

Mao, X. and Evans, A. G. (1997) The influence of blunting on crack growth at oxide/metal interfaces. Acta Metall. Mater. **45**, 4263-4270.

Mao, X. and Li, M. Z. (1998) Mode mixity effect on interface crack initiation and growth in metal/ceramic layered materials. J. Mech. Phys. Solids, accepted (paper No. 98/56, JMPS).

Marsh, P. G., Zielinske, W., Huang, H. and Gerverich, W. W. (1992) Crack-tip dislocation emission arrangements for equilibrium - III. application to larger applied stress intensities. Acta Metall. Mater. **40**, 2883-2894.

Mason, D. D. (1979) Segregation-induced embrittlement of grain boundaries. Phil. Mag. **39**, 455-468.

McMeeking, R. M. (1977) Finite deformation analysis of crack-tip opening in elastic-plastic materials and implications for fracture. J. Mech. Phys. Solids **25**, 357-381.

Muskhelishvili, N. I. (1953) Singular integral equations: boundary problems of function theory and their application to mathematical physics. Groningen, Netherlands: P. Noordhoff.

Nabarro, F. R. N. (1979) Dislocation in solids (volume 4) . Norh-Holland, New York.

Nakahara, S. and Willis, J. R. (1973) Some remarks on interfacial dislocations. J. Phys. F: Metal Phys. **3**, L249-L254.

O'Dowd, N. P., Stout, M. G. and Shih, C. F. (1992) Fracture toughness of alumina-niobium interfaces: experiments and analyses. Phil. Mag. **A66**, 1037-1064.

Orowan, E. (1934) Z. Phys. **89**, 605-613; 634-659.

Park, J. H. and Earmme, Y. Y. (1986) Applications of conservation integrals to interfacial crack problems. Mech. Mater. **5**, 261-276.

Peach, M. and Koehler, J. S. (1950) The forces exerted on dislocations and the stress fields produced by them. Phy. Rev. **80**, 436-439.

Polanyi, M. (1934) Z. Phys. **89**, 660-664.

Reimanis, I. E., Dalgleish, B. J. and Evans, A. G. (1991) The fracture resistance of a model metal/ceramic interface. Acta Metall. Mater. **39**, 3133-3141.

Rice, J. R. (1968) Mathematical analysis in the mechanics of fracture. In Fracture Volume II (ed. H. Liebowitz), pp. 191-311.

Rice, J. R. (1985) Conserved integrals and energetic force. In Fundamentals of deformation and fracture (Eshelby memorial symposium) (ed. B. A. Bilby, K. J. Miller and J. R. Willis), pp. 33-56. Cambridge University Press.

Rice, J. R. (1987) Mechanics of brittle cracking of crystal lattices and interfaces. In Chemistry and physics of Fracture (ed. R. M. latanision and R. H. Jones), pp. 22-43. Martinus Nijhoff Publishers BV, Dordrecht, The Netherlands.

Rice, J. R. (1988) Elastic fracture mechanics concepts for interfacial cracks. J. Appl. Mech. **55**, 98-103.

Rice , J. R. and Sih, G. C. (1965) Plane problems of cracks in dissimilar media. J. Appl. Mech. **32**, 418-423.

Rice, J. R. and Thomson, R. (1974) Ductile versus brittle behavior of crystals. Phil. Mag. **29**, 73-97.

Rice, J. R. and Wang, J. S. (1989) Embrittlement of interface by solute segregation. Mater. Sci. Engng. **A107**, 13-40.

Rice, J. R., Beltz, G. E. and Sun, Y. (1992) Peierls framework for dislocation nucleation from a crack tip. In Fundamentals of fracture and Fatigue (ed. A. S. Argon), pp. 1-58. Springer, Berlin.

Rice, J. R., Suo, Z. and Wang, J. S. (1990) Mechanics and thermodynamics of brittle interfacial failure in bimaterial systems. In Metal-Ceramic Interfaces (ed. M. Rühle , A. G. Evans, M. F. Ashby, and J. P. Hirth), pp. 161-179. Pergamon Press, New York.

Ritchie, R. O., Knot, J. F. and Rice, J. R. (1973) On the relationship between critical tensile stress and fracture toughness in mild steel. J. Mech. Phys. Solids **21**, 395-410.

Rogers, C. A. (1995) Intelligent materials. Scientific American September Issue, 154-157.

Ruhle, M., Evans, A. G., Asheby, M. F. and Hirth, J. P., eds. (1990) Metal-ceramic interfaces. Acta-Scripta Metallurgica Proc. Series **4**, Pergamon Press, New York.

Shaw, M. C., Clyne, T. W., Cocks, A. C. F., Fleck, N. A. and Pateras, S. K. (1996) Cracking patterns in metal-ceramic laminates: effects of plasticity. J. Mech. Phys. Solids **44**, 801-822.

Shen, Y. L. and Suresh, S. (1995a) Elastoplastic deformation on multilayered materials during thermal cycling. J. Mater. Res. **10**, 1200-1215.

Shen, Y. -L. and Suresh, S. (1995b) Thermal cycling and stress relaxation response of Si-Al and Si-Al-SiO_2 layered thin films. Acta Metall. Mater. **43**, 3915-3926.

Shih, C. F. (1991) Cracks on bimaterial interfaces: elasticity and plasticity aspects. Mater. Sci. Engng. **A143**, 77-90.

Shih, C. F. and Asaro, R. J. (1988) Elastic-plastic analysis of cracks on bimaterial interfaces: part I - small scale yielding. J. Appl. Mech. **55**, 299-316.

Shilkrot, L. E. and Srolovitz, D. J. (1998) Elastic analysis of finite stiffness bimaterial interfaces: application to dislocation-interface interaction. Acta Metall. Mater. **46**, 3063-3075.

Shu, J. Y., Blume, J. A. and Shih, C. F. (1995) Fracture toughness niobium/alumina interfaces: an analysis based on a micromechanical model. Acta Metall. Mater. **43**, 4301-4307.

Suo, Z. (1989) Singularities interacting with interfaces and cracks. Int. J. Solids Structures **25**, 1133-1142.

Suo, Z. (1990) Failure of brittle adhesive joints. Appl. Mech. Rev. **43**, S276-S279.

Suo, Z. and Hutchinson, J. W. (1989) Sandwich test specimens for measuring interface crack toughness. Mater. Sci. Engng. **A107**, 135-143.

Tada, H., Paris, P. C. and Irwin, G. R. (1985) The Stress Analysis of Cracks Handbook (2nd edition). Paris Productions Incorporated, St Louis, MI.

Taylor, G. I. (1934) The mechanism of plastic deformation of crystals. Proc. Roy. Soc. A145, 362-404.

Thomson, R. (1986) Solid State Physics (ed. H. Ehrenreich and D. Turnbull) **39**, 1

Thomson, R. M. and Sinclair, J. E. (1982) Mechanics of cracks screened by dislocations. Acta Metall. Mater. **30**, 1325-1334.

Thouless, M. D. (1990) Fracture of a model interface under mixed-mode loading. Acta Metall. Mater. **38**, 1135-1140.

Trantina, G. C. (1972) Combined mode crack extension in adhesive joints. J. Composite Materials **6**, 271-285.

Turner, M. R. and Evans, A. G. (1996) Experimental study of the mechanisms of crack extension along an oxide/metal interface. Acta Metall. Mater. **44**, 863-871.

Tvergaard, V. and Hutchinson, J. W. (1993) The influence of plasticity on mixed mode interface toughness. J. Mech. Phys. Solids **41**, 1119-1135.

Tvergaard V. and Hutchinson, J. W. (1994) Toughness of an interface along a thin ductile layer joining elastic solids. Phil. Mag. **A70**, 641-656.

Tvergaard, V. and Hutchinson, J. W. (1996) On the toughness of ductile adhesive joints. J. Mech. Phys. Solids **44**, 789-800.

Uchino, K. (1995) Advances in ceramic actuator materials. Mater. Lett. **22**, 1-4.

Varias, A. G., Suo, Z. and Shih, C. F. (1991) Ductile failure of a constrained metal foil. J. Mech. Phys. Solids **39**, 963-986.

Volterra, V. (1907) Ann. Ec. Norm. **24**, 401.

Wang, J. S. and Anderson, P. M. (1991) Fracture behavior of embrittled F.C.C metal bicrystals. Acta Metall. Mater. **39**, 779-792.

Wang, J. S. and Suo, Z. (1990) Experimental determination of interfacial toughness using Brazil-nut-sandwich. Acta. Metall. Mater. **38**, 1279-1290.

Wei, Y. G. and Hutchinson, J. W. (1996) Mixed mode interface toughness of metal/ceramic joints. Mat. Res. Soc. Symp. Proc. **409**, 163-170.

Williams, M. L. (1957) On the stress distribution at the base of a stationary crack. J. Appl. Mech. **3**, 109-114.

Williams, M. L. (1959) the stresses around a fault or crack in dissimilar media. Bull. Seismol. Soc. America **49**, 199-204.

Willis, J. R. (1971) Fracture mechanics of interfacial cracks. J. Mech. Phys. Solids **19**, 353-368.

Yang, W. and Suo, Z. (1994) Cracking in ceramic actuators caused by electrostriction. J. Mech. Phys. Solids **42**, 649-663.

Zielinski, W., Lii, M. J. and Gerverich. W. W. (1992) Crack-tip dislocation mission arrangements for equilibrium-I. In situ TEM observations of Fe-2wt%Si. Acta Metall. Mater. **40**, 2861-2871.

Zywicz, E. and Parks, D. M. (1992) Small-scale yielding interfacial crack-tip fields. J. Mech. Phys. Solids **40**, 511-536.